ACS Energy LETTERS

http://pubs.acs.org/journal/aelccp

FOCUS REVIEW

Electroreduction of CO_2: Advances in the Continuous Production of Formic Acid and Formate

Kevin Fernández-Caso, Guillermo Díaz-Sainz,* Manuel Alvarez-Guerra, and Angel Irabien

Cite This: *ACS Energy Lett.* 2023, 8, 1992−2024

Read Online

ACCESS | Metrics & More | Article Recommendations

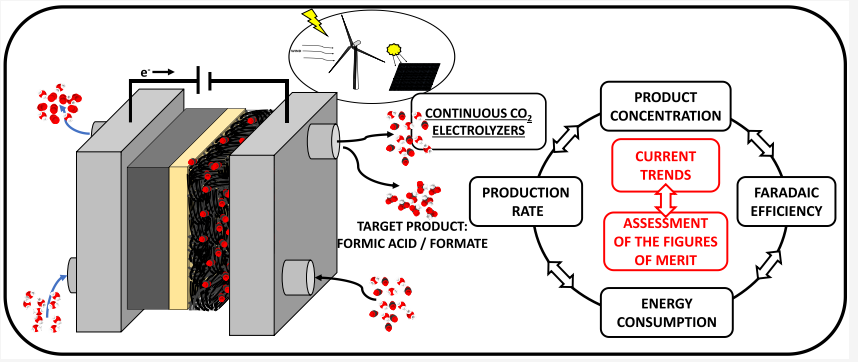

ABSTRACT: **The study of the electrochemical CO_2 reduction to obtain formate ($HCOO^-$) or formic acid (HCOOH) is receiving much attention as a promising technology. Since continuous−mode operation has become necessary for practical implementation of electrochemical CO_2 reduction, recent years have seen a rapid increase in the number of research approaches focusing on this aspect. This Focus Review provides a unified discussion of the available studies on the continuous electroreduction of CO_2 to $HCOO^-$/HCOOH, considering the different important features of process design. Moreover, this paper quantitatively assesses the performance of different studies that involve continuous electrochemical reactors for converting CO_2 to HCOOH/$HCOO^-$, comparing relevant typically used figures of merit, including energy consumption. Although some relevant trade-offs have already been achieved, the simultaneous optimization of all the figures of merit remains a challenge. Finally, concluding remarks highlight the detected trends and discuss relevant aspects that will have to be tackled by future studies in this field.**

One of the goals at the recent United Nations Climate Change Conference (COP26) hosted in Glasgow was to limit the increase of global temperature by up to 1.5 °C above the pre-industrial level.[1] For this purpose, the estimated remaining carbon budget is 420 Gt of CO_2.[2] Thus, it is necessary to reduce CO_2 emissions to mitigate climate change.[3,4] Different strategies are available for reducing CO_2 emissions, such as (i) improving the energy efficiency of processes, (ii) employing carbon-free fuels, and (iii) developing approaches based on CO_2 capture, utilization, and storage (CCUS).[5,6] The CCUS strategies have received special attention since they lower the CO_2 emissions in the atmosphere while extracting value-added products from CO_2 conversion.[7]

In this regard, electroreduction of CO_2 to form value-added chemicals can be considered as a promising option because it requires low temperature and pressure and stores energy from renewable and intermittent sources (e.g., solar and wind energy) in the form of chemicals.[8,9] Various compounds can be obtained by CO_2 electroreduction, such as carbon monoxide (CO),[10−13] hydrocarbons (e.g., methane (CH_4) or ethylene (C_2H_4)),[14−17] alcohols (e.g., methanol (CH_3OH) or ethanol (C_2H_6O)),[18,19] formic acid (HCOOH), and formate ($HCOO^-$).[20−22]

Received: March 7, 2023
Accepted: March 17, 2023

https://doi.org/10.1021/acsenergylett.3c00489
ACS Energy Lett. 2023, 8, 1992−2024

Among them, $HCOO^-$ and HCOOH (depending on pH value) are among the most valuable products that can be obtained by CO_2 electrocatalytic reduction. The global market for HCOOH was around 710 000 tonnes in 2021, and it is expected to be increased to 1 300 000 tonnes by 2035, conditioned in part by its possible future emerging applications.[23] In September 2022, the price of HCOOH in the USA was USD$1099 per ton,[24] while the main alkali formates such as sodium formate (HCOONa) and calcium formate ($(HCOO)_2Ca$) have an estimated value of USD$444 and 1123 per ton, respectively.[25,26] These compounds can be used as precursors for the production of other value-added chemicals and feedstock for fuels.[27] Furthermore, they are used as raw materials in different industries, such as for silage preservation, as additives in animal feeds, for textile finishing, and as anti-icing agents, and as intermediates in the chemical and pharmaceutical industries.[27] $HCOO^-$ can also be used as a more effective and environmentally friendly treatment for slippery (icy) roads than salts.[28] HCOONa specifically can also be employed for various uses such as the production of sodium hydrosulfate ($NaHSO_4$) or the generation of HCOOH. Moreover, HCOONa can be directly employed in leather tanning and printing processes, as a food additive, and as an enzyme stabilizer in detergents.[29] Additionally, $(HCOO)_2Ca$ can also be used in leather tanning, as a cement additive, for silage treatment, in gas generation and flue gas desulfurization, for safety explosives, and as a de-icing agent, among others.[30]

Among the current number of uses of HCOOH or $HCOO^-$, the most promising applications are as reactants in fuel cells and as renewable hydrogen carrier molecules. $HCOO^-$ and HCOOH are being considered as a starting reagents for direct formic acid or formate fuel cells in small portable appliances.[31−33] Moreover, HCOOH is a promising material for hydrogen storage. Hydrogen as an energy vector could be a solution for storing and delivering energy from renewable sources, but it is very difficult to use due to the extremely low critical point and density; hence, the problems associated with hydrogen storage hinder its implementation in fuel cells on a larger scale.[34,35] Therefore, alternative chemical hydrogen storage mechanisms have been developed using HCOOH due to its high storage density (53 $g{\cdot}L^{-1}$ of hydrogen).[36] Furthermore, with the use of a suitable catalyst, HCOOH can be easily decomposed into CO_2 and H_2.[37,38]

HCOOH production is currently based on the thermochemical processes of methanol carbonylation and hydrocarbon oxidation.[39−42] Conventional plants mainly synthesize HCOOH by the hydrolysis of methyl formate in a process that involves two stages: (i) liquid-phase carbonylation of methanol with carbon monoxide to methyl formate in the presence of a basic catalyst such as sodium or potassium methoxide ($CH_3OH + CO \rightarrow HCOOCH_3$) and (ii) hydrolysis of methyl formate to HCOOH and CH_3OH ($CH_3OOCH + H_2O \rightarrow HCOOH + CH_3OH$), where the methanol liberated in the second stage (ii) is returned to the first stage (i).[40] Another route for the production of HCOOH entails the formation of the acid from its salts. The main $HCOO^-$ salts (HCOONa and $(HCOO)_2Ca$) are available industrially as byproducts from the production of polyhydric alcohols.[40,43] For example, pentaerythritol ($C(CH_2OH)_4$) is produced by the reaction between formaldehyde (HCHO) and acetaldehyde (CH_3CHO) in alkaline conditions ($3HCHO + CH_3CHO \rightarrow (HOCH_2)_3CCHO$). Consequently, $(HOCH_2)_3CCHO$ also reacts with HCHO by Cannizaro rearrangement ($(HOCH_2)_3CCHO + HCHO + H_2O \rightarrow C(CH_2OH)_4 + HCOOH$) to give pentaerythritol and HCOOH, which is inevitably converted into the corresponding $HCOO^-$ salt ($HCOOH + NaOH \rightarrow HCOONa + H_2O$ or $2HCOOH + Ca(OH)_2 \rightarrow (HCOO)_2Ca + 2H_2O$) due to the presence of a basic medium.[40,43] The formation of the acid HCOOH from $HCOO^-$ salts involves an additional final step of acidolysis ($2HCOONa + H_2SO_4 \rightarrow 2HCOOH + Na_2SO_4$ or $(HCOO)_2Ca + H_2SO_4 \rightarrow 2HCOOH + CaSO_4$), which requires the addition of a chemical reagent like sulfuric acid (H_2SO_4) or phosphoric acid (H_3PO_4) and the consequent unavoidable co-production of salts.[40] HCOOH produced can be purified to different commercial concentrations for several uses, mainly by energy-intensive distillation-based separation processes such as azeotropic or extractive distillation, among others.[40] Exploring the production of HCOOH and $HCOO^-$ by means of alternatives to the conventional routes, and particularly, the possibility of obtaining these products through the electrochemical valorization of CO_2, is very attractive. Some studies have demonstrated that, under certain conditions and improvements, continuous electroreduction of CO_2 could be techno-economically and environmentally sustainable for producing HCOOH.[39,44−46] $HCOO^-$ and HCOOH must be differentiated as a function of their pH and electrochemical potentials versus standard hydrogen electrode (SHE) (eqs 1 and 2). On the one hand, since $pK_a = 3.8$, HCOOH is produced at strongly acidic pHs, while $HCOO^-$ is formed at slightly acidic, neutral, or basic pHs.[28]

$$CO_{2(g)} + H_2O_{(l)} + 2e^- \rightarrow HCOO^-_{(l)} + OH^- \qquad E^\circ = -0.43\ \text{V vs SHE (pH = 7)} \tag{1}$$

$$CO_{2(g)} + 2H^+ + 2e^- \rightarrow HCOOH_{(l)} \qquad E^\circ = -0.61\ \text{V vs SHE (pH = 7)} \tag{2}$$

Alkaline conditions are necessary to suppress the hydrogen evolution reaction (HER), enabling high Faradaic efficiencies (FEs) toward CO_2 reduction products such as $HCOO^-$.[47,48] Locally on the catalyst layer, alkaline conditions are predominant during the CO_2 reduction reaction by the production hydroxide anion radicals (eq 1).[47] Nevertheless, these conditions generate in turn a competing reaction of CO_2 with hydroxide, producing carbonates and bicarbonates (eqs 3 and 4).

$$CO_2 + OH^- \rightarrow HCO_3^- \qquad pK_a = 6.3 \tag{3}$$

$$HCO_3^- + OH^- \rightarrow CO_3^{2-} + H_2O \qquad pK_a = 10.3 \tag{4}$$

Classic reviews discussing the mechanical aspects and reaction pathways (e.g., refs 49−52), as well as the fundamentals and general characteristics of CO_2 electroreduction (e.g., refs 27, 53−55) can be found in the literature. Recent studies also highlight the advances and challenges of electrochemical CO_2 reduction (e.g., ref 56). The increasing interest in the electroreduction of CO_2 to obtain useful products has rapidly increased the number of studies conducted in this field over the past decade. The high volume of publications explains the recent appearance of numerous review articles focusing on certain aspects and components involved in CO_2 electrochemical reduction. The catalysts

https://doi.org/10.1021/acsenergylett.3c00489
ACS Energy Lett. 2023, 8, 1992−2024

involved in CO_2 electroreduction have been given particular attention, with excellent general reviews (e.g., refs 57, 58) and reviews focusing on metal-based (e.g., refs 59−63), homogeneous (e.g., refs 64, 65), and carbon-based heterogeneous catalysts (e.g., refs 66−70). For example, the effects of the oxidation state of nanomaterials on the structure and catalytic performance of the cathode catalysts have been studied,[71] while Wang et al.[72] have reviewed the regulation of the coordination structure of single metal atoms and their effect on the selectivity and activity of the CO_2 reduction reaction. The type of electrodes used as cathodes (particularly gas-diffusion electrodes, GDEs; refs 73−76), as well as the configuration and type of reactor/electrolyzer (e.g., refs 77−84), including specific types like membrane reactors (e.g., refs 85, 86), have also been reviewed, and different innovative strategies (e.g., tandem catalysts, upgraded electrodes, promising electrolytes, advanced devices; refs 87−89) and approaches of electrode engineering (considering the key roles of morphology and interface of electrode materials; ref 90) have been considered to improve the performance of CO_2 electroreduction systems.

This review paper aims to provide a unified discussion of the studies on the electroreduction of CO_2 to $HCOO^-$ or HCOOH that operate in a continuous mode. The review discusses the current trends and assesses the most relevant figures of merit.

Notably, most of the studies on the electroreduction of CO_2 to form HCOOH or $HCOO^-$ use either discontinuous (e.g., refs 20, 91−94) or semi-continuous (e.g., refs 95−97) modes. Most of the studies in discontinuous operation use H-type reactors to test new catalysts since the operation is simple.[98] However, compared with discontinuous cells, continuous electrochemical equipment can minimize the limitation of mass transport, improving the CO_2 conversion rate to a meaningful level;[83] thus, continuous operation increases the FE for the target product, resulting in reduced energy consumption (EC), higher selectivities, and lower electrolyte loadings.[99] Particular emphasis should be placed on the possibility of operating continuous-flow reactors at higher currents than batch reactors, thus achieving higher production rates.[99] These advantages make continuous operation necessary for future practical and industrial implementation. Studies on continuous CO_2 electroreduction has gained momentum in the recent years. Several recent excellent specific reviews exist on the electrochemical conversion of CO_2 to $HCOO^-$ or HCOOH,[28,100−105] with particular emphasis on the reaction mechanisms involved and the different types of electrocatalysts used as cathodes, and involving Sn-based catalysts.[104,105] However, a comprehensive review on continuous CO_2 electroreduction to form HCOOH or $HCOO^-$ is still lacking. Moreover, the state of the art for continuous electrochemical reduction of CO_2 conversion to form HCOOH or $HCOO^-$, which analyzes and compares these studies with respect to the relevant figures of merit used to assess the performance, has not yet been assessed in detail, and would interest the scientific community.

To fill this gap, this Focus Review aims to provide a unified discussion of the studies on the electroreduction of CO_2 to $HCOO^-$ or HCOOH that operate in a continuous mode. The review is structured into two main parts. Section 1 reviews and discusses the current trends, considering aspects related to process design, such as configuration of the electrochemical reactor, type of feed, nature of the catalyst, configuration of the working electrode, type of counter electrode used in the anode, and the different membranes implemented for separating the reactor compartments. Additionally, this work also assesses the results of the continuous CO_2 electroreduction studies to form HCOOH or $HCOO^-$ considering the most relevant figures of merit that are used to measure the performance of these electrochemical processes: HCOOH/$HCOO^-$ concentration, FE of HCOOH/$HCOO^-$, production rate, EC, and current density used in the continuous operation. All these aspects are discussed in Section 2 that presents a quantitative comparative assessment, analyzes the trends, and detects relevant trade-offs, based on important design aspects, such as type of feed, reactor configuration, and nature of the catalyst or membrane used as separator. Finally, the conclusions section, Section 3, highlights the detected trends and mentions relevant challenges that need to be tackled and could guide future research efforts for the practical development of continuous electrochemical processes to convert CO_2 into HCOOH or $HCOO^-$.

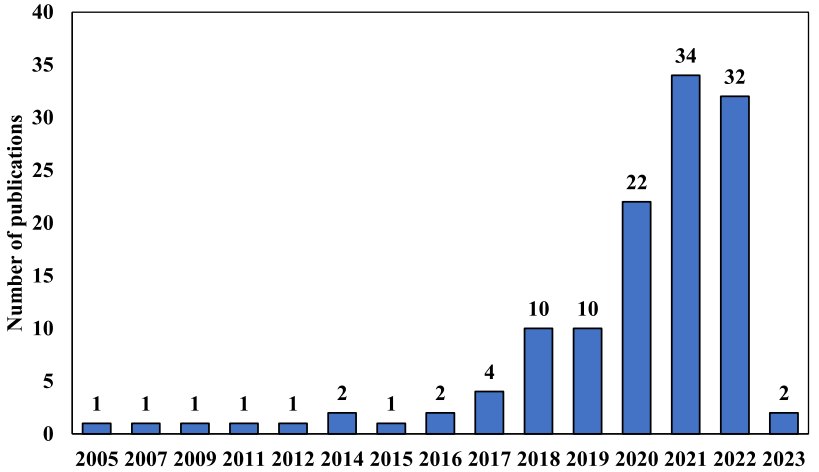

Figure 1. Number of reported publications per year for the continuous CO_2 electroreduction to HCOOH/$HCOO^-$. Studies published until 5 January 2023 in Scopus and Web of Science have been used.

https://doi.org/10.1021/acsenergylett.3c00489
ACS Energy Lett. 2023, 8, 1992−2024

Table 1. Main Features, Aspects, and Figures of Merit of Studies Reported in the Literature for the Continuous Electrocatalytic Reduction of CO_2 to HCOOH and $HCOO^-$ in Terms of (i) Reactor Configuration, (ii) Type of Feed with the Corresponding Concentration for Liquids Feeds, (iii) Catalyst Nature and Configuration of the Working Electrode, (iv) Type of Counter Electrode Used in the Anode, and (v) Type of Membrane (When Applicable)[a]

Reference	Electrochemical reactor configuration	Feed (C/#/A)	Cathode	Anode	Membrane	Current density [mA·cm^{-2}]	Concentration of the target product [g·L^{-1}]	Faradaic efficiency [%]	Product rate [mmol·m^{-2}·s^{-1}]	Energy consumption per kmol of product [kWh·kmol^{-1}]	Icons of graphical representations of section 3
106	Undivided reactor	Na_2SO_4 (0.1 M)	Sn plate	DSA	No membrane	(-)	19.20	(-)	(-)	(-)	
						50	17.20	55	1.42	(-)	
107	Two-compartment reactor	$KHCO_3$ (0.5 M) / KOH (1.0 M)	Sn plate	Ir-MMO	BPM (Fumasep)	100	20.07	65	4.00	277*	
108	Two - compartment reactor	Humidified CO_2 / KOH (1.0 M)	Sn-CCME	Pt/C-CCME	CEM (Nafion 115)	40	116.20	78	1.61*	152*	
109	Three-compartment reactor	Humidified CO_2 / DI water / DI water	Sn-GDE	IrO_2-GDE	AEM (Sustainion) / CEM (Nafion 212)	(-)	186.04	(-)	(-)	(-)	
				IrO_2 on expanded Ti	AEM (Sustainion) / CEM (Nafion 324)	140	94.00	94	6.82	200*	
110	Two-compartment reactor	$KHCO_3$ (0.45 M) + KCl (0.5 M) / KOH (1.0 M)	Sn-GDE	DSA	CEM (Nafion 117)	200	16.90	42	4.38	545*	
111	Two-compartment reactor	Humidified CO_2 / KOH (1.0 M)	Sn-CCME	DSA	CEM (Nafion 117)	45	19.20	49	1.15	244	
112	Two-compartment reactor	$KHCO_3$ (0.45 M) / KOH (1.0 M)	Copper tinned foil	Pt on Ti plate	CEM (Nafion 450)	133	2.02	50	(-)	300	
113	Two-compartment reactor	$KHCO_3$ (0.1 M) / H_2	Sn-GDE	Pt-GDE	CEM (Nafion 212)	3	(-)	64	(-)	(-)	
114	Two-compartment reactor	$KHCO_3$ (0.45 M) + KCl (2.0 M) / KOH (1.0 M)	Sn particulate fixed bed	316 SS, 10# screen	CEM (Nafion 117)	310	(-)	95	0.15*	(-)	
	Two-compartment reactor	$KHCO_3$ (0.45 M) + KCl (2.0 M) + $KHCO_2$ (3.0 M) / KOH (2.0 M)	Sn particulate fixed bed	316 SS, 10# screen	CEM (Nafion 117)	310	46.35	63	10.12*	340	
115	Two-compartment reactor	$KHCO_3$ (0.5 M) / $KHCO_3$ (0.5 M)	Sn-GDE	Pt foil	AEM (FAD)	50	1.91	51	1.47	398*	
116	Two-compartment reactor	Na_2SO_4 (0.5 M) / Na_2CO_3 (0.5 M)	Sn-GDE	Pt/C-GDE	CEM (Nafion 212)	214	1.80	74	7.40	182	
	Two-compartment reactor	Na_2SO_4 (0.5 M) / Na_2CO_3 (0.5 M)	Sn-GDE	Pt/C-GDE	CEM (Nafion 212)	385	3.64	72	14.90	163	
117	Two-compartment reactor	K_2SO_4 (0.4 M) / KOH (1.0 M)	Sn-GDE	Ni foam	BPM	500	3.94*	90	23.31*	351*	
118	Two-compartment reactor	Humidified CO_2 / KOH (2.0 M)	Sn-GDE	Ni foam	CEM (Nafion 117)	100	65.40	80	4.14*	181*	
119	Two-compartment reactor	$KHCO_3$ (0.5 M) / $KHCO_3$ (0.5 M)	Sn-GDE	Pt sheet	CEM (Nafion)	47	(-)	73	1.77	(-)	
120	Two-compartment reactor	KOH (1.0 M) / KOH (1.0 M)	Sn-GDE	Pt wire	CEM (Nafion 117)	306*	10.51	81	12.85*	(-)	
121	Two-compartment reactor	Humidified CO_2 and H_2 / KOH (1.0 M)	Sn-GDE	Pt-GDE	CEM (Nafion 117)	15*	(-)	14	0.14	(-)	
122	Two-compartment reactor	$KHCO_3$ (0.5 M) / KOH (2.0 M)	Sn-GDE	Pt on Ti screen	CEM (Nafion 117)	100	0.85*	76	3.94*	(-)	
123	Two-compartment reactor	$KHCO_3$ (0.5 M) / KOH (2.0 M)	Sn-GDE	Pt on Ti electrode	CEM (Nafion 117)	109	(-)	68	4.63	(-)	
124	Two-compartment reactor	$KHCO_3$ (0.5 M) / $KHCO_3$ (0.5 M)	Sn-GDE	DSA	CEM (Nafion 117)	10	(-)	71	0.37*	250	
125	Two-compartment reactor	$KHCO_3$ (0.5 M) / $KHCO_3$ (0.5 M) + 10 mg MO	Sn-GDE	Co_3O_4 on graphite electrode	CEM (Nafion 117)	43*	(-)	70	1.57	(-)	
126	Two-compartment reactor	KOH (1.0 M) / KOH (1.0 M)	Sn-GDE	Pt mesh	AEM (Fumasep)	147	(-)	46	3.50*	(-)	
127	Two-compartment reactor	$KHCO_3$ (0.5 M) / Na_2SO_4 (0.6 M)	Sn plate	DSA	CEM (Nafion 117)	10	0.46	70	3.05	216	
128	Two-compartment reactor	$KHCO_3$ (1.0 M) / H_2SO_4 (1.0 M)	Sn-GDE	Ir plate	CEM (Nafion 212)	30	15.75**	63	1.00	(-)	
129	Two-compartment reactor	$KHCO_3$ (0.5 M) / H_2SO_4 (0.5 M)	Sn-GDE	Ir/RuO_2 on Ti mesh	CEM (Nafion 324)	200	0.55*	98	10.57*	(-)	
130	Two-compartment reactor	$KHCO_3$ (0.45 M) + KCl (0.5 M) / KOH (1.0 M)	Sn-GDE	DSA	CEM (Nafion 117)	300	27.00	45	7.00	752	
131	Two-compartment reactor	$KHCO_3$ (0.45 M) + KCl (0.5 M) / KOH (1.0 M)	Sn-GDE	DSA	CEM (Nafion 117)	150	1.96	53	4.15	532*	
132	Two-compartment reactor	$KHCO_3$ (0.45 M) + KCl (0.5 M) / KOH (1.0 M)	Sn-plate	DSA	CEM (Nafion 117)	22	0.15	27	0.31	615*	

https://doi.org/10.1021/acsenergylett.3c00489
ACS Energy Lett. 2023, 8, 1992−2024

Table 1. continued

Reference	Electrochemical reactor configuration	Feed (C/#/A)	Cathode	Anode	Membrane	Current density [$mA \cdot cm^{-2}$]	Concentration of the target product [$g \cdot L^{-1}$]	Faradaic efficiency [%]	Product rate [$mmol \cdot m^{-2} \cdot s^{-1}$]	Energy consumption per kmol of product [$kWh \cdot kmol^{-1}$]	Icons of graphical representations of section 3
133	Two-compartment reactor	KOH (1.0 M) / KOH (1.0 M)	Sn-GDE	Ir/C-GDE	AEM (Selemion)	100*	0.66*	90	4.66*	(-)	●
134	Two-compartment microfluidic reactor	KOH (1.0 M) / KOH (1.0 M)	Sn-GDE	IrO_2-GDE	AEM (Selemion AMV AGC. Inc.)	471	12.41*	94	22.99*	(-)	●
135	Two-compartment reactor	KOH (1.0 M) / KOH (1.0 M)	Sn-GDE	IrO_2-GDE	AEM (FAA-3, Fumatech)	557*	6.50*	84	24.10*	(-)	●
136	Three-compartment reactor	Humidified CO_2 / N_2 vapour / H_2	Bi-GDE	Pt/C-GDE	AEM (PSMIM) / CEM (Nafion film)	200	556.00	40	4.14*	368*	▲
137	Two-compartment reactor	$KHCO_3$ (0.45 M) + KCl (0.5 M) / KOH (1.0 M)	Bi-GDE	DSA	CEM (Nafion 117)	200	18.02	45	4.67	535	△
138	Two-compartment reactor	Humidified CO_2 / KOH (1.0 M)	Bi-CCME	DSA	CEM (Nafion 117)	200	43.20	43	2.84	434	△
139	Two-compartment reactor	Humidified CO_2 / KOH (1.0 M)	Bi-GDE	DSA	CEM (Nafion 117)	45	337.00	89	2.10	180	△
140	Two-compartment reactor	$KHCO_3$ (0.5 M) / $KHCO_3$ (0.5 M)	Dendritic Bi on Pb plate	Pt gauze	CEM (Nafion 117)	95	(-)	92	4.53*	(-)	△
141	Two-compartment reactor	$KHCO_3$ (0.5 M) / KCl (0.5 M) + 500 mg/L of MO	Bi-GDE	Ti/SnO_2-Sb electrode	CEM (Nafion)	39	(-)	91	1.85	452*	△
142	Three-compartment reactor	Humidified CO_2 / Humidified N_2 / Humidified H_2	Bi-GDE	Pt/C-GDE	AEM / CEM (Nafion film)	200	1228.00	20	2.07*	429*	▲
143	Two-compartment reactor	KOH (1.0 M) / KOH (1.0 M) + CH_3OH (0.5 M)	Bi-GDE	Ni $(OH)_2$ nanosheets on Ni foam	AEM	117	(-)	92	8.80	90	▲
144	Two-compartment reactor	KOH (1.0 M) / KOH (1.0 M)	Bi-GDE	Ni foam	AEM (FAB-PK-130)	1000	1.30*	93	48.20*	(-)	▲
145	Two-compartment reactor	KOH (1.0 M) / KOH (1.0 M)	Bi-GDE	Fe/Ni foam	CEM (Nafion 1110)	816*	3.13*	83	35.08*	(-)	△
146	Three-compartment reactor	Humidified CO_2 / DI water / DI water	Bi-GDE	IrO_2-GDE	AEM (Sustainion) / CEM (Nafion 324)	200	151.80	76	7.89*	246*	▲
147	Two-compartment reactor	$KHCO_3$ (2.0 M) / $KHCO_3$ (2.0 M)	Bi-GDE	Pt foil	n.a.	200	(-)	90	9.33*	(-)	(-)
148	Two-compartment reactor	$KHCO_3$ (0.5 M) / $KHCO_3$ (0.5 M)	Bi-GDE	Pt wire	CEM (Nafion 117)	104*	0.21*	72	3.87*	(-)	△
149	Two-compartment reactor	KOH (1.0 M) / KOH (1.0 M)	Bi-GDE	Ir/C-GDE	AEM (Selemion)	210	4.60*	98	10.66*	(-)	▲
150	Two-compartment reactor	$KHCO_3$ (2.0 M) / $KHCO_3$ (2.0 M)	Bi-GDE	Pt foil	CEM (Nafion 117)	80*	0.75*	87	3.59	(-)	△
151	Two-compartment reactor	KOH (1.0 M) / KOH (1.0 M)	Bi-GDE	Ni foam	AEM (Fumapem FAA-3-PK-130)	405	2.74*	89	18.68*	(-)	▲
152	Two-compartment reactor	KOH (1.0 M) / KOH (1.0 M)	Bi-GDE	Al foil	n.a.	400	(-)	100	20.72*	(-)	(-)
153	Two-compartment reactor	KOH (1.0 M) / KOH (1.0 M)	Bi-GDE	RuO_2 plate	n.a.	200	(-)	96	9.97*	(-)	(-)
154	Two-compartment reactor	$KHCO_3$ (0.1 M) / Na_2SO_4 (0.3 M)	Bi on Cu plate	DSA	CEM (Nafion 117)	5*	$4 \cdot 10^{-3}$	100	0.27	164	△
155	Two-compartment reactor	KOH (1.0 M) / KOH (1.0 M)	Bi-GDE	Pt wire	CEM (Nafion)	500	3.42*	91	24.14	(-)	△
156	Two-compartment reactor	$KHCO_3$ (1.0 M) / $KHCO_3$ (1.0 M)	Bi-GDE	Ir-GDE	AEM	105	0.14*	97	5.32*	(-)	▲
157	Two-compartment reactor	KOH (1.0 M) / KOH (1.0 M)	Bi-GDE	Pt sheet	CEM (Nafion 212)	224*	0.29*	93	10.78*	(-)	△
158	Two-compartment flow reactor	$KHCO_3$ (1.0 M) / KOH (1.0 M)	Bi-GDE	RuO_2-GDE	BPM	200	0.31*	100	10.36*	(-)	▲
159	Two-compartment reactor	$KHCO_3$ (0.5 M) / $KHCO_3$ (0.5 M)	Bi-GDE	Pt foil	CEM (Nafion 117)	50*	$4 \cdot 10^{-2}$*	85	2.19	(-)	△
160	Two-compartment reactor	KOH (1.0 M) / KOH (1.0 M)	Bi-GDE	Ir/C-GDE	BPM	194*	0.06*	93	9.33*	144*	▲
161	Two-compartment reactor	Humidified CO_2 / KOH (1.0 M)	Bi-GDE	DSA	AEM (Sustainion 37 - 50)	600	10.80	74	22.90	342	▲

https://doi.org/10.1021/acsenergylett.3c00489
ACS Energy Lett. 2023, 8, 1992−2024

Table 1. continued

Reference	Electrochemical reactor configuration	Feed (C/#/A)	Cathode	Anode	Membrane	Current density [mA·cm^{-2}]	Concentration of the target product [g·L^{-1}]	Faradaic efficiency [%]	Product rate [mmol·m^{-2}·s^{-1}]	Energy consumption per kmol of product [kWh·kmol^{-1}]	Icons of graphical representations of section 3
162	Two-compartment reactor	KOH (1.0 M) / KOH (1.0 M)	Bi-GDE	NiFe LDH / Ni foam	AEM (Fumasep FAB-PK-130)	160	(-)	74	(-)	(-)	▲
163	Two-compartment reactor	KOH (1.0 M) / KOH (1.0 M)	Bi-GDE	Pt-foil	CEM (Nafion 117)	300*	(-)	95	14.77*	(-)	△
164	Two-compartment reactor	KOH (1.0 M) / KOH (1.0 M)	Bi-GDE	Pt-foil	CEM (Nafion 117)	350	(-)	92	(-)	(-)	△
165	Two-compartment reactor	KOH (1.0 M) / KOH (1.0 M)	Bi-GDE	Ni foam	AEM (Fumapem FAB-PK-130)	570	0.36*	91	26.88*	(-)	▲
166	Undivided microfluidic reactor	H_2SO_4 (0.5 M) + K_2SO_4 (0.5 M) / KOH (1.0 M)	Pb-GDE	Pt-Ru-GDE	No membrane	346	(-)	96	17.10*	(-)	◆
167	Two-compartment reactor	$KHCO_3$ (0.45 M) + KCl (0.5 M) / KOH (1.0 M)	Pb plate	DSA	CEM (Nafion 117)	12	0.13	44	0.28	(-)	◇
168	Two-compartment reactor	NaOH (0.5 M) / H_2SO_4 (0.5 M)	Pb plate	DSA	CEM (Nafion 423)	3	(-)	90	0.12	(-)	◇
169	Two-compartment reactor	Na_2CO_3 (1.0 M) + $NaHCO_3$ (1.0 M) / NaOH (10 % w/v) + $NaHCO_3$ (1.0 M)	Mixture of Pb and In-GDE	Pt/C-GDE	AEM (Polimeric alkaline membrane)	40	(-)	80	1.66*	(-)	◆
170	Flow-through reactor	K_2SO_4 (0.2 M) / K_2SO_4 (0.2 M)	Ag-Sn alloy dental almagam electrode	2 DSA mesh type	CEM (Nafion 117) / CEM (Nafion 117)	50	108.00**	85	(-)	(-)	◇
171	Two-compartment reactor	KOH (3.0 M) / KOH (3.0 M)	In-GDE	Ni foam	AEM	1000*	(-)	93	48.30	(-)	◆
172	Two-compartment reactor	Na_2SO_4 (0.1 M) / Na_2SO_4 (0.1 M)	Sn-Sb alloy film	Pt-plate	CEM (Nafion 117)	7*	(-)	83	0.31	(-)	◇
173	Two-compartment reactor	KCl (0.5 M) / KOH (1.0 M)	BDD	Pt plate	CEM (Nafion NRE-212)	2	7.36**	95	0.10	(-)	◇
174	Undivided microfluidic reactor	H_2SO_4 (0.5 M) + K_2SO_4 (0.5 M) / K_2SO_4 (0.5 M)	Pb-GDE	Pt-Ru-GDE	No membrane	144	0.39	94	7.01*	176*	◆
175	Two-compartment reactor	Humidified CO_2 / $KHCO_3$ (0.3 M)	Pb-GDE	Pt-GDE	CEM (Nafion 117)	16	(-)	(-)	$2\cdot10^{-3}$	(-)	◇
176	Two-compartment reactor	$KHCO_3$ (2.0 M) / $KHCO_3$ (2.0 M)	Bi-Sn alloy-GDE	(-)	CEM (Nafion 115)	250	0.33*	92	11.92*	(-)	◇
177	Two-compartment reactor	CO_2 saturated DI water / DI water	Fe/BCNNS-GDE	BCN-GDE	CEM (Nafion 117)	(-)	3.45**	94	(-)	(-)	◇
178	Two-compartment reactor	CO_2 saturated DI water / DI water	Fe_3C@NCNTs-GDE	Fe_3C@NCNTs-GDE	CEM (Nafion 117)	(-)	2.67**	90	(-)	(-)	◇
179	Two-compartment reactor	$KHCO_3$ (0.1 M) / $KHCO_3$ (0.1 M)	Bi-Sn on glassy carbon electrode	Graphite carbon rod	CEM (Nafion 117)	10	(-)	94	(-)	(-)	◇
180	Two-compartment reactor	KCl (0.5 M) / K_2SO_4 (0.5 M)	BDD	BDD	CEM (Nafion NRE-212)	11*	0.57**	96	0.53*	(-)	◇
181	Two-compartment reactor	$KHCO_3$ (0.5 M) / $KHCO_3$ (0.5 M)	Ag-Bi on graphite felt	2 DSA	CEM (Nafion 417) / CEM (Nafion 417)	76	(-)	88	3.82	(-)	◇
182	Two-compartment reactor	KOH (1.0 M) / KOH (1.0 M)	Zn-In-GDE	Pt sheet	CEM (Nafion 212)	260*	0.34*	94	12.60*	(-)	◇
183	Two-compartment reactor	KOH (1.0 M) / KOH (1.0 M)	Cu-Sn alloy-GDE	IrO_2-GDE	AEM (Selemion)	148	(-)	87	(-)	(-)	◆
184	Two-compartment reactor	$KHCO_3$ (0.5 M) / $KHCO_3$ (0.5 M)	Dendritic Sn-Pb alloy	Pt mesh	CEM (Nafion 117)	17	$2\cdot10^{-3}$*	92	0.83*	(-)	◇
185	Two-compartment reactor	KOH (1.0 M) / KOH (1.0 M)	In-GDE	Carbon electrode	CEM (Nafion 115)	46	0.12*	91	2.17	(-)	◇
186	Two-compartment reactor	Humidified CO_2 / KOH (1.0 M)	In-GDE	Ni foam	AEM (Sustainion 37 - 50)	258*	(-)	92	12.33*	157*	◆
187	Two-compartment reactor	KOH (1.0 M) / KOH (1.0 M)	Mixture of Bi and Sn-GDE	Pt sheet	BPM	220	(-)	91	10.37*	(-)	◆
188	Two-compartment reactor	Humidified CO_2 / $KHCO_3$ (0.1 M)	Bi-Sn alloy-GDE	IrO_x on Ti foam	CEM (Nafion 117)	60	153.00	82	2.50*	267*	◇
189	Two-compartment reactor	$KHCO_3$ (0.5 M) / KOH (1.0 M)	Cu-Bi-GDE	Pt sheet	AEM (FAA-3-PK-130)	57	(-)	98	2.90*	(-)	◆
190	Two-compartment reactor	KOH (1.0 M) / KOH (1.0 M)	Cu-Sn-GDE	Pt	n.a.	223	(-)	90	11.22	(-)	(-)

https://doi.org/10.1021/acsenergylett.3c00489
ACS Energy Lett. 2023, 8, 1992−2024

Table 1. continued

Reference	Electrochemical reactor configuration	Feed (C/#/A)	Cathode	Anode	Membrane	Current density [mA·cm^{-2}]	Concentration of the target product [g·L^{-1}]	Faradaic efficiency [%]	Product rate [mmol·m^{-2}·s^{-1}]	Energy consumption per kmol of product [kWh·kmol^{-1}]	Icons of graphical representations of section 3
191	Three-compartment reactor	Humidified CO_2 / DI water / H_2SO_4 (0.5 M)	Pb-Cu-GDE	IrO_2 on Ti mesh	AEM / CEM (Nafion film)	133*	7.36	94	6.60*	214*	◆
192	Two-compartment reactor	KOH (1.0 M) / KOH (1.0 M)	Bi-W-GDE	NiFe-LDHs-GDE	CEM (Nafion 117)	250	0.34*	98	12.63*	(-)	◇
193	Two-compartment reactor	$KHCO_3$ (1.0 M) / $KHCO_3$ (1.0 M)	In-Zn-GDE	Ni foam	CEM (Nafion 117)	500*	0.33*	95	24.70	(-)	◇
194	Two-compartment reactor	KOH (1.0 M) / KOH (1.0 M)	Sn-In-GDE	IrO_2-GDE	AEM (PK-75, Fumatech)	196*	9.57*	87	8.86*	197*	◆
195	Two-compartment reactor	KOH (10 M) / KOH (10 M)	Ag-GDE	Ni foam	n.a.	450	(-)	50	(-)	(-)	(-)
196	Two-compartment reactor	KOH (1.0 M) / KOH (1.0 M)	Bi-GDE	$Ni(Fe)O_xH_y$/ Ni foam	AEM (Fumasep FAB-PK-130)	400	(-)	90	18.66	460*	▲
197	Two-compartment reactor	CO_2 / KOH (0.1 M)	In-GDE	IrO_x-Ti mesh	CEM (Nafion 115)	150	(-)	52	4.04*	439*	◇
197	Two-compartment reactor	KOH (1.0 M) / KOH (1.0 M)	In-GDE	IrO_2-GDE	AEM (Fumatech FAB-PK-130)	200	(-)	85	8.81*	225*	◆
198	Two-compartment reactor	KOH (1.0 M) / KOH (1.0 M)	Bi-Cu-GDE	(-)	CEM (Nafion)	60	(-)	96	(-)	(-)	◇
199	Two-compartment reactor	KOH (1.0 M) / KOH (1.0 M)	Ag-In-GDE	Ni foam	AEM (FAB-PK-130)	600	(-)	94	9.75	(-)	◆
200	Three-compartment reactor	Humidified CO_2 / DI water / H_2SO_4 (1.0 M)	In-GDE	IrO_2 on Ti mesh	AEM (Sustainion 37 – 50) / CEM (Nafion 117)	30	5.52*	88	1.37*	219*	◆
201	Two-compartment reactor	KOH (1.0 M) / KOH (1.0 M)	In-GDE	Ni foam	AEM (FAA-3-PK-130)	44	(-)	91	(-)	(-)	◆
202	Two-compartment reactor	$KHCO_3$ (0.5 M) / KOH (1.0 M)	Bi-GDE	Ni foam	CEM (Nafion 115)	200	0.36*	95	9.97	223*	◇
203	Two-compartment reactor	KOH (1.0 M) / KOH (1.0 M)	Bi-GDE	Pt mesh	AEM	200	(-)	95	9.84*	(-)	▲
204	Two-compartment reactor	Humidified CO_2 + K_2SO_4 (0.4 M) / KOH (1.0 M)	Sn-GDE	Ni foam	BPM	500	3.54*	81*	20.99*	423*	◍
205	Two-compartment reactor	KOH (1.0 M) / KOH (1.0 M)	In-GDE	Ni plate	AEM (Fumapem FAA-3-PK-130)	134	(-)	90	(-)	(-)	◆
206	Two-compartment reactor	KOH (1.0 M) / KOH (1.0 M)	In-GDE	Pt foil	AEM (Sustainion X37-50)	100	(-)	90	(-)	(-)	◆
207	Two-compartment reactor	KOH (1.0 M) / KOH (1.0 M)	Sb-Bi-GDE	Pt foil	AEM (Fumasep FAB-PK-130)	800	1.01*	91.7	37.77	(-)	◆
208	Two-compartment reactor	$KHCO_3$ (0.5 M) / $KHCO_3$ (0.5 M)	SCuSn-GDE	20% wt. Ir@carbon XC72 (Premetek)	CEM (Nafion 117)	250*	3.37*	96	12.48*	(-)	◇
209	Two-compartment reactor	$KHCO_3$ (0.5 M) / $KHCO_3$ (0.5 M)	CuBi-HFGDE	(-)	AEM (Fumatech FAA-3-PK-130)	165*	(-)	85	(-)	(-)	◆
210	Two-compartment reactor	KOH (1.0 M) / KOH (1.0 M)	Bi-GDE	Pt foil	AEM (Sustainion X37-50)	1938	5.66*	69*	69.88*	(-)	▲
211	Two-compartment reactor	CsOH (1.0 M) / CsOH (1.0 M)	Bi-GDE	Ni foam	AEM (-)	870	(-)	90	40.57*	(-)	▲
212	Two-compartment reactor	KOH (1.0 M) / KOH (1.0 M)	Bi-GDE	Ni foam	AEM (FAA-3-PK-130)	186*	$8.49\cdot10^{-3}$*	98	9.43*	(-)	▲
213	Two-compartment reactor	KOH (1.0 M) / KOH (1.0 M)	Bi-GDE	IrO_2 on Ti sheet	(-)	400	0.53*	95	19.61*	(-)	(-)
214	Two-compartment reactor	$KHCO_3$ (0.5 M) / KOH (1.0 M) + GLY (0.1 M)	Ag-Bi-GDE	CoP on Ni foam	AEM (-)	(-)	(-)	130	5.08*	91	◆
215	Two-compartment reactor	$KHCO_3$ (0.1M) / $KHCO_3$ (0.1 M)	Sn-Cu-GDE	Ni electrode	CEM (-)	205	0.52*	90	9.65*	(-)	◇
216	Two-compartment reactor	KOH (1.0 M) / KOH (1.0 M)	Bi-GDE	Pt electrode	AEM (FAA-3-PK-130)	500	0.71*	100	26.66	(-)	▲
217	Two-compartment reactor	KOH (1.0 M) / KOH (1.0 M)	S-Cu-GDE	(-)	(-)	588*	(-)	71	(-)	(-)	(-)
218	Two-compartment microfluidic reactor	KOH (1.0 M) / KOH (1.0 M)	Sn-Bi-GDE	Pt foil	AEM (-)	200	0.12*	90	9.32*	(-)	◆
219	Two-compartment reactor	KOH (1.0 M) / KOH (1.0 M)	Sn-GDE	NiCoFe plate	CEM (Nafion)	200	3.34*	71	7.43*	(-)	○
220	Two-compartment reactor	$KHCO_3$ (0.5 M) / KOH (1.0 M)	Sn-GDE	Platinized titanium electrode	CEM (Nafion 117)	300	7.17*	85	13.28*	(-)	○

https://doi.org/10.1021/acsenergylett.3c00489
ACS Energy Lett. 2023, 8, 1992−2024

Table 1. continued

Reference	Electrochemical reactor configuration	Feed (C/#/A)	Cathode	Anode	Membrane	Current density [mA·cm^{-2}]	Concentration of the target product [g·L^{-1}]	Faradaic efficiency [%]	Product rate [mmol·m^{-2}·s^{-1}]	Energy consumption per kmol of product [kWh·kmol^{-1}]	Icons of graphical representations of section 3
221	Two-compartment reactor	KOH (1.0 M) / KOH (1.0 M)	Bi-W-GDE	(-)	CEM (Nafion 117)	110	(-)	78	4.49*	(-)	◇
222	Two-compartment reactor	CO_2 / KOH (0.1 M)	Bi-GDE	Pt-coated titanium flow field anode plate	AEM (QAPPT)	500	5.04*	90	23.32*	207*	▲
223	Two-compartment reactor	KOH (1.0 M) / KOH (1.0 M) + CH_3OH (0.5 M)	Bi-GDE	Ni_3N-Co_3N/NF on Ni foam	AEM (FAB-PK-130)	150	0.46*	90	10.39	142*	▲
		KOH (1.0 M) / KOH (1.0 M)	Bi-GDE	Ni foam	AEM (FAB-PK-130)	300*	0.66*	95	14.81	(-)	▲
224	Two-compartment reactor	KOH (1.0 M) / KOH (1.0 M)	Bi-GDE	IrO_2-electrode	CEM (Nafion 117)	200	2.10*	70	7.25*	(-)	△
225	Two-compartment reactor	KOH (1.0 M) / KOH (1.0 M)	Cu-Bi-GDE	Foamed Ni films	AEM (FAA-3-PK-130)	200	(-)	95	9.84	(-)	◆
226	Two-compartment reactor	KOH (1.0 M) / KOH (1.0 M)	Bi-In-GDE	Ni foam	AEM (FAA-3-PK-130)	300	(-)	92	14.36	(-)	◆
		Humidified CO_2 / $KHCO_3$ (0.1 M)	Bi-In-GDE	IrO_2 on Ti foam	AEM (Sustainion X37-50)	120	0.36*	80	4.97*	268*	◆
227	Two-compartment reactor	KOH (1.0 M) / KOH (1.0 M)	Bi-GDE	Pt electrode	AEM (-)	300	(-)	89	13.88*	(-)	▲
228	Two-compartment reactor	$KHCO_3$ (0.5 M) / KOH (0.5 M)	Cu-Sn-GDE	Pt film	AEM (FAD)	66	(-)	89	2.20*	189*	◆
229	Two-compartment reactor	$KHCO_3$ (0.45 M) + KCl (0.5M) / KOH (1.0 M)	Bi-GDE	NiO particulate electrode	CEM (Nafion 117)	150	13.73	45	3.56	545	△

CEM – Cation exchange membrane
AEM - Anion exchange membrane
BPM – Bipolar membrane
MO – Methyl orange
DI – Deionized water
BDD – Bored Doped Diamond

C: Feed of the cathode compartment
#: Feed of the central compartment in the cases of 3-compartment reactors
A: Feed of the anode compartment.
*Calculated values of figures of merit
**Accumulated $HCOO^-$ or HCOOH concentration
n.a. membrane not available
(-) figures of merit neither reported nor with enough information to be calculated

[a]The commercial houses and specifications of the membranes reported by each work are indicated in parentheses. The figures of merit analyzed to assess the performance of the electrochemical processes were current density, HCOOH or $HCOO^-$ concentration, Faradaic efficiency for the target product, the production rate, and energy consumption. Definitions of the figures of merit are explained in Section 2. The last column shows the icon used to represent each study in the graphical representations of Figures 12−15, according to the symbols and meanings detailed in Table 2.

1. STATE OF THE ART OF CONTINUOUS ELECTROCHEMICAL CO_2 REACTORS FOR $HCOO^-$ AND HCOOH

1.1. Summary of Studies. A total of 124 studies (from 2005 to 2023) on continuous electrocatalytic reduction of CO_2 to HCOOH or $HCOO^-$ were compiled. It was assumed that all these studies operate with a continuous feed of all the reactants (including CO_2) in the electrochemical reactor. The number of studies in this field has increased in the recent years, reaching up to 22 publications in 2020, 34 manuscripts in 2021, and 32 in 2022 (Figure 1).

The main features and aspects of these studies are summarized in Table 1. Table 1 also summarizes the main figures of merit obtained from all these studies. These figures of merit are defined at the beginning of Section 2, before the subsequent quantitative comparative assessment.

1.2. Electrochemical Reactor Configuration. The configuration of the electrochemical reactors for continuous CO_2 electroreduction to $HCOO^-$ and HCOOH is considered significant.[103] Generally, more than 90% of the published studies have used two-compartment electrochemical reactors, while the rest used three-compartment reactors and reactors without separation between compartments or undivided reactors.

Some studies have reported the use of electrochemical reactors that do not employ separators between the cathodic and anodic compartments.[106,166,174] The main advantage of this configuration is that they do not depend on the stability of the compartment separator. However, the $HCOO^-$ or HCOOH produced on the surface of the working electrode can diffuse to the counter electrode and consequently be oxidized, lowering the selectivity of CO_2 conversion to the target product process. This category includes compartmentless filter press and microfluidic reactors. Figure 2a shows the schematic diagram of a pressurized undivided filter-press reactor, and Figure 2b depicts the diagram of a microfluidic reactor. An example of an undivided filter press reactor can be found in Proietto et al.[106] CO_2 electroreduction is carried out at high pressures (23 bar) and current densities of 55 mA·cm^{-2}, reaching $HCOO^-$ concentrations, FEs and production rates of 17.20 g·L^{-1}, 55%, and 1.42 mmol·m^{-2}·s^{-1}, respectively. The Sn metal plate cathode remains stable for up to 41 h for the production of HCOOH. Nevertheless, the stability of the Sn metal plate cathode could be affected by degradation and/or deactivation under cathodic polarization.[86] For Sn catalysts and 2.0 M KCl solutions, the deactivation by cathodic polarization was due to the formation of intermetallic compounds (KSn) occurring in parallel to the reduction of CO_2 to $HCOO^-$ at different potentials.[230] Microfluidic reactors operate with two diverse electrolytes (known as dual electrolyte microfluidic reactor) in laminar conditions to avoid intermixing of the electrolyte flow lines.[166,174] Both studies[166,174] report that increasing the Reynolds number improves the energy efficiency of the electrochemical process. This configuration enhances mass transfer (because there is no membrane separator) and removes the neutralization of both

https://doi.org/10.1021/acsenergylett.3c00489
ACS Energy Lett. 2023, 8, 1992−2024

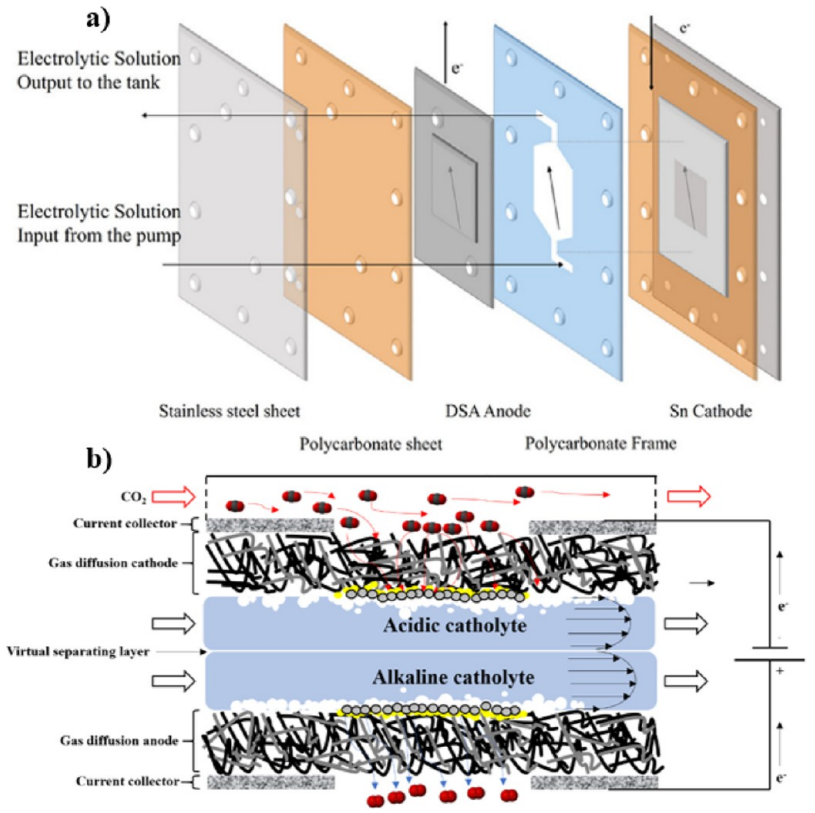

Figure 2. (a) Undivided filter-press reactor (reproduced with permission from ref 106, copyright 2018 Elsevier). (b) Microfluidic reactor configuration (adapted from ref 166 copyright 2017 Elsevier, and ref 174, copyright 2016 Elsevier).

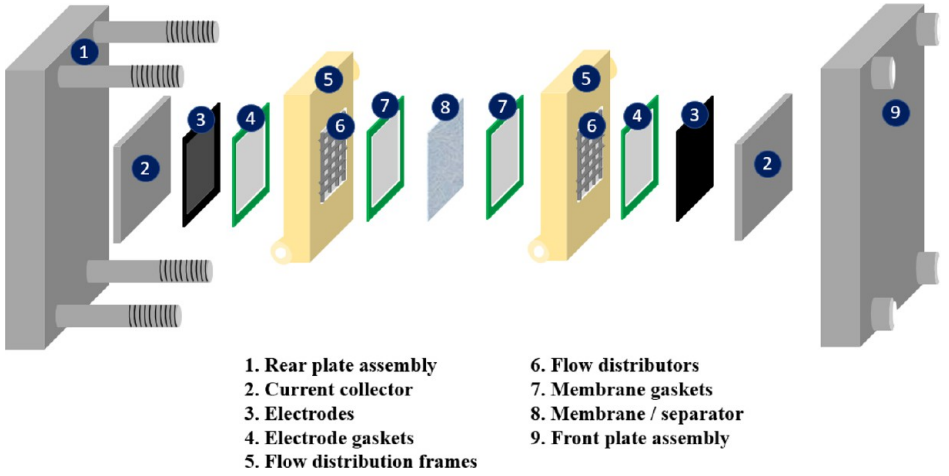

Figure 3. Two-compartment reactor based on a series of stacked components (adapted from ref 231, IOP Publishing Limited 2020, Creative Commons Attribution 4.0 License).

electrolytes (due to laminar flow) maintaining high concentrations of protons and hydroxyl radicals.

As previously mentioned, most studies on the electrocatalytic reduction of CO_2 to HCOOH or $HCOO^-$ have utilized a two-compartment reactor separated generally by an ion-exchange membrane (e.g., cationic-exchange membrane (CEM) and anionic-exchange membrane (AEM)). Reactor designs that involve the introduction of flow are often assembled from a series of stacked components, such as electrodes, current collectors, gaskets, separators, flow distribution frames, and housings (Figure 3).[231]

In particular, approximately 63% of the studies involving two-compartment laboratory reactors analyzed in this review employed a CEM as the compartment separator (Figure 4).[112,131,167] CEMs are solid components that usually consist of a backbone composed of various polymeric materials containing sulfonic acid, phosphoric acid, sulfonamide, or azole groups.[232] Majority of the two-compartment reactors use Nafion membranes (Nafion 115, 117, 212, 324, 417, 423, 450, and 1110) (Table 1),[110,155,185] the numbers of which represent different thicknesses (127, 183, 50.8, 279.4, 431.8, 250, 431.8, and 254 μm, respectively). Among them, Nafion 117 is the most widely used CEM.[123,124,179] These membranes show

https://doi.org/10.1021/acsenergylett.3c00489
ACS Energy Lett. 2023, 8, 1992−2024

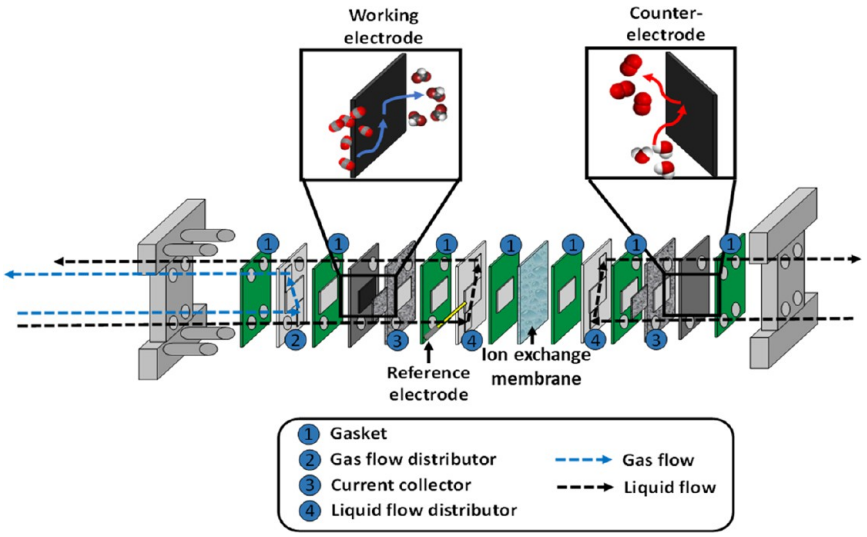

Figure 4. Simplified scheme of a typical two-compartment reactor configuration separated by an ion-exchange membrane (CEM, AEM, or BPM) (adapted from ref 137, copyright 2019 Elsevier).

good performance for the selective passage of cations, particularly protons.[233] The studies where $HCOO^-$ is generated at the cathode employ a CEM that restricts the passage of the $HCOO^-$ anions to the anode compartment, concentrating the product in the cathode outlet stream.[233] However, for aqueous feeds in the cathode compartment, the generated product can pass from the cathode into the anode compartment when the product is in high concentrations, reducing the selectivity of the electrochemical process.[114,130]

Only 31% of studies used AEM as the separator in two-compartment electrochemical reactors (Figure 4).[115,156,169] This type of membrane enables $HCOO^-$ anions to diffuse from the cathodic to the anodic compartment, with the possibility that part of the product generated in the cathode is re-oxidized over the anode surface. AEM are polymer electrolytes that conduct anions (like OH^- and Cl^-), as they typically contain positively charged groups bound covalently to a polymer backbone.[234] The main AEM employed in the reported studies were from commercial companies such as Fumatech (FAA-3-PK-130 and FAB-PK-130), Selemion (Selemion AMV, AGC Inc.), and Sustainion (Sustainion 37-50). Specifically, Wang et al. and Díaz-Sainz et al. successfully used a Sustainion 37-50 AEM with a humidified CO_2 inlet stream at the cathode side.[161,186] All the reported two-compartment reactors with AEM use aqueous alkaline electrolytes in both compartments,[126,151,183] because these membranes perform optimally under alkaline conditions. Furthermore, the high ionic conductivity of aqueous alkaline electrolytes allows increased operation at high current densities (<2 A·cm^{-2}). Despite the promising results obtained with the implementation of these membranes in continuous electrochemical reactors for CO_2 reduction to $HCOO^-$/HCOOH, rigorous studies such as the one by Salvatore et al.[235] conclude that AEMs should be further developed to avoid product crossover, increasing the mechanical and chemical stability, and minimizing energy losses.

In particular, Díaz-Sainz et al.[161] carried out an interesting comparison with the same system setup and operating conditions employing an AEM (Sustainion X37-50) and a CEM (Nafion 117). Notable performances were achieved with the two-compartment flow reactor equipped with the Sustainion X37−50 membrane, achieving promising FEs toward $HCOO^-$ of up to 93% at current densities of 200 mA·cm^{-2} at the expense of obtaining diluted $HCOO^-$ concentrations of 4.5 g·L^{-1} in the anolyte output stream. In contrast, under the same experimental conditions with the same filter-press reactor equipped with Nafion 117 membrane, $HCOO^-$ concentrations of up to 312 g·L^{-1} were achieved in the cathode side with the disadvantage of obtaining FEs toward this product of only 24.8%. Lei et al.[115] also tested up to four different ion-exchange membranes, showing that the best performance were achieved by FAD alkaline-exchange membranes, mainly attribute to the high ionic conductivity of this membrane, and thus, the reduction in the ohmic overpotential during the CO_2 electroreduction.

Studies implementing bipolar membranes (BPMs) in two-compartment reactor configurations have also been reported (Figure 4).[107,117,158] BPMs are composite membranes that consist of a layered ion-exchange structure composed of a cation-selective layer (with fixed negative charges) and an anion-selective layer (with fixed positive charges).[236] Fumatech commercial membranes, such as Fumasep FBM-PK,[107] are the most used BPMs in continuous CO_2 electrochemical reactors to obtain HCOOH and $HCOO^-$. Most of the studies with BPMs have employed electrolytes based on $KHCO_3$ and K_2SO_4 at the cathode side and alkaline electrolytes (based on KOH) at the anode side (Table 1).[107,117,158] The configuration of the BPM (Figure 5) favors the dissociation of water into its hydroxyl radicals (to anode) and protons (to cathode), improving the electrochemical performance of the reactor.[237] In all the studies that implement BPMs, operation is carried out at current densities >100 mA·cm^{-2}.

Several studies using three-compartment reactor configurations for continuous CO_2 electroreduction to $HCOO^-$ or HCOOH process also exist.[109,136,142,146] Three-compartment reactors are separated by an AEM in the cathodic compartment and a CEM in the anodic compartment, forming a central compartment in which the HCOOH is generated (Figure 6). The AEMs used are mainly Sustainion membranes, such as those of Yang et al.[109,146] The main objective of these membranes is to increase the transport of the $HCOO^-$ anions from the cathodic to the central compartment. In case of

https://doi.org/10.1021/acsenergylett.3c00489
ACS Energy Lett. 2023, 8, 1992−2024

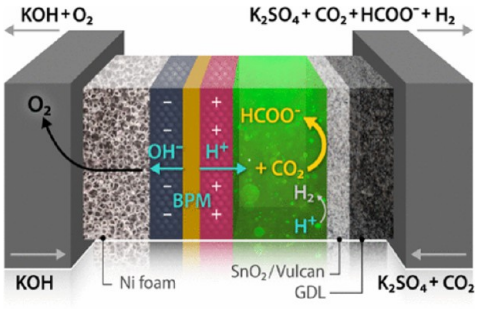

Figure 5. Schematic diagram of a two-compartment electrochemical reactor separated by a bipolar membrane (reproduced with permission from ref 117, copyright 2020 American Chemical Society).

CEMs, fluorinated ones, such as Nafion 324 used by Yang et al.[146] allow the passage of cations and protons from the anode compartment to the central one. In the central compartment, materials based on porous solid electrolytes (Figure 6a) (e.g., styrenedivinyl-benzene copolymer)[136,142,191] or ion-exchange resins (Figure 6b)[109,146] are used for the proper performance of the CO_2 electroreduction to the target product process. In particular, styrenedivinyl-benzene copolymer microspheres with sulfonic acid functional groups used by Fan et al.[142] increase the transport of protons from the anodic to cathodic compartment under room temperature. Other studies implemented Amberlite IR120 strong acid ion-exchange resins, that perform extremely well as ion conductors in the central compartment.[109,146] Currently, Dioxide Materials has started to develop three-compartment reactors achieving remarkable HCOOH concentrations (>15 wt%) for extended periods of time (>500 h).[238]

Park and Shin[170] have developed a novel reactor configuration in which the cathode is located in the central compartment, while the anodes are in the other two compartments separated by CEMs (Nafion 117) (Figure 7a). This configuration aims to increase the crossover of cation (K^+) and protons (H^+) through the two CEMs and promote electron generation through the two anodes. Another similar reactor configuration was implemented by Lou et al.,[181] in which the central compartment where the cathode is located is separated from the anodes by two CEMs (Nafion 417) (Figure 7b).

Two-compartment reactors were the most implemented configuration for the electrocatalytic reduction of CO_2 to HCOOH and $HCOO^-$ (Table 1). In particular, here CEM avoids the product crossover from the cathodic to the anodic compartment and therefore enhances the selectivity of CO_2 electroconversion. Undivided reactors and three-compartment reactors have also been considered for the CO_2 electroreduction to HCOOH and $HCOO^-$ in few studies. Undivided

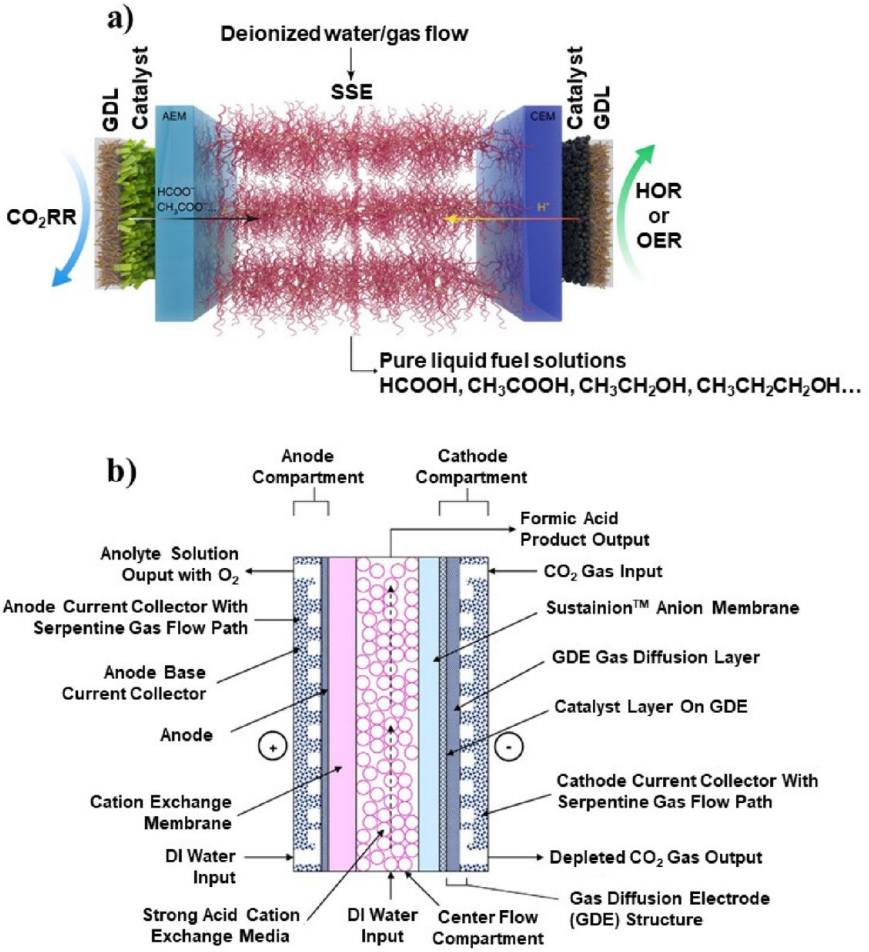

Figure 6. Schematic illustrations of three-compartment reactor configuration with (a) porous solid electrolyte (adapted from ref 136, copyright 2019 Springer Nature) and (b) ion-exchange resin in the central compartment (adapted from ref 109, copyright 2017 Elsevier).

https://doi.org/10.1021/acsenergylett.3c00489
ACS Energy Lett. 2023, 8, 1992−2024

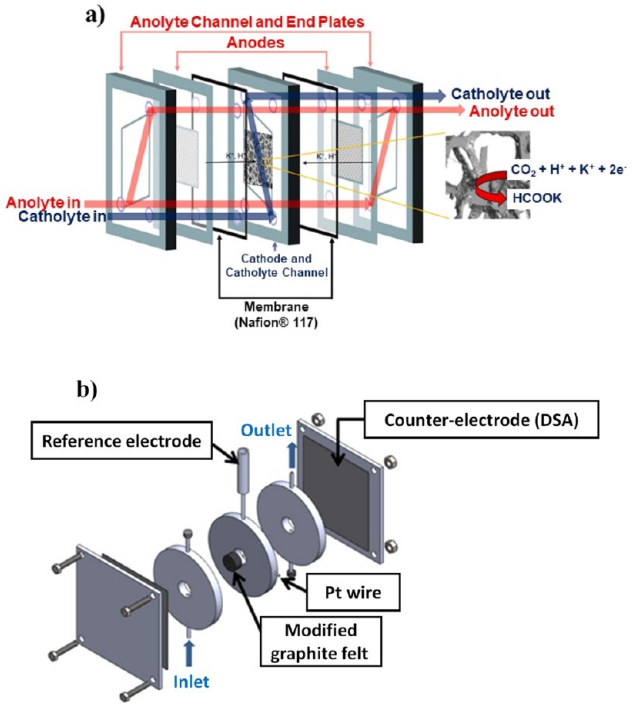

Figure 7. Schematic diagram of (a) the flow-through electrochemical cell implemented by Park and Shin (adapted from ref 170, copyright 2021 Elsevier) and (b) the home-made flow cell of Lou et al. (adapted from ref 181, copyright 2021 Elsevier).

reactors do not require a compartment separator, improving the transport of the ionic species through the reactor. However, a product crossover from the cathode to the anode compartment can occur, oxidizing the product and thus lowering the process selectivity. Meanwhile, a three-compartment reactor configuration allows obtaining the HCOOH in the central compartment through $HCOO^-$ (from the cathode through an AEM) and protons diffusion (from the anode through a CEM).

1.3. Types of Feeds at the Cathode. There are different ways for delivering the CO_2 to the electrochemical flow reactor. For better comprehension, Figure 8 depicts the main configurations of input feed stream used up to date for supplying CO_2 to the cathodic compartment of electrolyzer. Some part of the studies analyzed in this review employed aqueous feeds at the cathode compartment of the electrochemical reactor, particularly those in which the CO_2 input stream is bubbled until the saturation of the electrolyte (e.g., refs 140, 167, 168, 180). (Figure 8a). Moreover, there are numerous reported approaches in which CO_2 is fed directly to an interface between the catalyst of porous electrode and aqueous electrolyte (e.g., refs 110, 137) (Figure 8b).

The vast majority of studies on the continuous electrochemical reduction of CO_2 to $HCOO^-$/HCOOH analyzed in this review use a pure CO_2 gaseous stream at the cathode chamber of the electrochemical reactor at ambient pressure conditions. Only two approaches analyzed[219,220] have studied the effect of CO_2 concentration by reducing the CO_2 partial pressure of the input stream. On one side, Choi et al.[219] carried out CO_2 electrolysis experiments for 8 h using diluted streams of 15 vol% CO_2 (equivalent to a partial pressure of 0.15 atm) with SO_2 and NO impurities, and obtained notable performances. On the other hand, Van Daele et al.[220] successfully operated a continuous flow cell with a less concentrated gaseous stream (60 vol% CO_2 or CO_2 partial pressure of 0.6 atm) at current densities of up to 300 $mA \cdot cm^{-2}$. In contrast, to increase the CO_2 partial pressure, other approaches such as Proietto et al.[106] and Ramdin et al.[107] assessed the pressure effect inside the flow electrochemical cell to ensure a high CO_2 concentration near the catalyst surface, showing that the best results were obtained at elevated pressures of 23 and 50 bar, respectively, thereby increasing the CO_2 partial pressure.

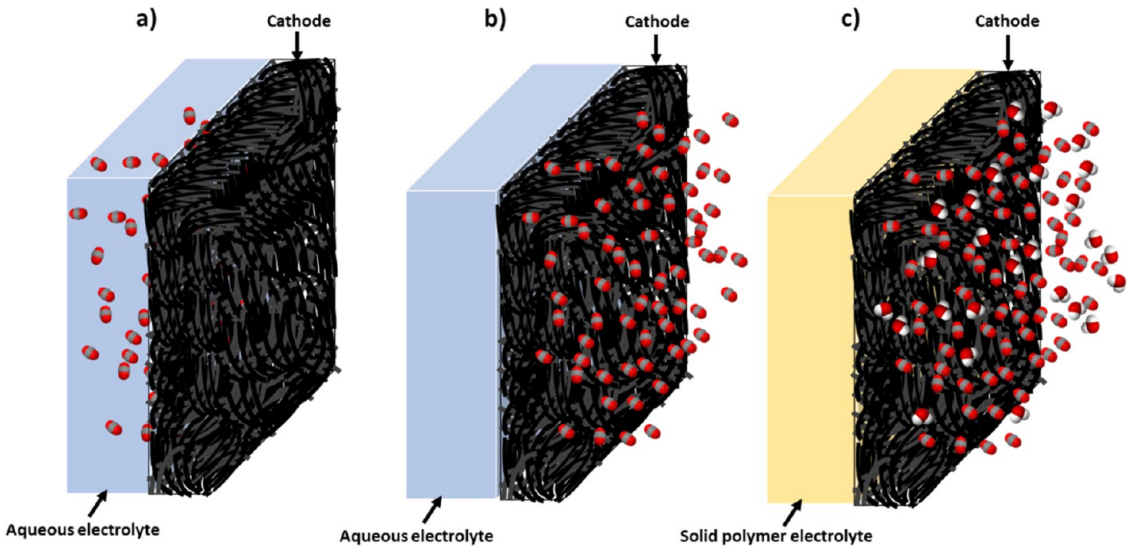

Figure 8. Simplified scheme showing the three main different input feed configurations that have been used for delivering CO_2 streams to the cathode of flow electrolyzers for the continuous production of HCOOH and $HCOO^-$ reported in this review: (a) a liquid feed in which the CO_2 input stream is bubbled until the saturation of the aqueous electrolyte, (b) a CO_2 input stream fed directly to an interface between the catalyst of cathode and a liquid electrolyte, and (c) a gaseous feed in which the CO_2 input stream is humidified, avoiding the use of the aqueous electrolyte since the ion-exchange membrane acts as a solid polymer electrolyte (adapted from ref 74, copyright 2018 American Chemical Society).

https://doi.org/10.1021/acsenergylett.3c00489
ACS Energy Lett. 2023, 8, 1992−2024

Aqueous electrolytes as cathode feeds increase the conductivity along the reactor and reduce the total reactor voltage. To date, liquid electrolytes based on potassium bicarbonate ($KHCO_3$),[127,130] sodium carbonate (Na_2CO_3), sodium bicarbonate ($NaHCO_3$),[169] and mixtures of carbonate compounds with potassium chloride solutions (KCl)[110,114,137] have been used. Thus, it has been proven that adding salts to the carbonate-based liquid electrolyte provides greater ionic conductivity.[239] Other electrolytes based on different salts, such as sodium sulfate (Na_2SO_4)[106,116] or potassium sulfate (K_2SO_4),[117,170] have also been considered for the electrocatalytic reduction of CO_2 to HCOOH and $HCOO^-$. The concentration of these electrolytes ranges between 0.1 and 3 M, mainly being 0.5 or 1 M (Table 1).

Other studies have used an acidic solution, particularly 0.5 M sulfuric acid (H_2SO_4), as the electrolyte in the cathode feed.[166,174] These studies employed an undivided microfluidic reactor in which laminar flow operates with an acid solution in the cathode side.

Despite the fact that alkaline electrolytes promote the formation/precipitation of (bi)carbonates,[240] they are used at the cathode side to improve the selectivity of the electrochemical process and reduce hydrogen production. (Bi)-carbonate formation can hinder the working electrode performances. Some excellent works have studied this undesirable event as well as different ways to reduce their formation, and thus, their impact during electrochemical tests, which is particularly important with operation at high current densities and for keeping long-term performances,[241] as well be discussed in section 2.5.

Nearly a third of the studies analyzed use alkaline liquid electrolytes. This has been proved by studies focused on potassium hydroxide (KOH) solutions at different concentrations (1.0 and 3.0 M).[143,144,171] For example, Grigioni et al.[171] employed a highly concentrated alkaline solution (KOH 3.0 M) as a cathode feed electrolyte, which considerably decreased the cathodic overpotential. Seifitokaldani et al.[195] obtained 50% FEs for $HCOO^-$ with current densities >450 $mA{\cdot}cm^{-2}$ using Ag-based catalysts at the cathode (more selective to give CO) and ultra-concentrated alkaline electrolytes (KOH 10 M). To a lesser extent, relatively low concentrations (0.5 M) of sodium hydroxide (NaOH)-based alkaline solutions have been used as a cathode feed electrolyte.[124,168]

Additionally, some studies use deionized water as an input stream at the cathode compartment of the electrochemical reactor.[177,178] For instance, Ghosh et al.[178] employed CO_2-saturated deionized water stream as an input in the cathodic compartment, and obtained remarkable accumulated product concentrations of 2.67 $g{\cdot}L^{-1}$ and FEs of up to 90% toward the target product.

Notably, some recent studies that operated in continuous mode avoided the use of liquid electrolytes, employing a humidified CO_2 stream at the cathode compartment of the electrochemical reactor.[175,186,191] Specifically, 12% of the reported studies operated with a humidified CO_2 feed to the cathode. This technique eliminated the need of an additional liquid electrolyte because the ion-exchange membrane acted as a solid polymer electrolyte (Figure 8c). Thus, the water vapor provide protons to carry out the reduction of CO_2 to $HCOO^-$ over the cathode surface, and simultaneously, the humidified CO_2 stream reduced the limitations associated with the solubility of CO_2 in aqueous phases.[98] In this context, the control of the CO_2 and water vapor ratio becomes crucial.[108,118,146] For example, in Lee et al.,[108] the water flow was controlled by a homemade bubble humidifier, and it was observed that the $HCOO^-$ concentration (116.20 $g{\cdot}L^{-1}$) and FE (78%) increased with a vapor supply of 0.65 $mg{\cdot}min^{-1}{\cdot}cm^{-2}$ and a temperature of 323 K without an appreciable increase of the cell voltage. Several works have designed experimental setups, such as a Vapour Delivery Module, which accurately controls and adjusting the feed gas temperature and the ratio between CO_2 flow and water vapor in the input stream at the cathode side.[111,138,139] Díaz-Sainz et al.[111] reported that the best results were obtained at ambient temperature of 293 K and water vapor stream of 500 $mg{\cdot}h^{-1}$ (56,1 mol $H_2O{\cdot}[mol\ CO_2{\cdot}m^2]^{-1}$) as input, providing of $HCOO^-$ concentrations, FEs, and EC of 19.20 g L^{-1}, 50%, and 244 $kWh{\cdot}kmol^{-1}$, respectively. De Mot et al.[118] controlled the flow of CO_2 (Brooks Instruments, GF040) and the flow of injected water by adjusting an HPLC pump (Watrex, P102) and mixing both compounds in a T-mixer. Employing this experimental setup, a product concentration and EC of 65.40 $g{\cdot}L^{-1}$ and 181 $kWh{\cdot}kmol^{-1}$, respectively, were achieved. Yang et al.[146] used a gas humidifier at room temperature (296−298 K) to control the CO_2 and vapor ratio with current densities of up to 200 $mA{\cdot}cm^{-2}$ and achieved excellent product concentrations of 151.80 $g{\cdot}L^{-1}$.

Some works, in which CO_2 input streams are humidified without employing a liquid catholyte, have studied the effect of temperature of the input stream. In this context, Lee et al.[108] observed that the best $HCOO^-$ concentrations of 116 $g{\cdot}L^{-1}$ were obtained at cell temperatures of 323 K. Díaz-Sainz et al., with catalyst-coated membrane electrodes based on Sn[111] and on Bi,[138] also assessed the influence of the temperature of the input stream in a two-compartment flow reactor, observing that the best performances in terms of $HCOO^-$ production were obtained at room temperature (293 K), which in both studies could be attributed to achieving in these conditions the optimal thickness of the liquid layer that coats the catalyst layer.

Literature review has revealed that aqueous electrolytes operate at higher current densities and with lower total reactor voltages. However, the problems associated with low CO_2 solubility of aqueous electrolytes generate mass-transfer limitations.[108] Humidified CO_2 input streams at the cathode side of the electrochemical reactor improve the mass-transfer phenomena for the CO_2 electroreduction to HCOOH and $HCOO^-$. Nevertheless, operation with humidified CO_2 gaseous feed for continuous electroreduction to HCOOH/$HCOO^-$ has resulted in general higher reactor voltages, which prevents efficient operation at high current densities. The causes to explain these higher voltages observed may be complex, probably related to resistances or ohmic drops due to liquid products formed that can flood the electrode, but they are currently being studied in order to understand their origin, minimize them, and thus improve energy efficiency.

1.4. Electrocatalyst and Working Electrode Configuration. Excellent detailed reviews have been focused on cathode electrocatalysts for the electrochemical conversion of CO_2 to $HCOO^-$ or HCOOH (e.g., refs 28, 100−105). This subsection presents a brief analysis of the cathode catalysts that have been used in the continuous electrocatalytic reduction of CO_2 to HCOOH and $HCOO^-$ (Table 1), with special attention on the catalyst arrangement and cathode configuration.

https://doi.org/10.1021/acsenergylett.3c00489
ACS Energy Lett. 2023, 8, 1992−2024

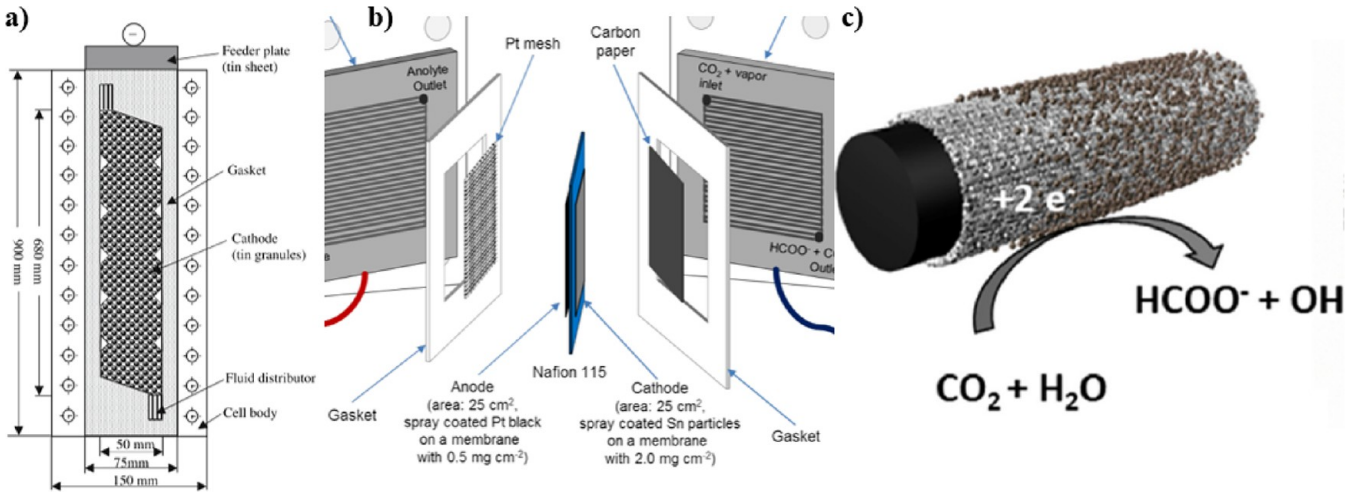

Figure 9. (a) Fixed-bed cathode of Li and Oloman (reproduced with permission from ref 114, copyright 2007 Springer Nature). (b) Catalyst-coated membrane electrode of Lee et al. (reproduced with permission from ref 108, copyright 2018 Wiley). (c) Graphite felt of Lou et al. (reproduced with permission from ref 181, copyright 2021 Elsevier).

The most common cathode materials used in the continuous electroreduction to CO_2 to $HCOOH/HCOO^-$ are Sn-[118,120,129] and Bi-based.[151−153] Nearly one-third of the reported works employ Sn-based catalysts. Within this group more than 30% employ tin oxide-based catalysts. Most of these studies used SnO_2 nanoparticles, while others researchers, such as Qian et al.[120] and Liu et al.,[135] have chosen to use SnO or Sn_3O_4, respectively. However, few studies have also used Pb-based[166−168] and In-based[171,185,186] electrocatalysts. Furthermore, boron-doped diamond[173,180] and nitrogen-doped[178] or boron and nitrogen co-doped carbon[177] materials encapsulating iron have also been used as cathode catalysts. Recent studies have explored the use of catalysts based on metallic alloys, particularly Sn alloys, such as Sn-Bi,[156] Sn-Cu,[163] and Sn-Pb.[164]

The electrocatalysts used are typically in the form of metal-based nanoparticles that increase the reaction-specific surface and improve the mass transfer of the compounds involved in CO_2 electroreduction. All the reported studies have used nanoparticles with a diameter <150 nm[109,110,115] that mainly average between 9 and 15 nm.[110,111,137] However, Wu et al.[143] conducted the CO_2 reduction reaction using Bi-based catalyst nanoparticles of 5 nm, and Merino-García et al.[130] employed SnO_2-based catalyst nanoparticles of 2 nm. Some studies have shown that the structure and size of the Bi-based catalyst nanoparticles have a great influence on the selectivity and behavior of electrochemical reduction.[242−244] Thus, it is important to highlight other physical configurations of catalyst nanomaterials, such as nanosheets,[159,182] which has demonstrated great performance in the reduction reaction. For instance, Fan et al. successfully and effectively employed ∼4.5 nm thick Bi-based nanosheets.[144]

Furthermore, porous support materials can effectively increase the reaction-specific surface (based on carbon materials). For example, carbon nanotubes employed as support for catalyst nanoparticles,[149,175,178] and other complex structures based on the metal−organic frames with different metallic catalysts, such as Bi[157,158] and In,[186] have demonstrated great performance. These structures achieved FEs of up to 90% for the target product at current densities >200 mA·cm^{-2}. Along with the material nature of the catalyst and its support, the physical configuration of the cathode employed for the CO_2 electroreduction to HCOOH and $HCOO^-$ also plays an important role.

Barely 5% of the 124 reported papers use foils/plates as physical working electrode configurations. First, Pb-[167,168] and Sn-based[106,107,132] metallic plates were reported as the simplest physical configurations of cathodes. However, the low specific reaction surfaces of metallic plates limited the mass transport of the compounds involved in reduction, limiting the current density supplied to the electrochemical reactor.[131] The highest current density in a continuous operation using a metallic plate of ∼100 mA·cm^{-2} was reported by Ramdin et al.[107] Lucas and Lima[172] used Sb-Sn alloy and showed a catalytic activity of 22 h, and the main figures of merit of the process were obtained in an acceptable range (FEs >96% and production rates of up to 0.28 mmol·m^{-2}·s^{-1}). As the surface area is a limiting issue in this type of configuration, numerous studies have been conducted on other cathode configurations.[114]

Figure 9a shows the configuration of the fixed-bed cathode implemented by Li and Oloman.[114] This configuration improved CO_2 transport, with CO_2 conversions of up to 75% per step. However, the Sn particles witnessed a loss of activity due to the accumulation of impurities on the surface of the catalyst and a loss of material due to corrosion.[114] Other innovative cathode configurations have also been proposed in the field of continuous CO_2 electroreduction to HCOOH and $HCOO^-$. For instance, the catalyst-coated membrane electrode (CCME) configuration deposits the catalyst over the ion-exchange membrane to increase the reaction-specific surface (Figure 9b). This approach solves the limitation of low CO_2 solubility in aqueous media that is associated with a humidified CO_2 input stream at the cathode side. Lee et al.[108] deposited Sn nanoparticles over a CEM (Nafion 115), and a carbon fibrous substrate was used as current collector that simultaneously corrected the distribution of the humidified CO_2 feed. Díaz-Sainz et al.[111,138] implemented CCMEs in two-compartment flow reactors. Sn[111] and Bi[138] carbon-supported nanoparticles were deposited over a CEM (Nafion 117) using a tinned steel mesh as a current collector. These studies showed the formation of liquid water on the catalyst surface of CCMEs during the experiments due to the accumulation of condensed water from the humidified CO_2 feeds. The thickness of the water layer was a critical factor and one of

https://doi.org/10.1021/acsenergylett.3c00489
ACS Energy Lett. 2023, 8, 1992−2024

the main mass-transfer resistances. Catalyst particles can be supported in different porous structures, such as graphite felts (Figure 9c).[181] This highly porous support improves transport by increasing the specific surface area and are available on a large scale at a low cost (Mersen, France).[181]

The most implemented cathode configuration in continuous CO_2 electroreduction to HCOOH and $HCOO^-$ has been the gas-diffusion electrode (GDE).[119,122,159] GDEs are composed of a catalytic layer and a gas-diffusion layer (GDL), which is a fibrous porous component that has two main functions: (i) to ensure uniform distribution of the reactant over the electrode surface, and (ii) to enhance the transport of electrons to or from the external electrical circuit.[245] Detailed reviews on GDEs for CO_2 reduction are available in literature.[73,76] In general, GDEs are composed of a carbon fibrous substrate, a microporous layer, which sometimes may not be present, and a catalytic layer (Figure 10). The different parts which conform

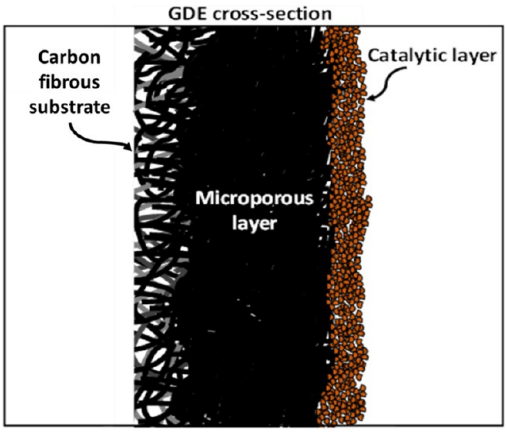

Figure 10. Schematic illustration of the cross-section of a gas diffusion electrode (GDE) with carbon support, an optional microporous layer, and a catalytic layer (adapted from ref 84, copyright 2022 Springer Nature).

to the GDEs are briefly discussed below. Compared to metallic plate electrodes, GDEs enhance the three-phase boundary area where the reduction reaction takes place,[131,246,247] decreasing the mass-transfer limitations and increasing the current density supply.[248,249]

Several studies have used Teflon-treated carbon fibrous substrates such as GDL.[110,137,139] This material is efficient in electron transport, is hydrophobic due to the polytetrafluoroethylene (PTFE) pretreatment, and permits the passage of CO_2 through the cathode.[250] The most commonly used carbon fibrous substrate consist PTFE-treated carbon paper of different total thicknesses (190, 255, 280, and 370 μm) from companies such as Toray Inc. of Japan or AvCarb (TGP-H-60, AvCarb P75t, TGP-H-90, and TGP-H-120).[109,110,137] A microporous layer is usually deposited over this carbon fibrous substrate (Figure 10) to improve CO_2 mass transport to the catalytic layer. For example, Díaz-Sainz et al. and Del Castillo et al. deposited a microporous layer consisting of a PTFE/carbon black mixture over the carbon fibrous substrate using an airbrush technique, with a corresponding load of 2 mg·cm^{-2}.[110,137,139]

Other studies used commercial GDLs as carbonaceous support from companies such as FuelCellStore, and they are composed jointly of the carbon fibrous substrate and a microporous layer. Different GDLs have been reported (mainly Sigracet 39BC, Sigracet 35BC, CeTech W1S1009, and CeTech W1S1010[117,118,143,171]). Qian et al.[120] used a PTFE-treated carbon fibrous substrate (TGP-H-60) equipped with mesoporous layers with a larger pore size (2−50 nm).

Although most of the approaches using GDEs compiled in Table 1 have employed carbon fibrous supports, other kind of substrates have also been reported, like carbon cloths,[128,129,171] PTFE gas-diffusion substrates,[188] copper hollow fiber supports,[209] metal copper meshes,[119,125] or metal copper foams.[189] In particular, tests with cloth substrates required PTFE treatment to prevent cathode flooding,[128,129,171] as well as a larger volume of electrolyte to dilute $HCOO^-$ and limit crossover.[171] GDEs prepared with Sn and Bi by using thermal evaporation on highly hydrophobic PTFE GDLs[188] were able to perform the continuous CO_2 electrocatalytic reduction to $HCOO^-$ with notable stability performances of up to 100 h, although at a current density of only 60 mA·cm^{-2}. On the one hand, the use of Cu hollow fiber as the substrate allowed Rabiee et al.[209] to prepare hollow fiber GDEs with free ionomer Bi-based catalysts. GDEs fabricated with other Cu-based substrates, such as meshes[119,125] or foams,[189] have also been reported due to their good properties of ductility, electrical conductivity, and low cost.

The catalytic layer (Figure 10) consists mainly of a mix of catalyst particles and an ionomer. The ionomer/binder holds the catalytic layer together and to the GDL. Binders/ionomers manipulate the hydrophobic−hydrophilic balance along with the ion transport in the three-phase boundary layer.[89,251] Perfluorinated sulfonic acid (PFSA) ionomers such as Nafion contain $-SO_3^-$ (hydrophilic) and $-CF_2$ (hydrophobic) groups.[251,252] However, a compromise is required, since excessive hydrophobicity will result in inferior electronic conduction because of a large amount of non-conducting hydrophobe, while not enough hydrophobicity will restrict the diffusion of CO_2 gas due to the tendency of flooding and accelerating the undesired HER.[83] Nafion solution (5 wt%) is the most implemented ionomer in the currently reviewed literature for the electrocatalytic reduction of CO_2 to HCOOH and $HCOO^-$.[115,141,145] In contrast, Sen et al.[116] employed the Nafion ionomer with a different mass ratio (LIQUion 1100 EW, Ion Power Inc., 15% w/w). However, certain studies report different anionic ionomer solutions, such as XA-9 (Dioxide Materials Inc., 5 wt%) or ionic liquid-based ionomers, such as imidazole (5 wt%).[109,146]

However, the catalytic layer of GDEs often compromises the catalytic activity and stability; hence, some strategies have been proposed to improve the essential requirements for the implementation of this technology on a larger scale. For example, Sen et al.[116] used a hydrophobized fibrous backing layer since it can act as a mechanical support for the Sn nanoparticles and correct the distribution of the gas flow through the catalytic layer. Xing et al.[145] studied a two-compartment reactor that operates with an aqueous feed (KOH 1.0 M) from the cathode side. PTFE was added to the ink that makes up the Bi-based catalytic layer. Specifically, the strong dependence of the CO_2 reduction reaction activity on the gas flow rate for the Bi/C/30% PTFE electrode suggests that the CO_2 mass transport inside the catalyst layer is partially mediated by gas-phase diffusion via the hydrophobic pores near PTFE, which enhances the CO_2 transport and CO_2 reduction reaction performance relative to the Bi/C electrode.[145]

https://doi.org/10.1021/acsenergylett.3c00489
ACS Energy Lett. 2023, 8, 1992−2024

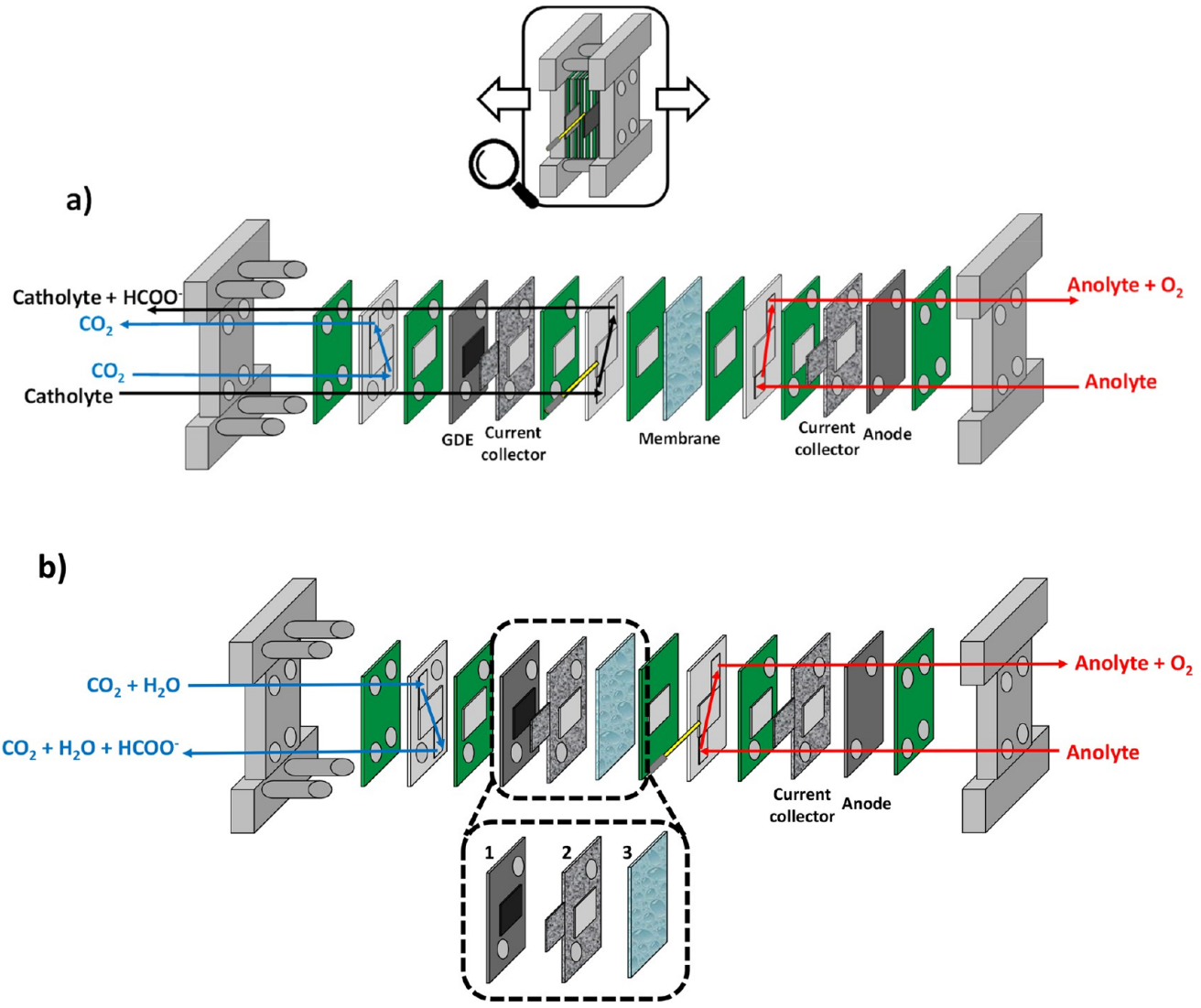

Figure 11. Schematic illustrations of examples of the implementation of a GDE in (a) a two-compartment reactor with an aqueous feed in cathode side and (b) a two-compartment reactor used for the study of the continuous electrocatalytic reduction of CO_2 to obtain $HCOO^-$ with a single pass of the inputs through the electrochemical reactor (1: gas diffusion electrode, 2: current collector, and 3: Nafion 117 membrane). (Adapted from ref 137, copyright 2019 Elsevier, and ref 139, copyright 2021 Elsevier.)

GDE disposition inside the electrochemical reactor plays an important role in the CO_2 electroreduction to HCOOH and $HCOO^-$, depending mainly on the type of the feed at the cathode side. Figure 11a shows a schematic view of the operation of a two-compartment reactor where the working electrode (GDE) is used with a liquid electrolyte feed at the cathode side. The product generated on the cathode surface was collected and analyzed with the aqueous electrolyte of the cathode side. A membrane electrode assembly (MEA) configuration (also called free-catholyte zero-gap reactor configuration), in which a humidified stream of CO_2 is used as an input at the cathode side, has also been studied and extracts higher $HCOO^-$ and HCOOH concentrations.[108,118,139,186] Figure 11b shows a schematic view of the MEA inside a two-compartment reactor. Li et al. employed a GDE in an MEA, achieving catalytic activity for 100 h with high $HCOO^-$ concentrations. Nevertheless, most works with a MEA at the cathode in a two-compartment flow reactor do not reach operation at commercially relevant current densities of 200 $mA{\cdot}cm^{-2}$.[253]

1.5. Counter Electrode Configuration and Anode Catalyst Implemented. In this section, the main electrocatalysts employed to carry out the anodic reaction and its configuration are discussed in detail. Oxygen evolution reaction (OER) is the most widely implemented reaction in the anodic compartment of the different reactor configurations for continuous CO_2 electroreduction to $HCOO^-$ and HCOOH. Numerous studies carried out the OER through the oxidation of aqueous solutions, such as KOH, $KHCO_3$ K_2SO_4, H_2SO_4, and deionized water, to obtain electrons, which were conducted through the external circuit to the working electrode of the reactor (Table 1). In contrast, only two studies have been reported in this review that use gaseous feeding in the anode compartment.[136,142] They carried out the hydrogen oxidation reaction (HOR) through the employment of Pt carbon-supported nanoparticle GDE in a three-compartment reactor. For different operating conditions (Table 1), Yang et al.[109] also employed a Pt carbon-supported nanoparticle electrode to carry out the HOR in the anode side of a three-compartment reactor with the consequent reduction of the cell

https://doi.org/10.1021/acsenergylett.3c00489
ACS Energy Lett. 2023, 8, 1992−2024

voltages (1.83 V), which registered low EC of 119 kWh·kmol^{-1}. Proton generation in the HOR promotes the formation of HCOOH in the central compartment of the reactor. Even though HOR in the anode compartment can reduce the reactor voltage, the high cost of H_2 feed can significantly increase the operational cost of the process.[146]

Pt-based anodes with different physical configurations (Pt-wire, Pt-sheet, Pt-mesh, and Pt-gauze) have been the most used in the continuous electrochemical reduction of CO_2 to HCOOH and $HCOO^-$ (Table 1).[121,140,173] He et al.[155] supplied the highest current density (500 mA·cm^{-2}) employing Pt-based anodes (Table 1). However, despite the high electron conductivity of Pt, its availability and cost are still limiting factors for its implementation on a larger scale.[254]

Dimensional stable anodes (DSAs) have also been widely implemented to carry out the OER (Table 1).[106,124,168] Different DSAs are available based on different catalysts and physical configurations. The commercial electrodes are typically metallic plates covered with materials based on IrO_2-Ta_2O_5 alloys. These electrodes are widely used in other electrochemical processes, such as electrooxidation of organic compounds, and have good performance in OER.[255,256] Currently, operations at current densities of ∼300 mA·cm^{-2} have been reported using DSA/O_2. However, Merino-García et al.[130] showed that DSA/O_2 can operate even at higher current densities of 500 mA·cm^{-2}, maintaining catalytic activity for 90−120 min. Moreover, Díaz-Sainz et al.[161] achieved remarkable figures of merit using a DSA/O_2 operating at current densities of up to 600 mA·cm^{-2}. Some studies have also used Pt catalyst-based DSAs.[168] Studies that operate with two interconnected DSAs are also available.[170,181] Thus, the geometric areas of the anode for a given reactor design can be doubled, thereby increasing the production of electrons. Park and Shin[170] used two interconnected DSA mesh anodes for long a period of time (180 h). Meanwhile, Lou et al.[181] operated with two interconnected DSAs (AC-2004, ECS International Electro Chemical Services, France). DSAs are generally very stable electrodes, but have a low specific surface area that limits the mass transfer of the anodic reaction.

Several recent studies have used particulate electrodes as anodes, which have higher active surface area with respect to that of the DSA plates.[149,166,183] These particulate electrodes are mainly based on IrO_2, Pt, and Ru materials. For example, Pt carbon-supported nanoparticles operates at current densities of up to 385 mA·cm^{-2}, achieving promising product rates of 14.90 mmol·m^{-2}·s^{-1}.[116] However, this anode configuration can be degraded under alkaline conditions due to binder/anolyte interaction, thus decreasing the activity and stability of the anode. Therefore, the choice of binder and its proportion in the catalytic ink is a critical factor in the proper development of an anodic reaction.[229]

The maximum current densities reported for Pt-based anodes, DSAs, and particulate anodes do not exceed 500 mA·cm^{-2}. However, Ni foams work at higher current densities (e.g., refs 117, 118, 186) due to their intrinsic porosity, which increasing mass transport of the species involved in the OER (Column 5, Table 1).[257] Different catalytic materials have been employed for Ni foam anodes. For example, Xing et al. used a nickel−iron foam as the counter electrode.[145] Moreover, other studies have used Ni foams in MEA configuration,[117,118,186] highlighting two-compartment reactors with humidified CO_2 feed in the cathode side operating at relatively high current densities of 100 and 258 mA·cm^{-2}, respectively.[118,186]

Ding et al.[152] employed an Al foil as a counter electrode for simultaneous CO_2 valorization and power generation. This electrode in alkaline conditions (KOH 1.0 M) oxidizes the Al to $Al(OH)_4^-$ and generates electrical energy. For a FE up to 100%, 1 g of Al can ideally convert 1.24 L of CO_2 to 2.45 g of HCOOH, releasing 5 kWh of electrical energy.

Few studies in continuous mode have carried out an oxidation reaction of interest at the anode. These studies took advantage of the oxidation potential of the anode instead of carrying out the OER, which had lower added value, e.g., oxidation of a methyl orange dye.[125,141] Wang et al.[141] oxidized methyl orange using a SnO_2−Sb electrode supported on Ti, obtaining 100% decolorization efficiencies. Similarly, Wang et al.[125] oxidized methyl orange with a Co_3O_4-coated graphite electrode. Furthermore, Wu et al.[143] co-produced $HCOO^-$ in a two-compartment reactor. In the cathode compartment, CO_2 was reduced to $HCOO^-$ and in the anode compartment, methanol (CH_3OH) was oxidized to $HCOO^-$. $HCOO^-$ was produced from CH_3OH in the anode compartment under alkaline conditions (KOH 1.0 M) using an $Ni(OH)_2$ foam anode. The $HCOO^-$ produced at the cathode diffused from the cathodic to the anodic compartments through an AEM, the product being concentrated in the anolyte outlet stream. Consequently, all figures of merit of the process were enhanced.[143] This shows that instead of OER, different oxidation reactions of interest can improve some process figures of merit and produce another valued-added product in the anodic compartment.

2. ASSESSMENT OF THE MAIN FIGURES OF MERIT

This section presents a quantitative comparison of the results obtained by the studies of continuous CO_2 electroreduction to HCOOH or $HCOO^-$, considering the most commonly used figures of merit, such as current density, concentration of the target product, FE, production rate, and EC. Table 1 reports the figures of merit corresponding to the conditions in which the highest product concentrations were obtained in each study. Certain studies did not explicitly include all the figures of merit; such figures of merit were calculated from the reported results (represented with an asterisk (*) in Table 1). Studies that report cumulative $HCOO^-$/HCOOH concentrations (marked with two asterisks (**) in Table 1) have not been shown in the different representations of the figures of merit for a fair comparison. Therefore, all the studies of this comparative evaluation involved continuous single-pass reactors. Some studies have reported figures of merit for different reactor configurations and different cathode electrocatalysts.[114,116] All the figures of merit addressed in Table 1 are shown for these studies. The meaning of the figures of merit is briefly explained below.

First, the FE for $HCOO^-$ or HCOOH is defined as the percentage of the total charge supplied, which is used to obtain the desired product.[258] FE can be obtained by eq 5:

$$\mathrm{FE}\ (\%) = \frac{zFn}{I} \times 100 \tag{5}$$

where z is the number of electrons exchanged in the electrochemical process (for $HCOO^-$ and HCOOH z = 2), F is the Faraday constant (96485 C·mol^{-1}), n is the number of moles of $HCOO^-$ or HCOOH produced per unit of time (expressed in mol·s^{-1}), and I is the current supplied to the electrochemical reactor (A).

https://doi.org/10.1021/acsenergylett.3c00489
ACS Energy Lett. 2023, 8, 1992−2024

Table 2. Symbology, Abbreviations, and Meanings of the Icons in the Graphical Representation of the Figures of Merit[a]

Symbol	Abbreviation	Meaning
△	G-2-Bi-CEM	Gaseous feed two-compartment reactors with Bi-based cathode catalysts and cation exchange membranes.
○	G-2-Sn-CEM	Gaseous feed two-compartment reactors with Sn-based cathode catalysts and cation exchange membranes.
◇	G-2-X-CEM	Gaseous feed two-compartment reactors with X-based cathode catalysts and cation exchange membranes.
▲	G-2-Bi-AEM	Gaseous feed two-compartment reactors with Bi-based cathode catalysts and anion exchange membranes.
◆	G-2-X-AEM	Gaseous feed two-compartment reactors with X-based cathode catalysts and anion exchange membranes.
▲	G-3-Bi	Gaseous feed three-compartment reactors with Bi-based cathode catalysts.
●	G-3-Sn	Gaseous feed three-compartment reactors with Sn-based cathode catalysts.
◆	G-3-X	Gaseous feed three-compartment reactors with X-based cathode catalysts.
●	L-1-Sn	Aqueous feed undivided reactors with Sn-based cathode catalysts.
◆	L-1-X	Aqueous feed undivided reactors with X-based cathode catalysts.
△	L-2-Bi-CEM	Aqueous feed two-compartment reactors with Bi-based cathode catalysts and cation exchange membranes.
○	L-2-Sn-CEM	Aqueous feed two-compartment reactors with Sn-based cathode catalysts and cation exchange membranes.
◇	L-2-X-CEM	Aqueous feed two-compartment reactors with X-based cathode catalysts and cation exchange membranes.
▲	L-2-Bi-AEM	Aqueous feed two-compartment reactors with Bi-based cathode catalysts and anion exchange membranes.
●	L-2-Sn-AEM	Aqueous feed two-compartment reactors with Sn-based cathode catalysts and anion exchange membranes.
◆	L-2-X-AEM	Aqueous feed two-compartment reactors with X-based cathode catalysts and anion exchange membranes.
▲	L-2-Bi-BPM	Aqueous feed two-compartment reactors with Bi-based cathode catalysts and bipolar membranes.
●	L-2-Sn-BPM	Aqueous feed two-compartment reactors with Sn-based cathode catalysts and bipolar membranes.
◆	L-2-X-BPM	Aqueous feed two-compartment reactors with X-based cathode catalysts and bipolar membranes.

G – Gaseous cathode feed ; **L** – Aqueous cathode feed
1 – Undivided reactor ; **2** – Two-compartment reactor ; **3**-Three-compartment reactor
Bi – Bi-based catalyst ; **Sn** – Sn-based catalyst ;
X – Pb-based catalyst, In-based catalyst, bimetallic alloy, mixture of metal catalysts, BDD, and nitrogen-doped catalyst;
CEM – Cation exchange membrane ; **AEM** – Anion exchange membrane, and
BPM - Bipolar membranes

[a]The external line represents the reactor configuration: icons with the dashed black external line are undivided reactors; two-compartment reactors are represented by icons with continuous blue and red external lines; symbols with continuous black external lines indicate three-compartment reactors. Blue icons represent the figures of merit for continuous reactors with humidified CO_2 feeds at the cathode side. Red icons show the figures of merit of reactors with aqueous feeds on the cathode side. The nature of the cathode catalysts has been considered with different symbol forms: the triangles represent Bi-based catalysts, circles represent Sn-based electrocatalysts, and other metallic catalysts, such as In, Pb, alloys, boron-doped diamond, and nitrogen-doped carbon materials, are represented by a diamond icon. The nature of the membrane of two-compartment reactors is represented with unfilled symbols for CEMs, blue and red filled icons for AEMs, and gray filled icons for BPMs.

The $HCOO^-$ or HCOOH production rate (r) represents their total amount produced per unit area of working electrode and unit of time. This figure of merit is defined by eq 6:

$$r\ (\mathrm{mmol{\cdot}m^{-2}{\cdot}s^{-1}}) = \frac{n_m}{A} \tag{6}$$

where n_m is the number of moles of $HCOO^-$ or HCOOH produced per unit of time (expressed in $\mathrm{mmol{\cdot}s^{-1}}$) and A is the geometric area of the cathode (m^2).

The EC per kmol of $HCOO^-$ or HCOOH is expressed as the amount of energy used in the electrochemical reactor to a produce certain amount of $HCOO^-$ or HCOOH. The EC can be calculated by eq 7:

$$\mathrm{EC}\ (\mathrm{kWh{\cdot}kmol^{-1}}) = \frac{IU}{n_{kh}} \tag{7}$$

where I is the current supplied to the electrochemical reactor (kA), U is the voltage of the electrochemical reactor (V), and n_{kh} is also the number of moles of $HCOO^-$ or HCOOH produced per unit of time (expressed in $\mathrm{kmol{\cdot}h^{-1}}$).

The quantitative comparison is supported by graphic representations of the combinations of the figures of merit to ease the analysis and considers reactor configuration, type of feed at the cathode side, electrocatalysts used in the cathode, and the type of membrane. The figures of merit analyzed have been represented in the graphs with different icons according to the symbols and meanings explained in Table 2.

2.1. Assessment of Concentration of the Target Product. Figure 12 shows the product concentration of the different reported studies as a function of the current density. Due to the variation in the reported product concentration

https://doi.org/10.1021/acsenergylett.3c00489
ACS Energy Lett. 2023, 8, 1992−2024

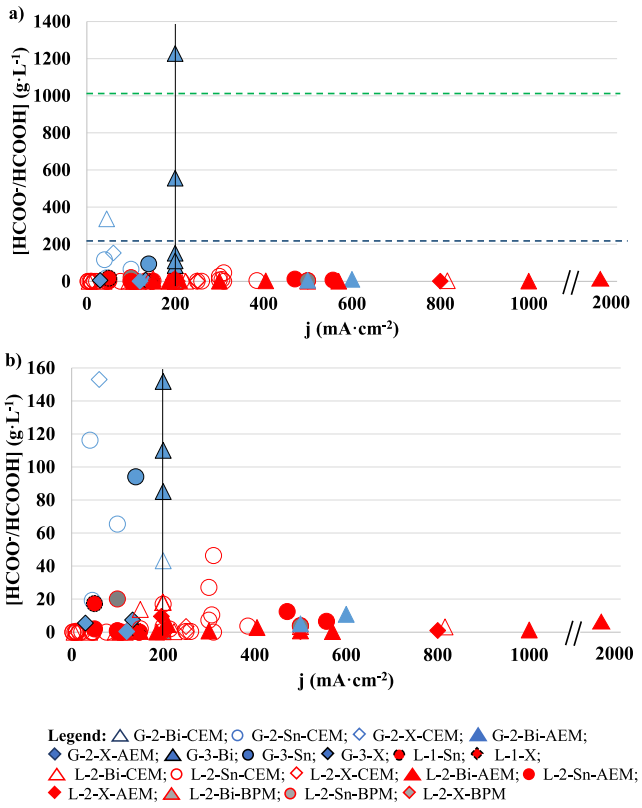

Figure 12. $HCOO^-$/HCOOH concentration versus current density (j): (a) displays in a higher Y-axis scale (0−1400 g·L^{-1}) for the highest product concentrations reported by reactors with gaseous feeds; (b) presents a lower Y-axis scale (0−160 g·L^{-1}) showing mainly $HCOO^-$/HCOOH concentrations of reactors with aqueous feeds. The abbreviations and symbols are detailed in Table 2. The horizontal green dashed line is set as the most common commercial product concentration value (1020 g·L^{-1}) and the horizontal dashed blue line represents the target product concentration (218 g·L^{-1}) for environmentally sustainable processes. The vertical black line is the threshold from which the current densities applied are commercially relevant (200 mA·cm^{-2}).

values, this figure has been divided in two graphs at different scales: Figures 12a and 12b.

Although $HCOO^-$ and HCOOH concentrations above 85 wt% (1020 g·L^{-1}) are desired for commercial use (depicted as green dashed line in Figure 12a), it has been found that product concentrations close to 21 wt% (218 g·L^{-1}, blue dashed line of Figure 12a) can reduce the energy costs associated with the downstream purification steps, thus making continuous electrochemical $HCOO^-$ and HCOOH processes environmentally sustainable.[39] Moreover, current densities >200 mA·cm^{-2} have been suggested as commercially relevant to minimize the capital-expenditure of the conversion unit to economically compelling levels.[75] Considering these thresholds, Figure 12a shows that there are no studies located in the top right area; i.e., there are no approaches yet that combine achieving concentrations above the most common commercial value of 85%, with operating current density >200 mA·cm^{-2}. The highest concentrations of $HCOO^-$ or HCOOH reported in continuous studies used a CO_2 humidified input stream at the cathode compartment of the electrochemical reactor and Bi-based electrocatalysts, although they were obtained at a maximum current density of ∼200 mA·cm^{-2} (Figure 12a). Fan et al.[142] achieved the highest product concentration (up to 1228.00 g·L^{-1}, becoming the only approach that exceeds the most common commercial HCOOH concentrations) by using a three-compartment reactor with Bi-GDE at current density of 200 mA·cm^{-2}. Xia et al.[136] also obtained remarkable results in terms of the concentration (556.00 g·L^{-1}) employing a three-compartment reactor with Bi-based cathode at current densities of 200 mA·cm^{-2}. As shown in Figure 12a, the third study that reports concentrations above the threshold of 218 g·L^{-1} suggested for the process to be environmentally sustainable[39] is that by Díaz-Sainz et al.,[139] which achieved $HCOO^-$ concentrations of 337.00 g·L^{-1} at current densities of 45 mA·cm^{-2} with a CEM-separated two-compartment reactor also using Bi-GDE.

Figure 12a also shows that some approaches with gaseous-fed electrochemical reactors (blue filled symbols) obtain product concentrations close to 21 wt% at current densities ≤200 mA·cm^{-2}. In contrast, the approaches that use liquid feed can operate at even higher current densities (up to almost 2 A·cm^{-2}, Figure 12), due to the higher ionic conductivity of the aqueous electrolyte. However, Figure 12b also clearly reveals that the product concentrations in approaches using liquid catholyte (red color) are lower (<50.00 g·L^{-1}, reaching even <5.00 g·L^{-1}) compared to those with gaseous feed (blue color). In this sense, aqueous-fed CEM-separated two-compartment electrochemical reactors with Sn-based cathode catalysts report product concentrations close to 50 g·L^{-1} at current densities >200 mA·cm^{-2} (representing one-third of the studies in this analysis). For instance, Li and Oloman[114] reported the highest product concentrations of 46.35 g·L^{-1} at current densities of 310 mA·cm^{-2} for reactors with aqueous feed (white circle with a red outline, Figure 12b). Recently, Merino-García et al.[130] obtained $HCOO^-$ concentrations of 27.00 g·L^{-1} employing a two-compartment reactor at current densities of 300 mA·cm^{-2}. This study implemented SnO_2 nanoparticles with an average size of 2 nm as electrocatalysts in the cathode. It has also been noted that two-compartment cells with Bi-based cathode catalysts allow supplying current densities up to almost 2 A·cm^{-2} and obtaining product concentrations <11 g·L^{-1}.[144,145]

Finally, it should be noted that more than 60% of the studies located in the lower left part of Figure 12b ($HCOO^-$/HCOOH concentrations <50 g·L^{-1} and current densities <200 mA·cm^{-2}) employ aqueous-fed two-compartment reactors with CEMs.

2.2. Analysis of the Faradaic Efficiency (FE) for the Target Product. Figure 13 represents the FE values as a function of current densities. To facilitate analysis, Figure 13 can be divided into sections considering as representative thresholds FE for $HCOO^-$ or HCOOH of 90% and current density of 200 mA·cm^{-2}. FE for $HCOO^-$ or HCOOH above 90% lowers the separation needs and reduces the total current required for a target production rate.[58,259] Furthermore, these high FEs may be combined with commercially relevant current densities above 200 mA·cm^{-2}.[75,76] In general, Figure 13 shows that reactors with aqueous feeds obtain high FEs for $HCOO^-$ or HCOOH at higher current densities than those by gaseous feed reactors.

Looking at the top right area of Figure 13, it can be seen that studies with FEs >90% and current densities >200 mA·cm^{-2} have mainly employed aqueous-fed two-compartment reactors (representing 90% of the studies located in that section). Specifically, these configurations used AEMs and Bi- and In-

https://doi.org/10.1021/acsenergylett.3c00489
ACS Energy Lett. 2023, 8, 1992−2024

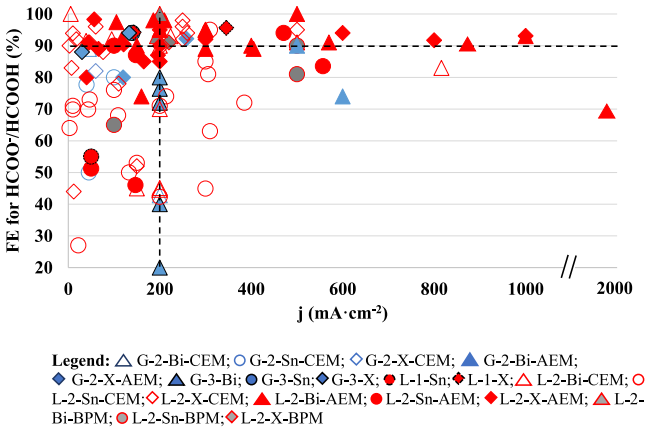

Figure 13. Faradaic efficiency (FE) for $HCOO^-$ or HCOOH versus current density (j). The abbreviations and symbols are detailed in Table 2. The horizontal black dashed line shows the value of FE of 90% established. The vertical black dashed line is the threshold from which the current densities applied are commercially relevant (200 mA·cm^{-2}).

based electrocatalysts, achieving FEs of 93% at current densities of up to 1 A·cm^{-2}.[144,171]

The upper left section of Figure 13 is dominated by aqueous-fed electrochemical reactors, achieving FEs >90% for $HCOO^-$ or HCOOH, but at current densities ≤200 mA·cm^{-2}. Some studies have shown high FEs (∼100%) with aqueous feeds at the cathode side. Cao et al.[158] used Bi-based electrocatalysts to obtain FEs ∼100% at current densities of up to 200 mA·cm^{-2} using a two-compartment reactor separated by a BPM. Only a few approaches using humidified CO_2 streams at the cathode can be found in this upper left section of Figure 13. Specifically, three-compartment reactors achieve FEs (up to 94%) at higher current densities (<140 mA·cm^{-2}) than those achieved by two-compartment electrochemical cells (<100 mA·cm^{-2}). For instance, Yang et al.[109] obtained FEs of 94% at current densities of 140 mA·cm^{-2} using a three-compartment reactor with Sn-based catalysts.

Only a few approaches, mainly using aqueous-fed two-compartment reactors with CEM and Sn-based cathode catalysts, are located in the lower right section of Figure 13; i.e., they operate at high current densities >200 mA·cm^{-2} but achieve FEs <90%. In this sense, Sen et al.[116] obtained FEs of 72% at current densities of 385 mA·cm^{-2}. Li and Oloman[114] attained FEs of 63% at current densities of 310 mA·cm^{-2}. However, Díaz-Sainz et al.[161] reached FEs of 74% at higher current densities of 600 mA·cm^{-2} by using a gaseous-fed two-compartment reactor with AEM (Sustainion 37-50) and Bi-based cathode catalysts, and Zelocualtecalt et al.[210] obtained FEs of 69% at current densities up to 1936 mA·cm^{-2}.

Finally, the lower left section of Figure 13 shows the studies with FEs <90% at current densities ≤200 mA·cm^{-2}. The majority of the works described in this section employ aqueous-fed two-compartment reactors. Moreover, Sn-based cathode catalysts obtain a wide range of FEs values (27−76%) at current densities <150 mA·cm^{-2}. On the other hand, studies that use Bi-based cathode catalysts achieve increasing current densities above 160 mA·cm^{-2}. Nevertheless, Bi-based catalysts are mostly employed by three-compartment reactors with humidified CO_2 streams at the cathode side. The studies with the highest product concentrations (<1228.00 g·L^{-1}) reported low FEs (<40%) at current densities of 200 mA·cm^{-2} (blue triangle with a black outline).[136,142] However, these studies also reported better FEs for HCOOH for different operating conditions. For instance, by increasing the humidified N_2 flow rate in the central compartment with a flow rate of 100 mL·min^{-1}, FEs of 80% were achieved at current densities of 200 mA·cm^{-2} at the expenses of reducing product concentration to 85.10 g·L^{-1}.[136] Similar result was observed by Fan et al.,[142] in which by raising the humidified N_2 flow rate in the central compartment from 20 to 100 mL·min^{-1}, product concentrations of 110.40 g·L^{-1} were obtained with FEs of 72% at current densities of 200 mA·cm^{-2}.

2.3. Analysis of the Production Rate. Production rates have been obtained for operating conditions with highest product concentrations. Figure 14 shows the influence of the

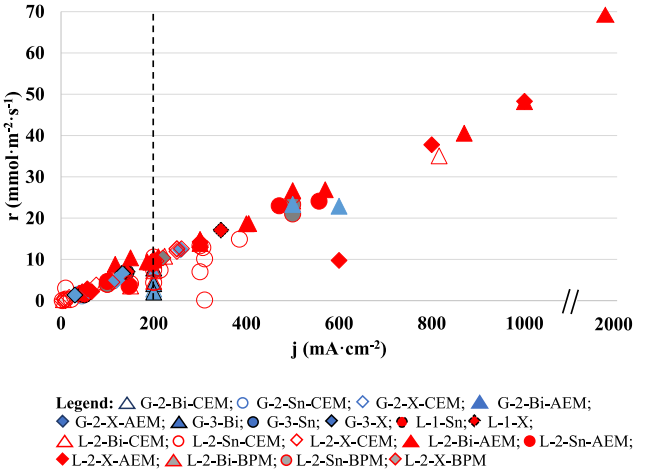

Figure 14. Production rate (r) versus total current density (j). The abbreviations and symbols are detailed in Table 2. The vertical black dashed line is the threshold from which the current densities applied are commercially relevant (200 mA·cm^{-2}).

production rate as a function of current density. The production rate generally follows an expected almost linear increasing trend with increasing current density (Figure 14).

In Figure 14, only 35% of the studies are located beyond the threshold (black dashed line of Figure 14) of commercially relevant current densities,[75] operating at current densities >200 mA·cm^{-2}. All these studies have employed two-compartment reactors with aqueous feed at the cathode, with the exception of Lu et al.[166] (undivided reactor), Wang et al.,[186] and Díaz-Sainz et al.[161] (both using a gaseous fed reactor). Aqueous-fed two-compartment reactors separated by AEM have reported the best results in terms of production rates. Zelocualtecalt et al.[210] reached production rates of 69.88 mmol·m^{-2}·s^{-1} at the highest current densities of up to almost 2 A·cm^{-2} by using aqueous-fed two compartment flow reactor equipped with AEM. Similarly, Fan et al. and Grigioni et al. also used high current densities of 1 A·cm^{-2} and obtained relevant production rates of up to 48.00 mmol·m^{-2}·s^{-1}.[144,171] The use of alkaline aqueous feed in both compartments improved the electrochemical performance of the AEM in these studies. Xing et al.[145] decreased the current densities and used a CEM (Nafion 1110) that operated with alkaline aqueous feed in both compartments. This configuration operated at current densities of 816 mA·cm^{-2} and obtained production rates of 35.08 mmol·m^{-2}·s^{-1}.

https://doi.org/10.1021/acsenergylett.3c00489
ACS Energy Lett. 2023, 8, 1992−2024

Notably, while the reactors with CO_2 humidified input stream achieved the highest product concentrations (Section 2.1), this configuration could not obtain production rates higher than 22.9 mmol·m^{-2}·s^{-1}. This could be attributed to the fact that these studies did not operate at current densities higher than 600 mA·cm^{-2}, mainly due to the low ionic conductivity of gaseous media compared to the aqueous one.[161] In this context, Díaz-Sainz et al.[161] achieved the highest production rates of 22.90 mmol·m^{-2}·s^{-1} at current densities of 600 mA·cm^{-2} with a two-compartment cell with AEM (Sustainion 37-50). Wang et al.[186] obtained production rates of 12.33 mmol·m^{-2}·s^{-1} at current densities of 258 mA·cm^{-2} by using the same reactor configuration as Díaz-Sainz et al.[161] and AEM (Sustainion 37-50).

From the nature of the employed cathode electrocatalysts, it can be concluded that Bi- and Sn-based catalysts achieve the best performances in terms of production rates, with the exception of Grigioni et al.,[171] who used In-based catalysts, and Lu et al.,[166] who used Pb-based catalysts. Bi- and Sn-based catalysts have been widely studied under broad ranges of current densities in the development of continuous CO_2 electrochemical reduction to $HCOO^-$ or HCOOH, which has resulted in a wide range of production rates.

2.4. Analysis of the Energy Consumption (EC) per kmol of Product. Figure 15 depicts the analysis of the performance in terms of a combination of EC per kmol of $HCOO^-$/HCOOH and FE for these products. Several studies have not reported the EC per kmol of $HCOO^-$ or HCOOH; hence, the amount of data for analysis in this section is lower than in previous ones. Less than 15% of the studies have explicitly reported EC and, another 23% have reported enough information to allow estimating the EC.

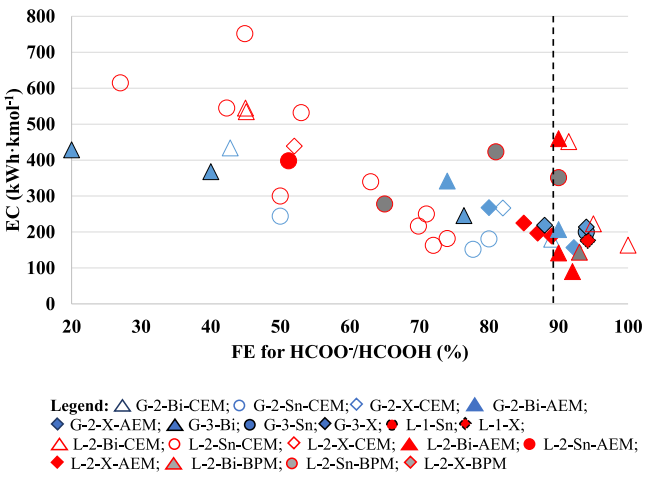

Figure 15. Energy consumption (EC per kmol of $HCOO^-$ or HCOOH) versus Faradaic efficiency (FE for $HCOO^-$ or HCOOH). The abbreviations and symbols are detailed in Table 2. The vertical black dashed line is the value of FE of 90%.

The most favorable scenario would be as close as possible to the lower right corner in Figure 15 (i.e., highest FE combined with lowest EC). Only a few approaches can be found in this lower right area of Figure 15 and they are mainly based on aqueous-fed two-compartment electrochemical reactors. Specifically, the approaches that use this reactor setup with Bi-based cathode catalysts achieve low ECs (<164 kWh·kmol^{-1}) at high FEs toward the target product (>92%). In this context, Wu et al.[143] achieved the lowest EC (90 kWh·kmol^{-1}) at 92% FE among the studies analyzed in this review, employing an AEM-separated two-compartment reactor with Bi-based catalyst at the cathode. The co-production of $HCOO^-$ in both electrodes and the implementation of an AEM were responsible for such low EC.

Other approaches with humidified CO_2 streams at the cathode have also reported ECs <200 kWh·kmol^{-1} at FEs >90%. Wang et al.[186] used an AEM-separated two-compartment reactor with In-based cathode catalysts to obtain a low EC of 157 kWh·kmol^{-1} at 92% FE. Employing CEM-separated two-compartment reactor with Bi-based cathode catalysts, Díaz-Sainz et al.[139] obtained a low EC of 180 kWh·kmol^{-1} at high FE of almost 90%. On the other side, the three-compartment reactor with Sn-based catalysts implemented by Yang et al.[109] slightly increased the EC to 200 kWh·kmol^{-1} at 94% FE.

Two studies with CEM-separated two-compartment reactors with Sn-based cathode catalysts have reported ECs 200 kWh·kmol^{-1} with FEs <90%, which are located in the lower left section of Figure 15. On the one hand, Lee et al.[108] achieved an EC of only 152 kWh·kmol^{-1} at FEs of 78% for the product, operating with an humidified CO_2 stream at the cathode side. On the other hand, Sen et al.[116] obtained ECs of 163 and 182 kWh·kmol^{-1} at FEs of 74 and 72%, respectively, by using different Sn-based cathode catalysts in an aqueous-fed electrochemical cell.

Represented in the upper right part of Figure 15 (very good FEs >90% and EC >200 kWh·kmol^{-1}), gaseous-fed reactors with metal alloys and Bi-based cathode catalysts obtain lower ECs with FE values similar to those obtained in other approaches with aqueous-fed two-compartment electrochemical cells. Specifically, Zheng et al.[191] employed a three-compartment reactor with cathode catalysts of Cu and Pb alloys, achieving an EC of 214 kWh·kmol^{-1} at 94% FE. Jiang and co-workers[222] obtained an interesting EC of 207 kWh·kmol^{-1} at a FE of 90% with a MEA-flow reactor.

Finally, looking at Figure 15, it is important to note that most of the studies that report EC are situated in the upper left section; i.e., they have high EC with low FE. Nearly half of the papers with EC >200 kWh·kmol^{-1} and FEs <90% have been reported by aqueous-fed CEM-separated two-compartment reactors with Sn-based catalysts (white circle with red outline of the top left area in Figure 15). For instance, Merino-Garcia et al.[130] reported high EC of 752 kWh·kmol^{-1} at FEs of 45% for $HCOO^-$, and high current density of 300 mA cm^{-2} up to 10 h. This high EC was also partly attributed to electrical losses converted in heat due to Joule effect observed in the reactor during the electroreduction.

2.5. Long-Term Operation Performance. Long-term stability will play a key role for the future practical implementation of CO_2 electroreduction processes. To assess the stability of continuous approaches for the electrochemical reduction of CO_2 to $HCOO^-$ or HCOOH, long-term studies, with operating times in the order of hundreds or thousands of hours, are needed. However, barely a third of the 124 studies analyzed in this work have carried out some type of experiments with times of operation higher than 10 h, and only nine of them have operating times higher than 100 h.[109,136,142,146,165,170,188,191,199] The number of studies that have included some tests at times in order of thousands of hours is reduced to just two.[146,188]

https://doi.org/10.1021/acsenergylett.3c00489
ACS Energy Lett. 2023, 8, 1992−2024

A few studies that operate for 100 h or more, achieving excellent figures of merit, should be highlighted. For example, Zhang et al.[165] successfully operated a two-compartment reactor separated by a AEM at a high current density of 350 $mA{\cdot}cm^{-2}$, obtaining FEs >90% for 110 h. Li et al.[188] used a humidified CO_2 feeding in a two-compartment reactor reaching $HCOO^-$ concentrations of 153 $g{\cdot}L^{-1}$ during 100 h of operation. In this same work, with a liquid feed in the cathode, FEs >90% were obtained at current densities of 100 $mA{\cdot}cm^{-2}$ for 2400 h. Yang et al.[109] employed a three-compartment reactor with Sn-based catalysts achieving promising HCOOH concentrations above 15 wt% at cell potentials of 3.3−3.4 V for 550 h. Park et al.[170] obtained great results by being able to work at modest current densities of 50 $mA{\cdot}cm^{-2}$ for long periods of time of more than 900 h. Finally, the 1000 h of operation of the three-compartment reactor with Bi-based catalysts of Yang et al.[146] which allowed obtaining HCOOH concentrations above 10% by weight at commercially relevant current densities of 200 $mA{\cdot}cm^{-2}$, can be emphasized.

To achieve efficient, long-term performance of reactors for CO_2 electroreduction to HCOOH or $HCOO^-$, solutions to mitigate salt formation will need to be developed and improved in future research. However, these solutions may negatively impact other figures of merit, and trade-offs will need to be made.

Salt formation can be an significant issue in maintaining the long-term performance of the reactors for CO_2 electrochemical reduction, particularly when operated at high current densities. At high reaction rates, electrochemical reactions on the cathode can generate large amounts of hydroxide ions that can interact with CO_2, leading to the formation of considerable quantities of (bi)carbonate anions. The solubility limits of these species are met in the presence of enough electrolyte cations, leading to "salting out" conditions in cathode compartments.[241] The precipitation of salts in porous cathode structures can progressively reduce CO_2 mass transport, thereby reducing the CO_2 conversion efficiency, and limiting the selective and long-term operation of CO_2 electrolyzers.[260]

Several studies for the continuous electroreduction of CO_2 to $HCOO^-$ or HCOOH analyzed in this work have reported the problem of detrimental carbonate salt formation after several hours of operation (e.g., refs 122, 144, 217, 222, 223, 226). A few works have reported strategies for tackling this problem, essentially based on periodically refreshing the electrolytes (e.g., refs 188, 219) or increasing water availability.[118] For example, Li et al.[188] changed the electrolytes every 48 h during the 2400 h continuous operation to reduce the carbonate precipitates. In their 25 h stability tests, De Mot et al. avoided salt precipitation by increasing the water availability through direct water injection, although at the expense of diluting the concentration of $HCOO^-$ in the product stream.[118]

In the literature, various strategies and operational approaches have been proposed to prevent or reverse salt precipitation and keep long-term CO_2 electroreduction to different products other than HCOOH or $HCOO^-$. All these strategies aim to avoid the solubility limits of carbonate salts, by targeting the concentration of either the cation, anion, or water.[241] Some of these approaches are based on the effect of modifying the electrolyte concentration and composition, i.e., decreasing the concentration of cations in the electrolyte or eliminating them entirely from the system (see, e.g., ref 47), or changing the nature of the cation of the electrolyte (see, e.g., Cofell et al.,[261] who reported that the rate of carbonate deposition was slowed by switching the electrolyte from KOH to CsOH in long-term tests for CO_2 electroreduction to CO). Other approaches for dealing with salt precipitation are based on operating the reactor using a pulsed electrolysis mode with a periodic regeneration voltage that aims to redistribute the cations and carbonate anions and therefore keep their concentration within levels that prevent precipitation.[260,262] An excellent example is the work of Xu et al.,[260] where they avoided salt formation by alternating the applied cell voltage between an operational voltage and a lower regeneration voltage, enabling the electrolyzer to operate for 157 h at high current densities up to 250 mA cm^{-2} and keeping FEs to C2 products of 80%. The performance of CO_2 electroreduction in acidic media has also been suggested as an avenue to reduce carbonate formation to near zero.[89] Alkaline and neutral environments have typically been considered because, under acidic conditions, the HER is kinetically more favorable and outcompetes the reduction of CO_2. However, the use of acidic conditions should be carefully considered for future studies, encouraged by excellent results like those by Huang et al.,[89] who reported a cation augmenting strategy to accelerate CO_2 activation kinetics and achieved efficient CO_2 electroreduction to multicarbon products (ethylene, ethanol, and 1-propanol) at 1.2 A cm^{-2} in strong acid. Finally, the use of bipolar membranes (BPMs) instead of a monopolar membrane, to reconvert any formed (bi)carbonates back into CO_2 by providing protons to the cathodic compartment, has also been suggested as an option to reduce salt formation.[241] However, using a BPM can also involve issues, such as a greater charge ohmic resistance, resulting in higher cell potentials, than a thinner monopolar membrane. In this sense, it is important to highlight that the different strategies mentioned for preventing or reversing salt formation can increase stability and operation time of the electrochemical reactor, but at the expense of decreasing other figures of merit; e.g., as mentioned, increasing water injection reduces the product concentration; or strategies like using a BPM, decreasing electrolyte concentration or eliminating it, imply higher cell potentials and thus higher EC. Therefore, to achieve an efficient long-term performance of reactors for CO_2 electroreduction to HCOOH or $HCOO^-$, solutions to avoid the problem of salt formation will need to be deployed and improved in future research, while also considering that they may likely negatively impact other figures of merit, and that trade-offs will have to be made.

3. CONCLUDING REMARKS AND FUTURE PERSPECTIVES

This Focus Review presents a quantitative assessment of the performance of the approaches of the continuous electrochemical reduction of CO_2 to $HCOO^-$/HCOOH, comparing relevant figures of merit typically used to measure the performance. Graphic representations were carefully designed

https://doi.org/10.1021/acsenergylett.3c00489
ACS Energy Lett. 2023, 8, 1992−2024

to facilitate the analysis and comparison of the figures of merit. The comparative assessment concluded that the different electrochemical approaches developed for a continuous production of HCOOH/$HCOO^-$ from CO_2 have achieved excellent results in some figures of merit, but the simultaneous optimization of all the different figures of merit is still a great challenge. The highest product concentrations have been obtained with humidified CO_2 input streams feeding three-compartment reactors and modest FE, working at a maximum current density of ~200 mA·cm^{-2} and higher EC than the other approaches. Moreover, less than 40% of studied manuscripts in this review operated at >200 mA·cm^{-2}, which has been considered as the minimum value of commercially relevant current densities for practical CO_2 electroreduction processes.[75] However, no studies were observed that combined obtaining concentrations above 85 wt%, the most common concentration in the market, with operation at high current densities above 200 mA·cm^{-2}. Although not reported and neglected in some studies, the product concentration could be a crucial factor for the practical implementation of the process. Apart from the high economic penalty that the purification of diluted solutions would imply, analyses of the environmental sustainability of formate production by continuous electroreduction of CO_2 alert that the energy requirements for conventional purification of the final formic acid/formate products cancel the expected benefits of the CO_2 electrovalorization in terms of global warming footprint.[44,263,264] In this sense, recent efforts are being developed in the practical application of pervaporation processes for the separation of mixtures made up of water/HCOOH, producing solutions of HCOOH products of higher concentration economically and with a lower capital cost.[265] A few approaches have been reported at current densities up to almost 2 A·cm^{-2} with liquid-fed two-compartments reactors separated by an AEM, which also achieved the highest production rates (50−70 mmol m^{-2} s^{-1}), but at the expense of low product concentrations (<6 g·L^{-1}). Although it was not conducted in a cell with continuous operation and, due to this, it has not been included in the set of works analyzed in this review, the study by Löwe et al.[97] should be highlighted, with FEs for $HCOO^-$ of 70% obtained at ultra-high current densities of 1.8 A cm^{-2}. Only three studies, using humidified CO_2 streams to feed Bi-GDEs cathodes, obtained concentrations above the threshold of 21 wt% that has been identified as the minimum product concentration that makes the process environmentally sustainable.[39] The EC of the continuous approaches lies in the range of 150−750 kWh per kmol of HCOOH/$HCOO^-$. Barely 20% of the studies managed to restrict EC below 200 kWh·$kmol^{-1}$ while keeping FE above 90%. Despite its importance due to economic implications, most reviewed studies did not explicitly report the EC, and few did not even offer enough information to calculate it. Therefore, future research should pay more attention to the evaluation of EC.

This review showed that significant progress has been made in the continuous CO_2 electroreduction to HCOOH or $HCOO^-$, with promising results for its practical implementation. This review highlights that continuous electrochemical processes will be prevalent in the future owing to the improved process control and the ability for an easy scale-up.[99] According to the reviewed data, it could be stated that currently (as of 5 Jan 2023) the development of continuous electrochemical conversion of CO_2 to HCOOH/$HCOO^-$ is at Technology Readiness Level 4−5. A pilot plant project of Mantra Venture Group to produce 35 t/yr of HCOOH has been reported.[266] DNV GL has also developed continuous processes at semi-pilot scale,[267−269] and lab-scale electrolyzers have been recently made commercially available (Dioxide Materials). However, the possibility of HCOOH/$HCOO^-$ production using continuous CO_2 electroreduction at industrial scale has not yet been implemented. It is necessary to continue research efforts to overcome the current limitations of these processes and explore their scaling. Improvements are still needed to simultaneously combine high FE and high production rates of concentrated HCOOH/$HCOO^-$ product with low EC to ensure its commercial viability. More research focused on the advanced electrocatalytic materials, innovative electrode configuration, and improved electrochemical reactors will result in significant advances toward commercialization. However, apart from this, demonstration projects are also required. These projects bridge the gap between the ideal lab conditions (i.e., studies carried out with pure CO_2 streams) and the real industrial environment, in which the performance of these processes, considering the influence of impurities in CO_2 streams from real combustion processes, could be investigated. Such projects are also related to durability of these systems, which is another issue that has been scarcely investigated. The performance of more long-term studies (more than a few hours; in the order of hundreds or thousands) will be required to assess the stability of high-performing electrodes. Analyses by Rumayor et al.,[39] for a baseline scenario in which an aqueous-fed flow filter-press cell equipped with Sn-GDE, DSA-O_2, and commercial Nafion 117 is considered, have demonstrated that cathode lifetimes over 210 h would be enough to neglect the influence of the cathode fabrication from an environmental perspective. Moreover, other results also indicate that cathode lifetime over 4.45 yr (close to 40 000 h) would keep the influence of the consumable cost in the total cost of production below 10%.[44] The development of "accelerated" durability tests can be suggested as a way to timely assess the process lifetimes.[270]

In general, most of the studies reported in the Table 1 do not provide direct information about full-cell energy efficiency (FEE) or the CO_2 conversion per pass (CO_2CPP). On the one hand, very few studies have explicitly reported the FEE,[146,188,204] with values ranging from 19 to 31%. In particular, Nguyen et al.[204] achieved FEE of 19.2% at current densities of 500 mA·cm^{-2}, with associated cell voltages of 6.4 V. Li and co-workers[188] reported FEEs of 27%, with a cell voltage of 4.2 V at a current density of 60 mA·cm^{-2}. Yang et al.[146] obtained an interesting FEE value of 30.8% using a three-compartment reactor, with a cell voltage of 3.52 V at a current density of 200 mA·cm^{-2}. Although most other studies analyzed did not report the full-cell voltages (necessary for the FEE calculation), an estimation of the FEE for some references[109,139,160,161] that have reported the best trade-offs among

The different electrochemical approaches developed for a continuous production of HCOOH or $HCOO^-$ from CO_2 have achieved excellent results in some figures of merit, but the simultaneous optimization of all the different figures of merit is still a great challenge.

https://doi.org/10.1021/acsenergylett.3c00489
ACS Energy Lett. 2023, 8, 1992−2024

the figures of merit analyzed in Section 2 of this paper, and that have included enough data to allow estimating them, reveals that the highest values of FEE obtained still barely exceed 50%. In this way, full-cell voltages of 2.5 and 3.0 V resulted in FEEs of almost 52 and 42% in the works of Wang et al.[160] and Díaz-Sainz et al.,[139] respectively, with FEE values of 38% in ref 109 and of only 22% in ref 161. Future studies should include FEEs in the figures of merit or at least report actual full-cell voltages to allow their assessment. On the other hand, the vast majority of the studies analyzed in Table 1 carried out the continuous electroreduction to HCOOH of $HCOO^-$ under conditions of great excess of CO_2, without considering the CO_2 conversion per pass (CO_2CPP). Only a few approaches[114,120,145,219,220,222] have reported the CO_2CPP, with ranges between 9 and 75%. In particular, continuous pure CO_2 flow rates lower than 10 mL_n $CO_2 \cdot min^{-1}$ make it possible to obtain interesting CO_2CPPs ranging from 33 to 44%.[120,145,222] In contrast, CO_2CPPs of 12 and 75% were obtained, respectively, by Van Daele et al.[220] and Li and Oloman[114] at higher CO_2 flow rates than 150 mL_n $CO_2 \cdot min^{-1}$. Choi et al.[219] operated the flow cell with a diluted gas inlet stream (with a CO_2 partial pressure of 0.15 atm, equivalent to a pure CO_2 flow rate of 4.5 mL_n $CO_2 \cdot min^{-1}$) and obtained a CO_2CPP of approximately of 9%. Furthermore, an estimation of the CO_2CPP of other seven additional references that have reported the best trade-offs in the figures of merit of section 2 have been also calculated.[136,139,142,144,160,171,210] In this sense, the CO_2CPP values obtained range from 1.5% (in the works of Díaz-Sainz et al. and Wang et al.[139,160]) to 25% in the study of Zelocualtecatl et al.;[210] CO_2CPP values of 13% in the works by Fan et al. and Grigioni et al.,[144,171] 11% CO_2CPP in the study by Xia et al.,[136] and 2.6% in the study by Fan et al.[142] were also obtained. Therefore, in future stages of research, especially at larger scales, more attention should also be paid to this figure of merit.

> The possibility of HCOOH or $HCOO^-$ production using continuous CO_2 electroreduction at industrial scale has not yet been implemented. It is necessary to continue research efforts to overcome the current limitations of these processes and explore their scaling.

We believe that ample opportunities exist for the improvement in the anode. This review clearly showed that the majority of the studies for continuous CO_2 electroreduction to $HCOOH/HCOO^-$ have focused on the cathode, leaving the anode for oxygen evolution (i.e., oxidation of water to give molecular oxygen). Few studies have successfully investigated the coupling of oxidation reactions of interest in the anodic compartment, such as the degradation of organic pollutants or the oxidation of methanol. Recent studies also support a thorough investigation of the more relevant alternative oxidative electrochemical reactions to the OER,[271,272] which could co-valorize CO_2 to $HCOOH/HCOO^-$ in the cathode together with other value-added products, lowering the global cell potential of the process. In this regard, glycerol is an important byproduct of biodiesel production and is produced in high amounts, resulting in a high surplus flooding the market over the last decades. Selective oxidation of glycerol is considered as a promising pathway to produce fine chemicals; even though the electrocatalytic pathway has not been widely investigated, there are already some studies reporting interesting results for C3 oxidation compounds, including high-value-added products, such as dihydroxyacetone (DHA),[273−275] which is currently produced mainly via a complex, time-consuming microbial fermentation process. Therefore, development of continuous electrochemical processes for co-valorization of CO_2 and glycerol is required in the future. Recent analyses have shown that anodic DHA concentrations of just 1.5 wt% are enough to achieve positive decarbonization when the integrated production of DHA and $HCOO^-$ is compared with the traditional route, which encourages further work in this direction.[276] Finally, it is important to note that, apart from the technical considerations, other aspects of the CO_2 electroreduction processes must also be analyzed holistically. This means that the development of continuous electrochemical processes for converting CO_2 into $HCOOH/HCOO^-$ will require a favorable economic balance and a positive environmental profile, based on a lifecycle assessment approach, together with social acceptance of these processes; thus, these processes need to be rigorously assessed for their sustainability and cost-effectiveness.

AUTHOR INFORMATION

Corresponding Author

Guillermo Díaz-Sainz − *Departamento de Ingenierías Química y Biomolecular, Universidad de Cantabria, 39005 Santander, Spain*; Email: diazsg@unican.es

Authors

Kevin Fernández-Caso − *Departamento de Ingenierías Química y Biomolecular, Universidad de Cantabria, 39005 Santander, Spain*

Manuel Alvarez-Guerra − *Departamento de Ingenierías Química y Biomolecular, Universidad de Cantabria, 39005 Santander, Spain*; orcid.org/0000-0002-3546-584X

Angel Irabien − *Departamento de Ingenierías Química y Biomolecular, Universidad de Cantabria, 39005 Santander, Spain*; orcid.org/0000-0002-2411-4163

Complete contact information is available at: https://pubs.acs.org/10.1021/acsenergylett.3c00489

Notes

The authors declare no competing financial interest.

Biographies

Kevin Fernández-Caso studied Chemical Engineering at Universidad de Cantabria (2019). At present, he is a Predoctoral Researcher in the Chemical and Biomolecular Engineering Department and member of the DePRO research group. The primary focus of his research is in the field of the electrocatalytic conversion of CO_2 into valuable products.

Guillermo Díaz-Sainz obtained a Ph.D. in Chemical Engineering, Energy, and Processes in 2021, and is now an Assistant Professor in the Chemical and Biomolecular Engineering Department at the Universidad de Cantabria. His goal is to innovate in CO_2 capture and convert it into valuable products using photo-/electrochemical methods.

Manuel Alvarez-Guerra received his Ph.D. in 2010, and he is currently Associate Professor ("Profesor Titular de Universidad") in the Department of Chemical and Biomolecular Engineering at the Universidad de Cantabria. His research is focused on developing and

https://doi.org/10.1021/acsenergylett.3c00489
ACS Energy Lett. 2023, 8, 1992−2024

evaluating innovative processes for the electrochemical conversion of CO_2 into valuable products.

Angel Irabien is a Full Professor of Chemical Engineering in the Department of Chemical and Biomolecular Engineering at the Universidad de Cantabria. His research interests primarily focus on the development of carbon capture and utilization processes, and the application of Life Cycle Thinking to Chemical and Process Engineering.

■ ACKNOWLEDGMENTS

The authors acknowledge the financial support from the Spanish State Research Agency (AEI) through the projects PID2019-108136RB-C31 and PID2020-112845RB-I00 (MCIN/AEI/10.13039/501100011033).

■ REFERENCES

(1) United Nations. Delivering the Glasgow Climate Pact, UN Climate Change Conference (COP26) at the SEC - Glasgow, 2021; https://ukcop26.org/ (accessed Dec 29, 2022).
(2) Global Carbon Project. Global carbon budget, 2022 http://www.globalcarbonproject.org/carbonbudget/index.htm (accessed Dec 16, 2022).
(3) Girardin, C. A. J.; Jenkins, S.; Seddon, N.; Allen, M.; Lewis, S. L.; Wheeler, C. E.; Griscom, B. W.; Malhi, Y. Nature-Based Solutions Can Help Cool the Planet - If We Act Now. *Nature* **2021**, *593* (7858), 191−194.
(4) Mcglade, C.; Ekins, P. The Geographical Distribution of Fossil Fuels Unused When Limiting Global Warming to 2°C. *Nature* **2015**, *517*, 187−190.
(5) Tapia, J. F. D.; Lee, J. Y.; Ooi, R. E. H.; Foo, D. C. Y.; Tan, R. R. A Review of Optimization and Decision-Making Models for the Planning of CO_2 Capture, Utilization and Storage (CCUS) Systems. *Sustain. Prod. Consum.* **2018**, *13*, 1−15.
(6) Norhasyima, R. S.; Mahlia, T. M. I. Advances in CO_2 Utilization Technology: A Patent Landscape Review. *J. CO_2 Util.* **2018**, *26*, 323−335.
(7) Zhang, W.; Hu, Y.; Ma, L.; Zhu, G.; Wang, Y.; Xue, X.; Chen, R.; Yang, S.; Jin, Z. Progress and Perspective of Electrocatalytic CO_2 Reduction for Renewable Carbonaceous Fuels and Chemicals. *Adv. Sci.* **2018**, *5* (1), 1700275.
(8) Lu, Q.; Jiao, F. Electrochemical CO_2 Reduction: Electrocatalyst, Reaction Mechanism, and Process Engineering. *Nano Energy* **2016**, *29*, 439−456.
(9) Jones, J.-P.; Surya Prakash, G. K.; Olah, G. A. Electrochemical CO_2 Reduction: Recent Advances and Current Trends. *Isr. J. Chem.* **2014**, *54* (10), 1451−1466.
(10) Gu, J.; Hsu, C. S.; Bai, L.; Chen, H. M.; Hu, X. Atomically Dispersed Fe^{3+} Sites Catalyze Efficient CO2 Electroreduction to CO. *Science.* **2019**, *364* (6445), 1091−1094.
(11) Dinh, C.-T.; Pelayo García De Arquer, F.; Sinton, D.; Sargent, E. H. High Rate, Selective, and Stable Electroreduction of CO_2 to CO in Basic and Neutral Media. *ACS Energy Lett.* **2018**, *3* (11), 2835−2840.
(12) Verma, S.; Hamasaki, Y.; Kim, C.; Huang, W.; Lu, S.; Jhong, H.-R. M.; Gewirth, A. A.; Fujigaya, T.; Nakashima, N.; Kenis, P. J. A. Insights into the Low Overpotential Electroreduction of CO_2 to CO on a Supported Gold Catalyst in an Alkaline Flow Electrolyzer. *ACS Energy Lett.* **2018**, *3* (1), 193−198.
(13) Lee, G.; Li, Y. C.; Kim, J. Y.; Peng, T.; Nam, D. H.; Sedighian Rasouli, A.; Li, F.; Luo, M.; Ip, A. H.; Joo, Y. C.; Sargent, E. H. Electrochemical Upgrade of CO_2 from Amine Capture Solution. *Nat. Energy* **2021**, *6* (1), 46−53.
(14) Cai, Y.; Fu, J.; Zhou, Y.; Chang, Y.-C.; Min, Q.; Zhu, J.-J.; Lin, Y.; Zhu, W. Insights on Forming N,O-Coordinated Cu Single-Atom Catalysts for Electrochemical Reduction CO_2 to Methane. *Nat. Commun.* **2021**, *12* (1), 586.
(15) Dinh, C. T.; Burdyny, T.; Kibria, G.; Seifitokaldani, A.; Gabardo, C. M.; Pelayo García De Arquer, F.; Kiani, A.; Edwards, J. P.; De Luna, P.; Bushuyev, O. S.; et al. CO_2 Electroreduction to Ethylene via Hydroxide-Mediated Copper Catalysis at an Abrupt Interface. *Science.* **2018**, *360* (6390), 783−787.
(16) Guan, A.; Chen, Z.; Quan, Y.; Peng, C.; Wang, Z.; Sham, T.-K.; Yang, C.; Ji, Y.; Qian, L.; Xu, X.; Zheng, G. Boosting CO_2 Electroreduction to CH_4 via Tuning Neighboring Single-Copper Sites. *ACS Energy Lett.* **2020**, *5* (4), 1044−1053.
(17) Ozden, A.; Li, F.; Pelayo García De Arquer, F.; Rosas-Hernándezhernández, A.; Thevenon, A.; Wang, Y.; Hung, S.-F.; Wang, X.; Chen, B.; Li, J.; et al. High-Rate and Efficient Ethylene Electrosynthesis Using a Catalyst/Promoter/ Transport Layer. *ACS Energy Lett.* **2020**, *5* (9), 2811−2818.
(18) Gonglach, S.; Paul, S.; Haas, M.; Pillwein, F.; Sreejith, S. S.; Barman, S.; De, R.; Müllegger, S.; Gerschel, P.; Apfel, U.-P.; et al. Molecular Cobalt Corrole Complex for the Heterogeneous Electrocatalytic Reduction of Carbon Dioxide. *Nat. Commun.* **2019**, *10* (1), 3864.
(19) Wang, Y.; Liu, X.; Han, X.; Godin, R.; Chen, J.; Zhou, W.; Jiang, C.; Thompson, J. F.; Bayazit Mustafa, K.; Shevlin, S. A.; Durrant, J. R.; Guo, Z.; Tang, J. Unique Hole-Accepting Carbon-Dots Promoting Selective Carbon Dioxide Reduction Nearly 100% to Methanol by Pure Water. *Nat. Commun.* **2020**, *11* (1), 2531.
(20) Zhang, X.; Sun, X.; Guo, S. X.; Bond, A. M.; Zhang, J. Formation of Lattice-Dislocated Bismuth Nanowires on Copper Foam for Enhanced Electrocatalytic CO_2 Reduction at Low Overpotential. *Energy Environ. Sci.* **2019**, *12* (4), 1334−1340.
(21) Han, N.; Wang, Y.; Yang, H.; Deng, J.; Wu, J.; Li, Y.; Li, Y. Ultrathin Bismuth Nanosheets from in Situ Topotactic Transformation for Selective Electrocatalytic CO_2 Reduction to Formate. *Nat. Commun.* **2018**, *9* (1), 1320.
(22) Margarit, C. G.; Asimow, N. G.; Costentin, C.; Nocera, D. G. Tertiary Amine-Assisted Electroreduction of Carbon Dioxide to Formate Catalyzed by Iron Tetraphenylporphyrin. *ACS Energy Lett.* **2020**, *5* (1), 72−78.
(23) Formic Acid Market Size, Growth | Industry Reports To 2035 https://www.chemanalyst.com/industry-report/formic-acid-market-688 (accessed Jan 2, 2023).
(24) Formic Acid Prices, Price, Pricing, News | ChemAnalyst https://www.chemanalyst.com/Pricing-data/formic-acid-1242 (accessed Nov 14, 2022).
(25) Sodium formate Price and Market Analysis - ECHEMI https://www.echemi.com/productsInformation/pd20150901132-sodium-formate.html (accessed Nov 7, 2022).
(26) Calcium Formate Prices, Price, Pricing, News | ChemAnalyst https://www.chemanalyst.com/Pricing-data/calcium-formate-1234 (accessed Nov 7, 2022).
(27) Irabien, A.; Alvarez-Guerra, M.; Albo, J.; Dominguez-Ramos, A. Electrochemical Conversion of CO_2 to Value-Added Products. In *Electrochemical Water and Wastewater Treatment*; Martínez-Huitle, C. A., Rodrigo, M. A., Scialdone, O., Eds.; Elsevier, 2018; pp 29−59.
(28) Du, D.; Lan, R.; Humphreys, J.; Tao, S. Progress in Inorganic Cathode Catalysts for Electrochemical Conversion of Carbon Dioxide into Formate or Formic Acid. *J. Appl. Electrochem.* **2017**, *47* (6), 661−678.
(29) Sodium Formate | Solvents | Hydrite.com https://www.hydrite.com/Product/industrial/Sodium-Formate.htm (accessed Nov 8, 2022).
(30) GOE. *Calcium Formate Product Data - Technical Data Sheet*, 2015; pp 2−5.
(31) Chiou, Y.-J.; Juchniewicz, K.; Kupiec, K. R.; Mikolajczuk-Zychora, A.; Mierzwa, B.; Lin, H.-M.; Borodzinski, A. Pd Nanoparticle Size Effect of Anodic Catalysts on Direct Formic Acid Fuel Cell Initial Performance: Development of a Mathematical Model and Comparison with Experimental Results. *ChemElectroChem* **2021**, *8* (17), 3348−3359.
(32) Yu, X.; Pickup, P. G. Recent Advances in Direct Formic Acid Fuel Cells (DFAFC). *J. Power Sources* **2008**, *182* (1), 124−132.

https://doi.org/10.1021/acsenergylett.3c00489
ACS Energy Lett. 2023, 8, 1992−2024

(33) Rice, C.; Ha, S.; Masel, R. I.; Waszczuk, P.; Wieckowski, A.; Barnard, T. Direct Formic Acid Fuel Cells. *J. Power Sources* **2002**, *111* (1), 83−89.
(34) Yadav, M.; Xu, Q. Liquid-Phase Chemical Hydrogen Storage Materials. *Energy Environ. Sci.* **2012**, *5* (12), 9698−9725.
(35) Mellmann, D.; Sponholz, P.; Junge, H.; Beller, M. Formic Acid as a Hydrogen Storage Material-Development of Homogeneous Catalysts for Selective Hydrogen Release. *Chem. Soc. Rev.* **2016**, *45* (14), 3954−3988.
(36) Chatterjee, S.; Dutta, I.; Lum, Y.; Lai, Z.; Huang, K. W. Enabling Storage and Utilization of Low-Carbon Electricity: Power to Formic Acid. *Energy Environ. Sci.* **2021**, *14* (3), 1194−1246.
(37) Tedsree, K.; Li, T.; Jones, S.; Chan, C. W. A.; Yu, K. M. K.; Bagot, P. A. J.; Marquis, E. A.; Smith, G. D. W.; Tsang, S. C. E. Hydrogen Production from Formic Acid Decomposition at Room Temperature Using a Ag-Pd Core-Shell Nanocatalyst. *Nat. Nanotechnol.* **2011**, *6* (5), 302−307.
(38) Carrales-Alvarado, D. H.; López-Olmos, C.; Dongil, A. B.; Kubacka, A.; Guerrero-Ruiz, A.; Rodríguez-Ramos, I. Effect of N-Doping and Carbon Nanostructures on NiCu Particles for Hydrogen Production from Formic Acid. *Appl. Catal. B Environ.* **2021**, *298*, 120604.
(39) Rumayor, M.; Dominguez-Ramos, A.; Irabien, A. Environmental and Economic Assessment of the Formic Acid Electrochemical Manufacture Using Carbon Dioxide: Influence of the Electrode Lifetime. *Sustain. Prod. Consum.* **2019**, *18*, 72−82.
(40) Hietala, J.; Vuori, A.; Johnsson, P.; Pollari, I.; Reutemann, W.; Kieczka, H. *Formic Acid*; Elvers, B., Ed.; Wiley-VCH, 2016.
(41) Bulushev, D. A.; Ross, J. R. H. Towards Sustainable Production of Formic Acid. *ChemSusChem* **2018**, *11* (5), 821−836.
(42) Dutta, I.; Chatterjee, S.; Cheng, H.; Parsapur, R. K.; Liu, Z.; Li, Z.; Ye, E.; Kawanami, H.; Low, J. S. C.; Lai, Z.; Loh, X. J.; Huang, K. W. Formic Acid to Power towards Low-Carbon Economy. *Adv. Energy Mater.* **2022**, *12*, 2103799.
(43) Werle, P.; Morawietz, M.; Lundmark, S.; Sörensen, K.; Karvinen, E.; Lehtonen, J. *Alcohols, Polyhydric*; Elvers, B., Ed.; Wiley-VCH, 2008.
(44) De Luna, P.; Hahn, C.; Higgins, D.; Jaffer, S. A.; Jaramillo, T. F.; Sargent, E. H. What Would It Take for Renewably Powered Electrosynthesis to Displace Petrochemical Processes? *Science* **2019**, *364*, eaav3506.
(45) Rumayor, M.; Dominguez-Ramos, A.; Perez, P.; Irabien, A. A Techno-Economic Evaluation Approach to the Electrochemical Reduction of CO_2 for Formic Acid Manufacture. *J. CO_2 Util.* **2019**, *34*, 490−499.
(46) Rumayor, M.; Dominguez-Ramos, A.; Irabien, A. Formic Acid Manufacture: Carbon Dioxide Utilization Alternatives. *Appl. Sci.* **2018**, *8* (6), 914.
(47) O'Brien, C. P.; Miao, R. K.; Liu, S.; Xu, Y.; Lee, G.; Robb, A.; Huang, J. E.; Xie, K.; Bertens, K.; Gabardo, C. M.; Edwards, J. P.; Dinh, C. T.; Sargent, E. H.; Sinton, D. Single Pass CO_2Conversion Exceeding 85% in the Electrosynthesis of Multicarbon Products via Local CO_2Regeneration. *ACS Energy Lett.* **2021**, *6* (4), 2952−2959.
(48) Larrazábal, G. O.; Ma, M.; Seger, B. A Comprehensive Approach to Investigate CO_2 Reduction Electrocatalysts at High Current Densities. *Acc. Mater. Res.* **2021**, *2* (4), 220−229.
(49) Jitaru, M.; Lowy, D. A.; Toma, M.; Toma, B. C.; Oniciu, L. Electrochemical Reduction of Carbon Dioxide on Flat Metallic Cathodes. *J. Appl. Electrochem.* **1997**, *27* (8), 875−889.
(50) Sánchez-Sánchez, C. M.; Montiel, V.; Tryk, D. A.; Aldaz, A.; Fujishima, A. Electrochemical Approaches to Alleviation of the Problem of Carbon Dioxide Accumulation. *Pure Appl. Chem.* **2001**, *73* (12), 1917−1927.
(51) Chaplin, R. P. S.; Wragg, A. A. Effects of Process Conditions and Electrode Material on Reaction Pathways for Carbon Dioxide Electroreduction with Particular Reference to Formate Formation. *J. Appl. Electrochem.* **2003**, *33* (12), 1107−1123.
(52) Gattrell, M.; Gupta, N.; Co, A. A Review of the Aqueous Electrochemical Reduction of CO_2 to Hydrocarbons at Copper. *J. Electroanal. Chem.* **2006**, *594* (1), 1−19.
(53) Masel, R.; Liu, Z.; Zhao, D.; Chen, Q.; Lutz, D.; Nereng, L. CO_2 Conversion to Chemicals with Emphasis on Using Renewable Energy/Resources to Drive the Conversion. In *Commercializing Biobased Products: Opportunities, Challenges, Benefits, and Risks*; Snyder, S. W., Ed.; RSC, 2016; pp 215−257.
(54) Qiao, J.; Liu, Y.; Zhang, J. *Electrochemical Reduction of Carbon Dioxide: Fundamentals and Techonologies*; Zhang, J., Ed.; CRC Press, 2016.
(55) Albo, J.; Alvarez-guerra, M.; Irabien, A. Electro-, Photo-, and Photoelectro-Chemical Reduction of CO_2. In *Heterogeneous Catalysts: Advanced Design, Characterization and Applications*, II; Teoh, W. Y., Urakawa, A., Ng, Y. H., Sit, P., Eds.; Wiley-VCH, 2021; pp 649−669.
(56) Birdja, Y. Y.; Pérez-Gallent, E.; Figueiredo, M. C.; Göttle, A. J.; Calle-Vallejo, F.; Koper, M. T. M. Advances and Challenges in Understanding the Electrocatalytic Conversion of Carbon Dioxide to Fuels. *Nat. Energy* **2019**, *4* (9), 732−745.
(57) Zhang, X.; Guo, S. X.; Gandionco, K. A.; Bond, A. M.; Zhang, J. Electrocatalytic Carbon Dioxide Reduction: From Fundamental Principles to Catalyst Design. *Mater. Today Adv.* **2020**, *7*, 100074.
(58) Kibria, M. G.; Edwards, J. P.; Gabardo, C. M.; Dinh, C. T.; Seifitokaldani, A.; Sinton, D.; Sargent, E. H. Electrochemical CO_2 Reduction into Chemical Feedstocks: From Mechanistic Electrocatalysis Models to System Design. *Adv. Mater.* **2019**, *31* (31), 1807166.
(59) Zhang, Q.; Xu, W.; Xu, J.; Liu, Y.; Zhang, J. High Performing and Cost-Effective Metal/Metal Oxide/Metal Alloy Catalysts/Electrodes for Low Temperature CO_2 Electroreduction. *Catal. Today* **2018**, *318*, 15−22.
(60) Hoang, V. C.; Gomes, V. G.; Kornienko, N. Metal-Based Nanomaterials for Efficient CO_2 Electroreduction: Recent Advances in Mechanism, Material Design and Selectivity. *Nano Energy* **2020**, *78*, 105311.
(61) Zhang, L.; Merino-Garcia, I.; Albo, J.; Sánchez-Sánchez, C. M. Electrochemical CO_2 Reduction Reaction on Cost-Effective Oxide-Derived Copper and Transition Metal-Nitrogen-Carbon Catalysts. *Curr. Opin. Electrochem.* **2020**, *23*, 65−73.
(62) Zhao, J.; Xue, S.; Barber, J.; Zhou, Y.; Meng, J.; Ke, X. An Overview of Cu-Based Heterogeneous Electrocatalysts for CO_2 Reduction. *J. Mater. Chem. A* **2020**, *8* (9), 4700−4734.
(63) Da Silva Freitas, W.; D'Epifanio, A.; Mecheri, B. Electrocatalytic CO_2 Reduction on Nanostructured Metal-Based Materials: Challenges and Constraints for a Sustainable Pathway to Decarbonization. *J. CO_2 Util.* **2021**, *50*, 101579.
(64) Zhang, S.; Fan, Q.; Xia, R.; Meyer, T. J. CO_2 Reduction: From Homogeneous to Heterogeneous Electrocatalysis. *Acc. Chem. Res.* **2020**, *53* (1), 255−264.
(65) Franco, F.; Fernández, S.; Lloret-Fillol, J. Advances in the Electrochemical Catalytic Reduction of CO_2 with Metal Complexes. *Curr. Opin. Electrochem.* **2019**, *15*, 109−117.
(66) Zhang, L.; Zhao, Z. J.; Gong, J. Nanostructured Materials for Heterogeneous Electrocatalytic CO_2 Reduction and Their Related Reaction Mechanisms. *Angew. Chem., Int. Ed.* **2017**, *56* (38), 11326−11353.
(67) Wu, J.; Sharifi, T.; Gao, Y.; Zhang, T.; Ajayan, P. M. Emerging Carbon-Based Heterogeneous Catalysts for Electrochemical Reduction of Carbon Dioxide into Value-Added Chemicals. *Adv. Mater.* **2019**, *31* (13), 1804257.
(68) Liu, S.; Yang, H.; Su, X.; Ding, J.; Mao, Q.; Huang, Y.; Zhang, T.; Liu, B. Rational Design of Carbon-Based Metal-Free Catalysts for Electrochemical Carbon Dioxide Reduction: A Review. *J. Energy Chem.* **2019**, *36*, 95−105.
(69) Jia, C.; Dastafkan, K.; Ren, W.; Yang, W.; Zhao, C. Carbon-Based Catalysts for Electrochemical CO_2 Reduction. *Sustain. Energy Fuels* **2019**, *3* (11), 2890−2906.

https://doi.org/10.1021/acsenergylett.3c00489
ACS Energy Lett. 2023, 8, 1992−2024

(70) Pérez-Sequera, A. C.; Díaz-Pérez, M. A.; Serrano-Ruiz, J. C. Recent Advances in the Electroreduction of CO_2 over Heteroatom-Doped Carbon Materials. *Catalysts* **2020**, *10* (10), 1179−1199.
(71) Wu, Z. Z.; Gao, F. Y.; Gao, M. R. Regulating the Oxidation State of Nanomaterials for Electrocatalytic CO_2 Reduction. *Energy Environ. Sci.* **2021**, *14* (3), 1121−1139.
(72) Wang, Y.; Liu, Y.; Liu, W.; Wu, J.; Li, Q.; Feng, Q.; Chen, Z.; Xiong, X.; Wang, D.; Lei, Y. Regulating the Coordination Structure of Metal Single Atoms for Efficient Electrocatalytic CO_2 Reduction. *Energy Environ. Sci.* **2020**, *13* (12), 4609−4624.
(73) Nguyen, T. N.; Dinh, C. T. Gas Diffusion Electrode Design for Electrochemical Carbon Dioxide Reduction. *Chem. Soc. Rev.* **2020**, *49* (21), 7488−7504.
(74) Higgins, D.; Hahn, C.; Xiang, C.; Jaramillo, T. F.; Weber, A. Z. Gas-Diffusion Electrodes for Carbon Dioxide Reduction: A New Paradigm. *ACS Energy Lett.* **2019**, *4* (1), 317−324.
(75) Burdyny, T.; Smith, W. A. CO_2 Reduction on Gas-Diffusion Electrodes and Why Catalytic Performance Must Be Assessed at Commercially-Relevant Conditions. *Energy Environ. Sci.* **2019**, *12* (5), 1442−1453.
(76) Rabiee, H.; Ge, L.; Zhang, X.; Hu, S.; Li, M.; Yuan, Z. Gas Diffusion Electrodes (GDEs) for Electrochemical Reduction of Carbon Dioxide, Carbon Monoxide, and Dinitrogen to Value-Added Products: A Review. *Energy Environ. Sci.* **2021**, *14* (4), 1959−2008.
(77) Chen, C.; Khosrowabadi Kotyk, J. F.; Sheehan, S. W. Progress toward Commercial Application of Electrochemical Carbon Dioxide Reduction. *Chem* **2018**, *4* (11), 2571−2586.
(78) Weekes, D. M.; Salvatore, D. A.; Reyes, A.; Huang, A.; Berlinguette, C. P. Electrolytic CO_2 Reduction in a Flow Cell. *Acc. Chem. Res.* **2018**, *51* (4), 910−918.
(79) Garg, S.; Li, M.; Weber, A. Z.; Ge, L.; Li, L.; Rudolph, V.; Wang, G.; Rufford, T. E. Advances and Challenges in Electrochemical CO_2 Reduction Processes: An Engineering and Design Perspective Looking beyond New Catalyst Materials. *J. Mater. Chem. A* **2020**, *8* (4), 1511−1544.
(80) Lin, R.; Guo, J.; Li, X.; Patel, P.; Seifitokaldani, A. Electrochemical Reactors for CO_2 Conversion. *Catalysts* **2020**, *10* (5), 473.
(81) Liang, S.; Altaf, N.; Huang, L.; Gao, Y.; Wang, Q. Electrolytic Cell Design for Electrochemical CO_2 Reduction. *J. CO_2 Util.* **2020**, *35*, 90−105.
(82) Yang, Y.; Li, F. Reactor Design for Electrochemical CO_2 Conversion toward Large-Scale Applications. *Curr. Opin. Green Sustain. Chem.* **2021**, *27*, 100419.
(83) Ma, D.; Jin, T.; Xie, K.; Huang, H. An Overview of Flow Cell Architecture Design and Optimization for Electrochemical CO_2 Reduction. *J. Mater. Chem. A* **2021**, *9* (37), 20897−20918.
(84) Wakerley, D.; Lamaison, S.; Wicks, J.; Clemens, A.; Feaster, J.; Corral, D.; Jaffer, S. A.; Sarkar, A.; Fontecave, M.; Duoss, E. B.; et al. Gas Diffusion Electrodes, Reactor Designs and Key Metrics of Low-Temperature CO_2 Electrolysers. *Nat. Energy* **2022**, *7* (2), 130−143.
(85) Merino-Garcia, I.; Alvarez-Guerra, E.; Albo, J.; Irabien, A. Electrochemical Membrane Reactors for the Utilisation of Carbon Dioxide. *Chem. Eng. J.* **2016**, *305*, 104−120.
(86) Ju, H. K.; Kaur, G.; Kulkarni, A. P.; Giddey, S. Challenges and Trends in Developing Technology for Electrochemically Reducing CO_2 in Solid Polymer Electrolyte Membrane Reactors. *J. CO_2 Util.* **2019**, *32*, 178−186.
(87) Tan, X.; Yu, C.; Ren, Y.; Cui, S.; Li, W.; Qiu, J. Recent Advances in Innovative Strategies for the CO_2 Electroreduction Reaction. *Energy Environ. Sci.* **2021**, *14* (2), 765−780.
(88) Bhargava, S. S.; Cofell, E. R.; Chumble, P.; Azmoodeh, D.; Someshwar, S.; Kenis, P. J. A. Exploring Multivalent Cations-Based Electrolytes for CO_2 Electroreduction. *Electrochim. Acta* **2021**, *394*, 139055.
(89) Huang, J. E.; Li, F.; Ozden, A.; Rasouli, A. S.; Garcia de Arquer, F. P. G.; Liu, S.; Zhang, S.; Luo, M.; Wang, X.; Lum, Y.; et al. CO_2 Electrolysis to Multicarbon Products in Strong Acid. *Science* **2021**, *372* (6546), 1074−1078.
(90) Pan, F.; Yang, Y. Designing CO_2 Reduction Electrode Materials by Morphology and Interface Engineering. *Energy Environ. Sci.* **2020**, *13* (8), 2275−2309.
(91) Shi, Y.; Ji, Y.; Long, J.; Liang, Y.; Liu, Y.; Yu, Y.; Xiao, J.; Zhang, B. Unveiling Hydrocerussite as an Electrochemically Stable Active Phase for Efficient Carbon Dioxide Electroreduction to Formate. *Nat. Commun.* **2020**, *11* (1), 3415.
(92) Zhang, X.; Jiao, M.; Chen, Z.; Ma, X.; Wang, Z.; Wang, N.; Zhang, X.; Liu, L. An Integrated Gradually Thinning and Dual-Ion Co-Substitution Strategy Modulated In-O-Ultrathin-SnS_2 Nanosheets to Achieve Efficient Electrochemical Reduction of CO_2. *Chem. Eng. J.* **2022**, *429*, 132145.
(93) Zheng, X.; De Luna, P.; García de Arquer, F. P.; Zhang, B.; Becknell, N.; Ross, M. B.; Li, Y.; Banis, M. N.; Li, Y.; Liu, M.; et al. Sulfur-Modulated Tin Sites Enable Highly Selective Electrochemical Reduction of CO_2 to Formate. *Joule* **2017**, *1* (4), 794−805.
(94) Klinkova, A.; De Luna, P.; Dinh, C.-T.; Voznyy, O.; Larin, E. M.; Kumacheva, E.; Sargent, E. H. Rational Design of Efficient Palladium Catalysts for Electroreduction of Carbon Dioxide to Formate. *ACS Catal.* **2016**, *6* (12), 8115−8120.
(95) Kopljar, D.; Inan, A.; Vindayer, P.; Wagner, N.; Klemm, E. Electrochemical Reduction of CO_2 to Formate at High Current Density Using Gas Diffusion Electrodes. *J. Appl. Electrochem.* **2014**, *44* (10), 1107−1116.
(96) Löwe, A.; Rieg, C.; Hierlemann, T.; Salas, N.; Kopljar, D.; Wagner, N.; Klemm, E. Influence of Temperature on the Performance of Gas Diffusion Electrodes in the CO_2 ReductionReaction. *ChemElectroChem* **2019**, *6* (17), 4497−4506.
(97) Löwe, A.; Schmidt, M.; Bienen, F.; Kopljar, D.; Wagner, N.; Klemm, E. Optimizing Reaction Conditions and Gas Diffusion Electrodes Applied in the CO_2 Reduction Reaction to Formate to Reach Current Densities up to 1.8 A cm^{-2}. *ACS Sustain. Chem. Eng.* **2021**, *9* (11), 4213−4223.
(98) Lin, R.; Guo, J.; Li, X.; Patel, P.; Seifitokaldani, A. Electrochemical Reactors for CO_2 Conversion. *Catalyst* **2020**, *10* (5), 473.
(99) Nicholls, T. P.; Schotten, C.; Willans, C. E. Electrochemistry in Continuous Systems. *Curr. Opin. Green Sustain. Chem.* **2020**, *26*, 100355.
(100) Ding, P.; Zhao, H.; Li, T.; Luo, Y.; Fan, G.; Chen, G.; Gao, S.; Shi, X.; Lu, S.; Sun, X. Metal-Based Electrocatalytic Conversion of CO_2 to Formic Acid/Formate. *J. Mater. Chem. A* **2020**, *8* (42), 21947−21960.
(101) Han, N.; Ding, P.; He, L.; Li, Y.; Li, Y. Promises of Main Group Metal-Based Nanostructured Materials for Electrochemical CO_2 Reduction to Formate. *Adv. Energy Mater.* **2020**, *10* (11), 1902338.
(102) Al-Tamreh, S. A.; Ibrahim, M. H.; El-Naas, M. H.; Vaes, J.; Pant, D.; Benamor, A.; Amhamed, A. Electroreduction of Carbon Dioxide into Formate: A Comprehensive Review. *ChemElectroChem* **2021**, *8* (17), 3207−3220.
(103) Duarah, P.; Haldar, D.; Yadav, V.; Purkait, M. K. Progress in the Electrochemical Reduction of CO_2 to Formic Acid: A Review on Current Trends and Future Prospects. *J. Environ. Chem. Eng.* **2021**, *9* (6), 106394.
(104) Proietto, F.; Patel, U.; Galia, A.; Scialdone, O. Electrochemical Conversion of CO_2 to Formic Acid Using a Sn Based Electrode: A Critical Review on the State-of-the-Art Technologies and Their Potential. *Electrochim. Acta* **2021**, *389*, 138753.
(105) Tay, Y. F.; Tan, Z. H.; Lum, Y. Engineering Sn-Based Catalytic Materials for Efficient Electrochemical CO_2 Reduction to Formate. *ChemNanoMat* **2021**, *7* (4), 380−391.
(106) Proietto, F.; Schiavo, B.; Galia, A.; Scialdone, O. Electrochemical Conversion of CO_2 to HCOOH at Tin Cathode in a Pressurized Undivided Filter-Press Cell. *Electrochim. Acta* **2018**, *277*, 30−40.

https://doi.org/10.1021/acsenergylett.3c00489
ACS Energy Lett. 2023, 8, 1992−2024

(107) Ramdin, M.; Morrison, A. R. T.; de Groen, M.; van Haperen, R.; de Kler, R.; van den Broeke, L. J. P.; Trusler, J. P. M.; de Jong, W.; Vlugt, T. J. H. High Pressure Electrochemical Reduction of CO_2 to Formic Acid/Formate: A Comparison between Bipolar Membranes and Cation Exchange Membranes. *Ind. Eng. Chem. Res.* **2019**, *58* (5), 1834−1847.
(108) Lee, W.; Kim, Y. E.; Youn, M. H.; Jeong, S. K.; Park, K. T. Catholyte-Free Electrocatalytic CO_2 Reduction to Formate. *Angew. Chem., Int. Ed.* **2018**, *130* (23), 6999−7003.
(109) Yang, H.; Kaczur, J. J.; Sajjad, S. D.; Masel, R. I. Electrochemical Conversion of CO_2 to Formic Acid Utilizing Sustainion™ Membranes. *J. CO_2 Util.* **2017**, *20*, 208−217.
(110) Del Castillo, A.; Alvarez-Guerra, M.; Solla-Gullón, J.; Sáez, A.; Montiel, V.; Irabien, A. Sn Nanoparticles on Gas Diffusion Electrodes: Synthesis, Characterization and Use for Continuous CO_2 Electroreduction to Formate. *J. CO_2 Util.* **2017**, *18*, 222−228.
(111) Díaz-Sainz, G.; Alvarez-Guerra, M.; Solla-Gullón, J.; García-Cruz, L.; Montiel, V.; Irabien, A. Catalyst Coated Membrane Electrodes for the Gas Phase CO_2 Electroreduction to Formate. *Catal. Today* **2020**, *346*, 58−64.
(112) Li, H.; Oloman, C. The Electro-Reduction of Carbon Dioxide in a Continuous Reactor. *J. Appl. Electrochem.* **2005**, *35* (10), 955−965.
(113) Wu, J.; Risalvato, F. G.; Ma, S.; Zhou, X. D. Electrochemical Reduction of Carbon Dioxide III. the Role of Oxide Layer Thickness on the Performance of Sn Electrode in a Full Electrochemical Cell. *J. Mater. Chem. A* **2014**, *2* (6), 1647−1651.
(114) Li, H.; Oloman, C. Development of a Continuous Reactor for the Electro-Reduction of Carbon Dioxide to Formate - Part 2: Scale-Up. *J. Appl. Electrochem.* **2007**, *37* (10), 1107−1117.
(115) Lei, T.; Zhang, X.; Jung, J.; Cai, Y.; Hou, X.; Zhang, Q.; Qiao, J. Continuous Electroreduction of Carbon Dioxide to Formate on Tin Nanoelectrode Using Alkaline Membrane Cell Configuration in Aqueous Medium. *Catal. Today* **2018**, *318*, 32−38.
(116) Sen, S.; Brown, S. M.; McLain, L.; Brushett, F. R. Electroreduction of Carbon Dioxide to Formate at High Current Densities Using Tin and Tin Oxide Gas Diffusion Electrodes. *J. Appl. Electrochem.* **2019**, *49*, 917−928.
(117) Chen, Y.; Vise, A.; Klein, W. E.; Cetinbas, F. C.; Myers, D. J.; Smith, W. A.; Deutsch, T. G.; Neyerlin, K. C. A Robust, Scalable Platform for the Electrochemical Conversion of CO_2 to Formate: Identifying Pathways to Higher Energy Efficiencies. *ACS Energy Lett.* **2020**, *5* (6), 1825−1833.
(118) De Mot, B.; Ramdin, M.; Hereijgers, J.; Vlugt, T. J. H.; Breugelmans, T. Direct Water Injection in Catholyte-Free Zero-Gap Carbon Dioxide Electrolyzers. *ChemElectroChem* **2020**, *7* (18), 3839−3843.
(119) Wang, Q.; Wang, X.; Wu, C.; Cheng, Y.; Sun, Q.; Dong, H.; Yu, H. Electrodeposition of Tin on Nafion-Bonded Carbon Black as an Active Catalyst Layer for Efficient Electroreduction of CO_2 to Formic Acid. *Sci. Rep.* **2017**, *7* (1), 13711.
(120) Qian, Y.; Liu, Y.; Tang, H.; Lin, B. L. Highly Efficient Electroreduction of CO_2 to Formate by Nanorod@2D Nanosheets SnO. *J. CO_2 Util.* **2020**, *42*, 101287.
(121) Thijs, B.; Rongé, J.; Martens, J. A. Selective Electrochemical Reduction of CO_2 to Formic Acid in Gas Phase Reactor with By-Product Recirculation. *Sustain. Energy Fuels* **2021**, *5* (6), 1867−1873.
(122) De Mot, B.; Hereijgers, J.; Duarte, M.; Breugelmans, T. Influence of Flow and Pressure Distribution inside a Gas Diffusion Electrode on the Performance of a Flow-by CO_2 Electrolyzer. *Chem. Eng. J.* **2019**, *378*, 122224.
(123) Duarte, M.; Daems, N.; Hereijgers, J.; Arenas-Esteban, D.; Bals, S.; Breugelmans, T. Enhanced CO_2 Electroreduction with Metal-Nitrogen-Doped Carbons in a Continuous Flow Reactor. *J. CO_2 Util.* **2021**, *50*, 101583.
(124) Irtem, E.; Andreu, T.; Parra, A.; Hernández-Alonso, M. D.; García-Rodríguez, S.; Riesco-García, J. M.; Penelas-Pérez, G.; Morante, J. R. Low-Energy Formate Production from CO_2 Electroreduction Using Electrodeposited Tin on GDE. *J. Mater. Chem. A* **2016**, *4* (35), 13582−13588.
(125) Wang, Q.; Wang, X.; Wu, C.; Cheng, Y.; Sun, Q.; Yu, H. Enhanced Electroreduction of CO_2 and Simultaneous Degradation of Organic Pollutants Using a Sn-Based Carbon Nanotubes/Carbon Black Hybrid Gas Diffusion Cathode. *J. CO_2 Util.* **2018**, *26*, 425−433.
(126) Liang, C.; Kim, B.; Yang, S.; Yang, L.; Francisco Woellner, C.; Li, Z.; Vajtai, R.; Yang, W.; Wu, J.; Kenis, P. J. A.; Ajayan, P. M. High Efficiency Electrochemical Reduction of CO_2 beyond the Two-Electron Transfer Pathway on Grain Boundary Rich Ultra-Small SnO_2 Nanoparticles. *J. Mater. Chem. A* **2018**, *6* (22), 10313−10319.
(127) Kong, Y.; Wang, L.; Jiang, H.; Li, F.; Zhao, T.; Zhuo, M.; Chen, Q.; Mao, M.; Xu, Y. Design of Counter Oxidation vs. CO_2 Electroreduction for Efficient Formate Production on a Tin Cathode. *J. Electroanal. Chem.* **2019**, *847*, 113264.
(128) Lim, J.; Kang, P. W.; Jeon, S. S.; Lee, H. Electrochemically Deposited Sn Catalysts with Dense Tips on a Gas Diffusion Electrode for Electrochemical CO_2 Reduction. *J. Mater. Chem. A* **2020**, *8* (18), 9032−9038.
(129) Pavesi, D.; van de Poll, R. C. J.; Krasovic, J. L.; Figueiredo, M.; Gruter, G.-J. M.; Koper, M. T. M.; Schouten, K. J. P. Cathodic Disintegration as an Easily Scalable Method for the Production of Sn- and Pb-Based Catalysts for CO_2 Reduction. *ACS Sustain. Chem. Eng.* **2020**, *8* (41), 15603−15610.
(130) Merino-Garcia, I.; Tinat, L.; Albo, J.; Alvarez-Guerra, M.; Irabien, A.; Durupthy, O.; Vivier, V.; Sánchez-Sánchez, C. M. Continuous Electroconversion of CO_2 into Formate Using 2 Nm Tin Oxide Nanoparticles. *Appl. Catal. B Environ.* **2021**, *297*, 120447.
(131) Del Castillo, A.; Alvarez-Guerra, M.; Solla-Gullón, J.; Sáez, A.; Montiel, V.; Irabien, A. Electrocatalytic Reduction of CO_2 to Formate Using Particulate Sn Electrodes: Effect of Metal Loading and Particle Size. *Appl. Energy* **2015**, *157*, 165−173.
(132) Alvarez-Guerra, M.; Del Castillo, A.; Irabien, A. Continuous Electrochemical Reduction of Carbon Dioxide into Formate Using a Tin Cathode: Comparison with Lead Cathode. *Chem. Eng. Res. Des.* **2014**, *92* (4), 692−701.
(133) Wang, X.; Li, F.; Yin, W.-J.; Si, Y.; Miao, M.; Wang, X.; Fu, Y. Atomically Dispersed Sn Modified with Trace Sulfur Species Derived from Organosulfide Complex for Electroreduction of CO_2. *Appl. Catal. B Environ.* **2022**, *304*, 120936.
(134) Li, J.; Jiao, J.; Zhang, H.; Zhu, P.; Ma, H.; Chen, C.; Xiao, H.; Lu, Q. Two-Dimensional SnO_2 Nanosheets for Efficient Carbon Dioxide Electroreduction to Formate. *ACS Sustain. Chem. Eng.* **2020**, *8* (12), 4975−4982.
(135) Liu, L. X.; Zhou, Y.; Chang, Y. C.; Zhang, J. R.; Jiang, L. P.; Zhu, W.; Lin, Y. Tuning Sn_3O_4 for CO_2 Reduction to Formate with Ultra-High Current Density. *Nano Energy* **2020**, *77*, 105296.
(136) Xia, C.; Zhu, P.; Jiang, Q.; Pan, Y.; Liang, W.; Stavitski, E.; Alshareef, H. N.; Wang, H. Continuous Production of Pure Liquid Fuel Solutions via Electrocatalytic CO_2 Reduction Using Solid-Electrolyte Devices. *Nat. Energy* **2019**, *4* (9), 776−785.
(137) Díaz-Sainz, G.; Alvarez-Guerra, M.; Solla-Gullón, J.; García-Cruz, L.; Montiel, V.; Irabien, A. CO_2 Electroreduction to Formate: Continuous Single-Pass Operation in a Filter-Press Reactor at High Current Densities Using Bi Gas Diffusion Electrodes. *J. CO_2 Util.* **2019**, *34*, 12−19.
(138) Díaz-Sainz, G.; Alvarez-Guerra, M.; Solla-Gullón, J.; García-Cruz, L.; Montiel, V.; Irabien, A. Gas-Liquid-Solid Reaction System for CO_2 Electroreduction to Formate without Using Supporting Electrolyte. *AIChE J.* **2020**, *66* (9), No. e16299.
(139) Díaz-Sainz, G.; Alvarez-Guerra, M.; Ávila-Bolívar, B.; Solla-Gullón, J.; Montiel, V.; Irabien, A. Improving Trade-Offs in the Figures of Merit of Gas-Phase Single-Pass Continuous CO_2 Electrocatalytic Reduction to Formate. *Chem. Eng. J.* **2021**, *405*, 126965.
(140) Fan, M.; Prabhudev, S.; Garbarino, S.; Qiao, J.; Botton, G. A.; Harrington, D. A.; Tavares, A. C.; Guay, D. Uncovering the Nature of Electroactive Sites in Nano Architectured Dendritic Bi for Highly

https://doi.org/10.1021/acsenergylett.3c00489
ACS Energy Lett. 2023, 8, 1992−2024

Efficient CO_2 Electroreduction to Formate. *Appl. Catal. B Environ.* **2020**, *274*, 119031.
(141) Wang, Q.; Zhu, C.; Wu, C.; Yu, H. Direct Synthesis of Bismuth Nanosheets on a Gas Diffusion Layer as a High-Performance Cathode for a Coupled Electrochemical System Capable of Electroreduction of CO_2 to Formate with Simultaneous Degradation of Organic Pollutants. *Electrochim. Acta* **2019**, *319*, 138−147.
(142) Fan, L.; Xia, C.; Zhu, P.; Lu, Y.; Wang, H. Electrochemical CO_2 Reduction to High-Concentration Pure Formic Acid Solutions in an All-Solid-State Reactor. *Nat. Commun.* **2020**, *11* (1), 3633.
(143) Wu, D.; Hao, J.; Song, Z.; Fu, X. Z.; Luo, J. L. All Roads Lead to Rome: An Energy-Saving Integrated Electrocatalytic CO_2 Reduction System for Concurrent Value-Added Formate Production. *Chem. Eng. J.* **2021**, *412*, 127893.
(144) Fan, T.; Ma, W.; Xie, M.; Liu, H.; Zhang, J.; Yang, S.; Huang, P.; Dong, Y.; Chen, Z.; Yi, X. Achieving High Current Density for Electrocatalytic Reduction of CO_2 to Formate on Bismuth-Based Catalysts. *Cell Rep. Phys. Sci.* **2021**, *2* (3), 100353.
(145) Xing, Z.; Hu, X.; Feng, X. Tuning the Microenvironment in Gas-Diffusion Electrodes Enables High-Rate CO_2 Electrolysis to Formate. *ACS Energy Lett.* **2021**, *6*, 1694−1702.
(146) Yang, H.; Kaczur, J. J.; Sajjad, S. D.; Masel, R. I. Performance and Long-Term Stability of CO_2 Conversion to Formic Acid Using a Three-Compartment Electrolyzer Design. *J. CO_2 Util.* **2020**, *42*, 101349.
(147) Pelayo García de Arquer, F.; Bushuyev, O. S.; De Luna, P.; Dinh, C.-T.; Seifitokaldani, A.; Saidaminov, M. I.; Tan, C.-S.; Na Quan, L.; Proppe, A.; Golam Kibria, M.; et al. 2D Metal Oxyhalide-Derived Catalysts for Efficient CO_2 Electroreduction. *Adv. Mater.* **2018**, *30* (38), 1802858.
(148) Yang, Q.; Wu, Q.; Liu, Y.; Luo, S.; Wu, X.; Zhao, X.; Zou, H.; Long, B.; Chen, W.; Liao, Y.; Li, L.; Shen, P. K.; Duan, L.; Quan, Z. Novel Bi-Doped Amorphous SnOx Nanoshells for Efficient Electrochemical CO_2 Reduction into Formate at Low Overpotentials. *Adv. Mater.* **2020**, *32* (36), 2002822.
(149) Gong, Q.; Ding, P.; Xu, M.; Zhu, X.; Wang, M.; Deng, J.; Ma, Q.; Han, N.; Zhu, Y.; Lu, J.; Feng, Z.; Li, Y.; Zhou, W.; Li, Y. Structural Defects on Converted Bismuth Oxide Nanotubes Enable Highly Active Electrocatalysis of Carbon Dioxide Reduction. *Nat. Commun.* **2019**, *10* (1), 2807.
(150) Zeng, J.; Jagdale, P.; Lourenco, M. A. O.; Farkhondehfal, M. A.; Sassone, D.; Bartoli, M.; Pirri, C. F. Biochar-Supported BiOx for Effective Electrosynthesis of Formic Acid from Carbon Dioxide Reduction. *Crystals* **2021**, *11* (4), 363.
(151) Yang, J.; Wang, X.; Qu, Y.; Wang, X.; Huo, H.; Fan, Q.; Wang, J.; Yang, L.-M.; Wu, Y. Bi-Based Metal-Organic Framework Derived Leafy Bismuth Nanosheets for Carbon Dioxide Electroreduction. *Adv. Energy Mater.* **2020**, *10* (36), 2001709.
(152) Ding, P.; Zhang, J.; Han, N.; Zhou, Y.; Jia, L.; Li, Y. Simultaneous Power Generation and CO_2 Valorization by Aqueous Al-CO_2 Batteries Using Nanostructured Bi2S3 as the Cathode Electrocatalyst. *J. Mater. Chem. A* **2020**, *8* (25), 12385−12390.
(153) Peng, C.-J.; Zeng, G.; Ma, D.-D.; Cao, C.; Zhou, S.; Wu, X.-T.; Zhu, Q.-L. Hydrangea-like Superstructured Micro/Nanoreactor of Topotactically Converted Ultrathin Bismuth Nanosheets for Highly Active CO_2 Electroreduction to Formate. *ACS Appl. Mater. Interfaces* **2021**, *13* (17), 20589−20597.
(154) Jiang, H.; Wang, L.; Li, Y.; Gao, B.; Guo, Y.; Yan, C.; Zhuo, M.; Wang, H.; Zhao, S. High-Selectivity Electrochemical CO_2 Reduction to Formate at Low Overpotential over Bi Catalyst with Hexagonal Sheet Structure. *Appl. Surf. Sci.* **2021**, *541*, 148577.
(155) He, S.; Ni, F.; Ji, Y.; Wang, L.; Wen, Y.; Bai, H.; Liu, G.; Zhang, Y.; Li, Y.; Zhang, B.; Peng, H. The P-Orbital Delocalization of Main-Group Metals to Boost CO_2 Electroreduction. *Angew. Chem., Int. Ed.* **2018**, *57* (49), 16114−16119.
(156) Ma, W.; Bu, J.; Liu, Z.; Yan, C.; Yao, Y.; Chang, N.; Zhang, H.; Wang, T.; Zhang, J. Monoclinic Scheelite Bismuth Vanadate Derived Bismuthene Nanosheets with Rapid Kinetics for Electrochemically Reducing Carbon Dioxide to Formate. *Adv. Funct. Mater.* **2021**, *31* (4), 2006704.
(157) Deng, P.; Yang, F.; Wang, Z.; Chen, S.; Zhou, Y.; Zaman, S.; Xia, B. Y. Metal-Organic Framework-Derived Carbon Nanorods Encapsulating Bismuth Oxides for Rapid and Selective CO_2 Electroreduction to Formate. *Angew. Chem. Int. Ed* **2020**, *59*, 10807−10813.
(158) Cao, C.; Ma, D.-D.; Gu, J.-F.; Xie, X.; Zeng, G.; Li, X.; Han, S.-G.; Zhu, Q.-L.; Wu, X.-T.; Xu, Q. Metal-Organic Layers Leading to Atomically Thin Bismuthene for Efficient Carbon Dioxide Electroreduction to Liquid Fuel. *Angew. Chem., Int. Ed.* **2020**, *59* (35), 15014−15020.
(159) Yi, L.; Chen, J.; Shao, P.; Huang, J.; Peng, X.; Li, J.; Wang, G.; Zhang, C.; Wen, Z. Molten-Salt-Assisted Synthesis of Bismuth Nanosheets for Long-Term ContinuousE Lectrocatalytic Conversion of CO_2 to Formate. *Angew. Chem., Int. Ed.* **2020**, *59* (45), 20112−20119.
(160) Wang, Y.; Xu, L.; Zhan, L.; Yang, P.; Tang, S.; Liu, M.; Zhao, X.; Xiong, Y.; Chen, Z.; Lei, Y. Electron Accumulation Enables Bi Efficient CO_2 Reduction for Formate Production to Boost Clean Zn-CO_2 Batteries. *Nano Energy* **2022**, *92*, 106780.
(161) Díaz-Sainz, G.; Alvarez-Guerra, M.; Irabien, A. Continuous Electroreduction of CO_2 towards Formate in Gas-Phase Operation at High Current Densities with an Anion Exchange Membrane. *J. CO_2 Util.* **2022**, *56*, 101822.
(162) Zou, J.; Lee, C.-Y.; Wallace, G. G. A Non-Noble Metal Catalyst-Based Electrolyzer for Efficient CO_2-to-Formate Conversion. *ACS Sustain. Chem. Eng.* **2021**, *9* (48), 16394−16402.
(163) Liu, S.-Q.; Shahini, E.; Gao, M.-R.; Gong, L.; Sui, P.-F.; Tang, T.; Zeng, H.; Luo, J.-L. Bi_2O_3 Nanosheets Grown on Carbon Nanofiber with Inherent Hydrophobicity for High-Performance CO_2 Electroreduction in a Wide Potential Window. *ACS Nano* **2021**, *15* (11), 17757−17768.
(164) Sui, P.-F.; Xu, C.; Zhu, N.; Liu, S.; Liu, Q.; Luo, J.-L. Interface-Induced Electrocatalytic Enhancement of CO_2-to-Formate Conversion on Heterostructured Bismuth-Based Catalysts. *Small* **2022**, *18* (1), 2105682.
(165) Zhang, M.; Wei, W.; Zhou, S.; Ma, D.-D.; Cao, A.; Wu, X.-T.; Zhu, Q.-L. Engineering Conductive Network of Atomically Thin Bismuthene with Rich Defects Enables CO_2 Reduction to Formate with Industry- Compatible Current Densities and Stability. *Energy Environ. Sci.* **2021**, *14* (9), 4998−5008.
(166) Lu, X.; Leung, D. Y. C.; Wang, H.; Xuan, J. A High Performance Dual Electrolyte Microfluidic Reactor for the Utilization of CO_2. *Appl. Energy* **2017**, *194*, 549−559.
(167) Alvarez-Guerra, M.; Quintanilla, S.; Irabien, A. Conversion of Carbon Dioxide into Formate Using a Continuous Electrochemical Reduction Process in a Lead Cathode. *Chem. Eng. J.* **2012**, *207−208*, 278−284.
(168) Innocent, B.; Liaigre, D.; Pasquier, D.; Ropital, F.; Léger, J. M.; Kokoh, K. B. Electro-Reduction of Carbon Dioxide to Formate on Lead Electrode in Aqueous Medium. *J. Appl. Electrochem.* **2009**, *39* (2), 227−232.
(169) Narayanan, S. R.; Haines, B.; Soler, J.; Valdez, T. I. Electrochemical Conversion of Carbon Dioxide to Formate in Alkaline Polymer Electrolyte Membrane Cells. *J. Electrochem. Soc.* **2011**, *158* (2), A167.
(170) Park, M.; Shin, W. Long-Term Stable and Selective Conversion of Carbon Dioxide to Formate Using Dental Amalgam Electrode. *J. CO_2 Util.* **2021**, *45*, 101435.
(171) Grigioni, I.; Sagar, L. K.; Li, Y. C.; Lee, G.; Yan, Y.; Bertens, K.; Miao, R. K.; Wang, X.; Abed, J.; Won, D. H.; et al. CO_2 Electroreduction to Formate at a Partial Current Density of 930 mA cm^{-2} with InP Colloidal Quantum Dot Derived Catalysts. *ACS Energy Lett.* **2021**, *6* (1), 79−84.
(172) Lucas, F. W. S.; Lima, F. H. B. Electrodeposited Tin-Antimony Alloys as Novel Electrocatalysts for Selective and Stable Carbon Dioxide Reduction to Formate. *ChemElectroChem* **2020**, *7* (18), 3733−3742.

https://doi.org/10.1021/acsenergylett.3c00489
ACS Energy Lett. 2023, 8, 1992−2024

(173) Natsui, K.; Iwakawa, H.; Ikemiya, N.; Nakata, K.; Einaga, Y. Stable and Highly Efficient Electrochemical Production of Formic Acid from Carbon Dioxide Using Diamond Electrodes. *Angew. Chem., Int. Ed.* **2018**, *57* (10), 2639−2643.
(174) Lu, X.; Leung, D. Y. C.; Wang, H.; Maroto-Valer, M. M.; Xuan, J. A PH-Differential Dual-Electrolyte Microfluidic Electrochemical Cells for CO_2 Utilization. *Renew. Energy* **2016**, *95*, 277−285.
(175) García, J.; Jiménez, C.; Martínez, F.; Camarillo, R.; Rincón, J. Electrochemical Reduction of CO_2 Using Pb Catalysts Synthesized in Supercritical Medium. *J. Catal.* **2018**, *367*, 72−80.
(176) Xing, Y.; Kong, X.; Guo, X.; Liu, Y.; Li, Q.; Zhang, Y.; Sheng, Y.; Yang, X.; Geng, Z.; Zeng, J. Bi@Sn Core-Shell Structure with Compressive Strain Boosts the Electroreduction of CO_2 into Formic Acid. *Adv. Sci.* **2020**, *7* (22), 1902989.
(177) Ghosh, S.; Ramaprabhu, S. Boron and Nitrogen Co-Doped Carbon Nanosheets Encapsulating Nano Iron as an Efficient Catalyst for Electrochemical CO_2 Reduction Utilizing a Proton Exchange Membrane CO_2 Conversion Cell. *J. Colloid Interface Sci.* **2020**, *559*, 169−177.
(178) Ghosh, S.; Garapati, M. S.; Ghosh, A.; Sundara, R. Nonprecious Catalyst for Three-Phase Contact in a Proton Exchange Membrane CO_2 Conversion Full Cell for Efficient Electrochemical Reduction of Carbon Dioxide. *ACS Appl. Mater. Interfaces* **2019**, *11* (43), 40432−40442.
(179) Wu, Z.; Wu, H.; Cai, W.; Wen, Z.; Jia, B.; Wang, L.; Jin, W.; Ma, T. Engineering Bismuth-Tin Interface in Bimetallic Aerogel with a 3D Porous Structure for Highly Selective Electrocatalytic CO_2 Reduction to HCOOH. *Angew. Chem., Int. Ed.* **2021**, *60* (22), 12554−12559.
(180) Irkham; Nagashima, S.; Tomisaki, M.; Einaga, Y. Enhancing the Electrochemical Reduction of CO_2 by Controlling the Flow Conditions: An Intermittent Flow Reduction System with a Boron-Doped Diamond Electrode. *ACS Sustain. Chem. Eng.* **2021**, *9* (15), 5298−5303.
(181) Lou, Y.; Fu, D.; Fabre, B.; Fourcade, F.; Amrane, A.; Pasturel, M.; Bourzami, R.; Merdrignac-Conanec, O.; Labasque, T.; Geneste, F. Bismuth Coated Graphite Felt Modified by Silver Particles for Selective Electroreduction of CO_2 into Formate in a Flow Cell. *Electrochim. Acta* **2021**, *371*, 137821.
(182) Wang, Z.; Qi, R.; Liu, D.; Zhao, X.; Huang, L.; Chen, S.; Chen, Z.; Li, M.; You, B.; Pang, Y.; Xia, B. Y. Exfoliated Ultrathin $ZnIn_2S_4$ Nanosheets with Abundant Zinc Vacancies for Enhanced CO_2 Electroreduction to Formate. *ChemSusChem* **2021**, *14* (3), 852−859.
(183) Wang, J.; Zou, J.; Hu, X.; Ning, S.; Wang, X.; Kang, X.; Chen, S. Heterostructured Intermetallic CuSn Catalysts: High Performance towards the Electrochemical Reduction of CO_2 to Formate. *J. Mater. Chem. A* **2019**, *7* (48), 27514−27521.
(184) Fan, M.; Eslamibidgoli, M. J.; Zhu, X.; Garbarino, S.; Tavares, A. C.; Eikerling, M.; Guay, D. Understanding the Improved Activity of Dendritic Sn_1Pb_3 Alloy for the CO_2 Electrochemical Reduction: A Computational-Experimental Investigation. *ACS Catal.* **2020**, *10* (18), 10726−10734.
(185) Zhang, A.; Liang, Y.; Li, H.; Zhang, B.; Liu, Z.; Chang, Q.; Zhang, H.; Zhu, C.-F.; Geng, Z.; Zhu, W.; Zeng, J. In-Situ Surface Reconstruction of InN Nanosheets for Efficient CO_2 Electroreduction into Formate. *Nano Lett.* **2020**, *20* (11), 8229−8235.
(186) Wang, Z.; Zhou, Y.; Xia, C.; Guo, W.; You, B.; Xia, B. Y. Efficient Electroconversion of Carbon Dioxide to Formate by a Reconstructed Amino-Functionalized Indium-Organic Framework Electrocatalyst. *Angew. Chem., Int. Ed.* **2021**, *60* (35), 19107−19112.
(187) Wang, X.; Wang, W.; Zhang, J.; Wang, H.; Yang, Z.; Ning, H.; Zhu, J.; Zhang, Y.; Guan, L.; Teng, X.; Zhao, Q.; Wu, M. Carbon Sustained SnO_2-Bi_2O_3 Hollow Nanofibers as Janus Catalyst for High-Efficiency CO_2 Electroreduction. *Chem. Eng. J.* **2021**, *426*, 131867.
(188) Li, L.; Ozden, A.; Guo, S.; Pelayo García de Arquer, F.; Wang, C.; Zhang, M.; Zhang, J.; Jiang, H.; Wang, W.; Dong, H.; Sinton, D.; Sargent, E. H.; Zhong, M. Stable, Active CO_2 Reduction to Formate via Redox-Modulated Stabilization of Active Sites. *Nat. Commun.* **2021**, *12* (1), 5223.
(189) Lou, W.; Peng, L.; He, R.; Liu, Y.; Qiao, J. CuBi Electrocatalysts Modulated to Grow on Derived Copper Foam for Efficient CO_2-to-Formate Conversion. *J. Colloid Interface Sci.* **2022**, *606*, 994−1003.
(190) Wang, W.; Wang, Z.; Yang, R.; Duan, J.; Liu, Y.; Nie, A.; Li, H.; Xia, B. Y.; Zhai, T. In Situ Phase Separation into Coupled Interfaces for Promoting CO_2 Electroreduction to Formate over a Wide Potential Window. *Angew. Chem., Int. Ed.* **2021**, *60* (42), 22940−22947.
(191) Zheng, T.; Liu, C.; Guo, C.; Zhang, M.; Li, X.; Jiang, Q.; Xue, W.; Li, H.; Li, A.; Pao, C.-W.; Xiao, J.; Xia, C.; Zeng, J. Copper-Catalysed Exclusive CO_2 to Pure Formic Acid Conversion via Single-Atom Alloying. *Nat. Nanotechnol.* **2021**, *16* (12), 1386−1393.
(192) Liu, S.; Wang, C.; Wu, J.; Tian, B.; Sun, Y.; Lv, Y.; Mu, Z.; Sun, Y.; Li, X.; Wang, F.; Wang, Y.; Tang, L.; Wang, P.; Li, Y.; Ding, M. Efficient CO_2 Electroreduction with a Monolayer Bi_2WO_6 through a Metallic Intermediate Surface State. *ACS Catal.* **2021**, *11* (20), 12476−12484.
(193) Chi, L.-P.; Niu, Z.-Z.; Zhang, X.-L.; Yang, P.-P.; Liao, J.; Gao, F.-Y.; Wu, Z.-Z.; Tang, K.-B.; Gao, M.-R. Stabilizing Indium Sulfide for CO_2 Electroreduction to Formate at High Rate by Zinc Incorporation. *Nat. Commun.* **2021**, *12* (1), 5835.
(194) Jhong, H.-R. M.; Nwabara, U. O.; Shubert-Zuleta, S.; Grundish, N. S.; Tandon, B.; Reimnitz, L. C.; Staller, C. M.; Ong, G. K.; Saez Cabezas, C. A.; Goodenough, J. B.; Kenis, P. J. A.; Milliron, D. J. Efficient Aqueous Electroreduction of CO_2 to Formate at Low Overpotential on Indium Tin Oxide Nanocrystals. *Chem. Mater.* **2021**, *33* (19), 7675.
(195) Seifitokaldani, A.; Gabardo, C. M.; Burdyny, T.; Dinh, C.-T.; Edwards, J. P.; Kibria, M. G.; Bushuyev, O. S.; Kelley, S. O.; Sinton, D.; Sargent, E. H. Hydronium-Induced Switching between CO_2 Electroreduction Pathways. *J. Am. Chem. Soc.* **2018**, *140*, 3833.
(196) Ning, B.; Xu, Q.; Liu, M.; Jiang, H.; Hu, Y.; Li, C. Bismuthene with Stable Bi[Sbnd]O Bonds for Efficient CO_2 Electroreduction to Formate. *Chem. Eng. Sci.* **2022**, *251*, 117409.
(197) Liu, Z.; Lv, X.; Zhang, J.; Guan, A.; Yang, C.; Yan, S.; Chen, Y.; Liu, K.; Zheng, G. Hydroxy-Group-Enriched In_2O_3 Facilitates CO_2 Electroreduction to Formate at Large Current Densities. *Adv. Mater. Interfaces* **2022**, *9*, 2101956.
(198) Zhang, X.; Peng, L.; Xu, B.; Liu, P.; Jiao, X.; Kang, H.; Song, Z.; Yan, X.; Mao, Y.; Qiao, J. Bi-Cu Bimetallic Electrocatalysts Prepared Using Electrochemical Deposition Effluent for Highly Converting CO_2 to Formate. *Process Saf. Environ. Prot.* **2022**, *158*, 560−566.
(199) Zhang, J.; Fan, T.; Huang, P.; Lian, X.; Guo, Y.; Chen, Z.; Yi, X. Electro-Reconstruction-Induced Strain Regulation and Synergism of Ag-In-S toward Highly Efficient CO_2 Electrolysis to Formate. *Adv. Funct. Mater.* **2022**, *32* (25), 2113075.
(200) Wang, Z.; Zhou, Y.; Liu, D.; Qi, R.; Xia, C.; Li, M.; You, B.; Xia, B. Y. Carbon-Confined Indium Oxides for Efficient Carbon Dioxide Reduction in a Solid-State Electrolyte Flow Cell. *Angew. Chem., Int. Ed.* **2022**, *61* (21), No. e202200552.
(201) Wang, Y.; Ding, J.; Zhao, J.; Wang, J.; Han, X.; Deng, Y.; Hu, W. Selective Electrocatalytic Reduction of CO_2 to Formate via Carbon-Shell-Encapsulated In_2O_3 Nanoparticles/Graphene Nanohybrids. *J. Mater. Sci. Technol.* **2022**, *121*, 220−226.
(202) Lee, J.; Liu, H.; Chen, Y.; Li, W. Bismuth Nanosheets Derived by In Situ Morphology Transformation of Bismuth Oxides for Selective Electrochemical CO_2 Reduction to Formate. *ACS Appl. Mater. Interfaces* **2022**, *14*, 14210−14217.
(203) Li, Y.; Chen, J.; Chen, S.; Liao, X.; Zhao, T.; Cheng, F.; Wang, H. In Situ Confined Growth of Bismuth Nanoribbons with Active and Robust Edge Sites for Boosted CO_2 Electroreduction. *ACS Energy Lett.* **2022**, *7* (4), 1454−1461.
(204) Nguyen-Phan, T.-D.; Hu, L.; Howard, B. H.; Xu, W.; Stavitski, E.; Leshchev, D.; Rothenberger, A.; Neyerlin, K. C.; Kauffman, D. R.

https://doi.org/10.1021/acsenergylett.3c00489
ACS Energy Lett. 2023, 8, 1992−2024

High Current Density Electroreduction of CO_2 into Formate with Tin Oxide Nanospheres. *Sci. Rep.* **2022**, *12* (1), 8420.
(205) Zhang, B.; Chang, Y.; Wu, Y.; Fan, Z.; Zhai, P.; Wang, C.; Gao, J.; Sun, L.; Hou, J.; et al. Regulating *OCHO Intermediate as Rate-Determining Step of Defective Oxynitride Nanosheets Enabling Robust CO_2 Electroreduction. *Adv. Energy Mater.* **2022**, *12* (27), 2200321.
(206) Zhang, Y.; Lan, J.; Xie, F.; Peng, M.; Liu, J.; Chan, T.-S.; Tan, Y. Aligned InS Nanorods for Efficient Electrocatalytic Carbon Dioxide Reduction. *ACS Appl. Mater. Interfaces* **2022**, *14* (22), 25257−25266.
(207) Yang, W.; Si, C.; Zhao, Y.; Wei, Q.; Jia, G.; Cheng, G.; Qin, J.; Zhang, Z. Activating Inert Antimony for Selective CO_2 Electroreduction to Formate via Bimetallic Interactions. *Appl. Catal. B Environ.* **2022**, *316*, 121619.
(208) Li, K.; Xu, J.; Zheng, T.; Yuan, Y.; Liu, S.; Shen, C.; Jiang, T.; Sun, J.; Liu, Z.; Xu, Y.; Chuai, M.; Xia, C.; Chen, W. In Situ Dynamic Construction of a Copper Tin Sulfide Catalyst for High-Performance Electrochemical CO_2 Conversion to Formate. *ACS Catal.* **2022**, *12* (16), 9922−9932.
(209) Rabiee, H.; Ge, L.; Zhang, X.; Hu, S.; Li, M.; Smart, S.; Zhu, Z.; Yuan, Z. Shape-Tuned Electrodeposition of Bismuth-Based Nanosheets on Flow-through Hollow Fiber Gas Diffusion Electrode for High-Efficiency CO_2 Reduction to Formate. *Appl. Catal. B Environ.* **2021**, *286*, 119945.
(210) Zelocualtecatl Montiel, I.; Dutta, A.; Kiran, K.; Rieder, A.; Iarchuk, A.; Vesztergom, S.; Mirolo, M.; Martens, I.; Drnec, J.; Broekmann, P. CO_2 Conversion at High Current Densities: Stabilization of Bi(III)-Containing Electrocatalysts under CO_2 Gas Flow Conditions. *ACS Catal.* **2022**, *12* (17), 10872−10886.
(211) Xu, J.; Yang, S.; Ji, L.; Mao, J.; Zhang, W.; Zheng, X.; Fu, H.; Yuan, M.; Yang, C.; Chen, H.; Li, R. High Current CO_2 Reduction Realized by Edge/Defect-Rich Bismuth Nanosheets. *Nano Res.* **2023**, *16*, 53−61.
(212) Wang, M.; Liu, S.; Chen, B.; Huang, M.; Peng, C. Co-Regulation of Intermediate Binding and Water Activation in Sulfur-Doped Bismuth Nanosheets for Electrocatalytic CO_2 Reduction to Formate. *Chem. Eng. J.* **2023**, *451*, 139056.
(213) Wu, J.; Yu, X.; He, H.; Yang, C.; Xia, D.; Wang, L.; Huang, J.; Zhao, N.; Tang, F.; Deng, L.; Liu, Y.-N. Bismuth-Nanosheet-Based Catalysts with a Reconstituted Bi0Atom for Promoting the Electrocatalytic Reduction of CO_2 to Formate. *Ind. Eng. Chem. Res.* **2022**, *61* (34), 12383−12391.
(214) Guo, X.; Xu, S.-M.; Zhou, H.; Ren, Y.; Ge, R.; Xu, M.; Zheng, L.; Kong, X.; Shao, M.; Li, Z.; Duan, H. Engineering Hydrogen Generation Sites to Promote Electrocatalytic CO_2 Reduction to Formate. *ACS Catal.* **2022**, *12* (17), 10551−10559.
(215) Jiang, X.; Li, X.; Kong, Y.; Deng, C.; Li, X.; Hu, Q.; Yang, H.; He, C. Oxidation State Modulation of Bimetallic Tin-Copper Oxide Nanotubes for Selective CO_2 Electroreduction to Formate. *Small* **2022**, *18* (47), 2204148.
(216) Wei, Q.; Qin, J.; Jia, G.; Zhao, Y.; Guo, Z.; Cheng, G.; Ma, W.; Yang, W.; Zhang, Z. Dealloying-Derived Nanoporous Bismuth for Selective CO_2 Electroreduction to Formate. *J. Phys. Chem. Lett.* **2022**, *13*, 9058−9065.
(217) Liu, L.-X.; Li, X.; Cai, Y.; Du, H.; Liu, F.; Zhang, J.-R.; Fu, J.; Zhu, W. Hierarchical S-Modified Cu Porous Nanoflakes for Efficient CO_2 Electroreduction to Formate. *Nanoscale* **2022**, *14* (37), 13679−13688.
(218) Wang, D.; Sun, T.; Xu, L.; Gong, L.; Chen, B.; Zhang, P.; Zheng, T.; Xu, Q.; Pan, H.; Zhang, Y.; Jiang, J. Interfacial Engineering of $SnO_2/Bi_2O_2CO_3$ Heterojunction on Heteroatoms-Doped Carbon for High-Performance CO_2 Electroreduction to Formate. *Nano Res.* **2023**, *16* (2), 2278−2285.
(219) Choi, B. U.; Tan, Y. C.; Song, H.; Lee, K. B.; Oh, J. System Design Considerations for Enhancing Electroproduction of Formate from Simulated Flue Gas. *ACS Sustain. Chem. Eng.* **2021**, *9* (5), 2348−2357.
(220) Van Daele, S.; Hintjens, L.; Van Den Hoek, J.; Neukermans, S.; Daems, N.; Hereijgers, J.; Breugelmans, T. Influence of the Target Product on the Electrochemical Reduction of Diluted CO_2in a Continuous Flow Cell. *J. CO_2 Util.* **2022**, *65*, 102210.
(221) Xie, S.; Mei, B.; Yu, L.; Nie, Z.; Li, M.; Jiang, L.; Duan, J.; Jiang, Z.; Chen, S. Size Separation of Bi2WO6 Nanolayers Promoting Electroreduction of Carbon Dioxide to Formate. *Appl. Surf. Sci.* **2023**, *611*, 155499.
(222) Jiang, X.; Lin, L.; Rong, Y.; Li, R.; Jiang, Q.; Yang, Y.; Gao, D. Boosting CO_2 Electroreduction to Formate via Bismuth Oxide. *Nano Res.* **2022**, DOI: 10.1007/s12274-022-5073-0.
(223) Zhang, Y.; Chen, Y.; Liu, R.; Wang, X.; Liu, H.; Zhu, Y.; Qian, Q.; Feng, Y.; Cheng, M.; Zhang, G. Oxygen Vacancy Stabilized $Bi_2O_2CO_3$ Nanosheet for CO_2 Electroreduction at Low Overpotential Enables Energy Efficient CO-Production of Formate. *InfoMat* **2023**, *5*, No. e12375.
(224) Liu, S.; Fan, Y.; Wang, Y.; Jin, S.; Hou, M.; Zeng, W.; Li, K.; Jiang, T.; Qin, L.; Yan, Z.; Tao, Z.; Zheng, X.; Shen, C.; Liu, Z.; Ahmad, T.; Zhang, K.; Chen, W. Surface-Oxygen-Rich Bi@C Nanoparticles for High-Efficiency Electroreduction of CO_2 to Formate. *Nano Lett.* **2022**, *22* (22), 9107−9114.
(225) Li, L.; Jin, X.; Yu, X.; Zhong, M. Bimetallic Cu-Bi Catalysts for Efficient Electroreduction of CO_2 to Formate. *Front. Chem.* **2022**, *10*, 983778.
(226) Yao, K.; Wang, H.; Yang, X.; Huang, Y.; Kou, C.; Jing, T.; Chen, S.; Wang, Z.; Liu, Y.; Liang, H. Metal-Organic Framework Derived Dual-Metal Sites for Electroreduction of Carbon Dioxide to HCOOH. *Appl. Catal. B Environ.* **2022**, *311*, 121377.
(227) Li, S.; Kang, Y.; Mo, C.; Peng, Y.; Ma, H.; Peng, J. Nitrogen-Doped Bismuth Nanosheet as an Efficient Electrocatalyst to CO_2 Reduction for Production of Formate. *Int. J. Mol. Sci.* **2022**, *23* (22), 14485.
(228) Liu, P. X.; Peng, L. W.; He, R. N.; Li, L. L.; Qiao, J. L. A High-Performance Continuous-Flow MEA Reactor for Electroreduction CO_2 to Formate. *J. Electrochem.* **2022**, *28* (1), 2104231.
(229) Díaz-Sainz, G.; Fernández-Caso, K.; Lagarteira, T.; Delgado, S.; Alvarez-Guerra, M.; Mendes, A.; Irabien, A. Coupling Continuous CO_2 Electroreduction to Formate with Efficient Ni-Based Anodes. *J. Environ. Chem. Eng.* **2023**, *11* (1), 109171.
(230) Anawati; Frankel, G. S.; Agarwal, A.; Sridhar, N. Degradation and Deactivation of Sn Catalyst Used for CO_2 Reduction as Function of Overpotential. *Electrochim. Acta* **2014**, *133*, 188−196.
(231) Perry, S. C.; Ponce de León, C.; Walsh, F. C. Review—The Design, Performance and Continuing Development of Electrochemical Reactors for Clean Electrosynthesis. *J. Electrochem. Soc.* **2020**, *167* (15), 155525.
(232) Ran, J.; Wu, L.; He, Y.; Yang, Z.; Wang, Y.; Jiang, C.; Ge, L.; Bakangura, E.; Xu, T. Ion Exchange Membranes: New Developments and Applications. *J. Membr. Sci.* **2017**, *522*, 267−291.
(233) Kim, J. M.; Beckingham, B. S. Transport and Co-Transport of Carboxylate Ions and Alcohols in Cation Exchange Membranes. *J. Polym. Sci.* **2021**, *59* (21), 2545−2558.
(234) Varcoe, J. R.; Atanassov, P.; Dekel, D. R.; Herring, A. M.; Hickner, M. A.; Kohl, P. A.; Kucernak, A. R.; Mustain, W. E.; Nijmeijer, K.; Scott, K.; et al. Anion-Exchange Membranes in Electrochemical Energy Systems. *Energy Environ. Sci.* **2014**, *7* (10), 3135−3191.
(235) Salvatore, D. A.; Gabardo, C. M.; Reyes, A.; O'Brien, C. P.; Holdcroft, S.; Pintauro, P.; Bahar, B.; Hickner, M.; Bae, C.; Sinton, D.; et al. Designing Anion Exchange Membranes for CO_2 Electrolysers. *Nat. Energy* **2021**, *6* (4), 339−348.
(236) Xu, T. Ion Exchange Membranes: State of Their Development and Perspective. *J. Membr. Sci.* **2005**, *263* (1−2), 1−29.
(237) Blommaert, M. A.; Sharifian, R.; Shah, N. U.; Nesbitt, N. T.; Smith, W. A.; Vermaas, D. A. Orientation of a Bipolar Membrane Determines the Dominant Ion and Carbonic Species Transport in Membrane Electrode Assemblies for CO_2reduction. *J. Mater. Chem. A* **2021**, *9* (18), 11179−11186.
(238) CO_2 Conversion To Formic Acid, Dioxide Materials, https://dioxidematerials.com/technology/formic-acid/ (accessed Nov 29, 2021).

https://doi.org/10.1021/acsenergylett.3c00489
ACS Energy Lett. 2023, 8, 1992−2024

(239) Li, H.; Oloman, C. Development of a Continuous Reactor for the Electro-Reduction of Carbon Dioxide to Formate-Part 1: Process Variables. *J. Appl. Electrochem.* **2006**, *36* (10), 1105−1115.
(240) Hernandez-Aldave, S.; Andreoli, E. Fundamentals of Gas Diffusion Electrodes and Electrolysers for Carbon Dioxide Utilisation: Challenges and Opportunities. *Catalyst* **2020**, *10* (6), 713.
(241) Sassenburg, M.; Kelly, M.; Subramanian, S.; Smith, W. A.; Burdyny, T. Zero-Gap Electrochemical CO_2Reduction Cells: Challenges and Operational Strategies for Prevention of Salt Precipitation. *ACS Energy Lett.* **2023**, *8*, 321−331.
(242) Dutta, A.; Kuzume, A.; Rahaman, M.; Vesztergom, S.; Broekmann, P. Monitoring the Chemical State of Catalysts for CO_2 Electroreduction: An In Operando Study. *ACS Catal.* **2015**, *5* (12), 7498−7502.
(243) Lv, W.; Zhou, J.; Kong, F.; Fang, H.; Wang, W. Porous Tin-Based Film Deposited on Copper Foil for Electrochemical Reduction of Carbon Dioxide to Formate. *Int. J. Hydrogen Energy* **2016**, *41* (3), 1585−1591.
(244) Won, D. H.; Choi, C. H.; Chung, J.; Chung, M. W.; Kim, E.-H.; Woo, S. I. Rational Design of a Hierarchical Tin Dendrite Electrode for Efficient Electrochemical Reduction of CO_2. *ChemSusChem* **2015**, *8* (18), 3092−3098.
(245) Abderezzak, B. Introduction to Hydrogen Technology. Introd. to Transf. Phenom. *PEM Fuel Cell* **2018**, 1−51.
(246) MacHunda, R. L.; Ju, H.; Lee, J. Electrocatalytic Reduction of CO_2 Gas at Sn Based Gas Diffusion Electrode. *Curr. Appl. Phys.* **2011**, *11* (4), 986−988.
(247) MacHunda, R. L.; Lee, J.; Lee, J. Microstructural Surface Changes of Electrodeposited Pb on Gas Diffusion Electrode during Electroreduction of Gas-Phase CO_2. *Surf. Interface Anal.* **2010**, *42* (6−7), 564−567.
(248) Wang, Q.; Dong, H.; Yu, H. Development of Rolling Tin Gas Diffusion Electrode for Carbon Dioxide Electrochemical Reduction to Produce Formate in Aqueous Electrolyte. *J. Power Sources* **2014**, *271*, 278−284.
(249) Wang, Q.; Dong, H.; Yu, H. Fabrication of a Novel Tin Gas Diffusion Electrode for Electrochemical Reduction of Carbon Dioxide to Formic Acid. *RSC Adv.* **2014**, *4* (104), 59970−59976.
(250) Becker, J.; Flückiger, R.; Reum, M.; Büchi, F. N.; Marone, F.; Stampanoni, M. Determination of Material Properties of Gas Diffusion Layers: Experiments and Simulations Using Phase Contrast Tomographic Microscopy. *J. Electrochem. Soc.* **2009**, *156* (10), B1175.
(251) García de Arquer, F. P.; Dinh, C. T.; Ozden, A.; Wicks, J.; McCallum, C.; Kirmani, A. R.; Nam, D. H.; Gabardo, C.; Seifitokaldani, A.; Wang, X.; et al. CO_2 Electrolysis to Multicarbon Products at Activities Greater than 1 A cm^{-2}. *Science* **2020**, *367* (6478), 661−666.
(252) Kusoglu, A.; Weber, A. Z. New Insights into Perfluorinated Sulfonic-Acid Ionomers. *Chem. Rev.* **2017**, *117* (3), 987−1104.
(253) Song, J. T.; Song, H.; Kim, B.; Oh, J. Towards Higher Rate Electrochemical CO_2 Conversion: From Liquid-Phase to Gas-Phase Systems. *Catalysts* **2019**, *9* (3), 224.
(254) Vij, V.; Sultan, S.; Harzandi, A. M.; Meena, A.; Tiwari, J. N.; Lee, W.-G.; Yoon, T.; Kim, K. S. Nickel-Based Electrocatalysts for Energy-Related Applications: Oxygen Reduction, Oxygen Evolution, and Hydrogen Evolution Reactions. *ACS Catal.* **2017**, *7* (10), 7196−7225.
(255) Coria, G.; Sirés, I.; Brillas, E.; Nava, J. L. Influence of the Anode Material on the Degradation of Naproxen by Fenton-Based Electrochemical Processes. *Chem. Eng. J.* **2016**, *304*, 817−825.
(256) Scialdone, O.; Randazzo, S.; Galia, A.; Silvestri, G. Electrochemical Oxidation of Organics in Water: Role of Operative Parameters in the Absence and in the Presence of NaCl. *Water Res.* **2009**, *43* (8), 2260−2272.
(257) Lu, X.; Zhao, C. Electrodeposition of Hierarchically Structured Three-Dimensional Nickel-Iron Electrodes for Efficient Oxygen Evolution at High Current Densities. *Nat. Commun.* **2015**, *6*, 6616.
(258) Zhu, D. D.; Liu, J. L.; Qiao, S. Z. Recent Advances in Inorganic Heterogeneous Electrocatalysts for Reduction of Carbon Dioxide. *Adv. Mater.* **2016**, *28* (18), 3423−3452.
(259) Bushuyev, O. S.; De Luna, P.; Dinh, C. T.; Tao, L.; Saur, G.; van de Lagemaat, J.; Kelley, S. O.; Sargent, E. H. What Should We Make with CO_2 and How Can We Make It? *Joule* **2018**, *2* (5), 825−832.
(260) Xu, Y.; Edwards, J. P.; Liu, S.; Miao, R. K.; Huang, J. E.; Gabardo, C. M.; O'Brien, C. P.; Li, J.; Sargent, E. H.; Sinton, D. Self-Cleaning CO_2Reduction Systems: Unsteady Electrochemical Forcing Enables Stability. *ACS Energy Lett.* **2021**, *6* (2), 809−815.
(261) Cofell, E. R.; Nwabara, U. O.; Bhargava, S. S.; Henckel, D. E.; Kenis, P. J. A. Investigation of Electrolyte-Dependent Carbonate Formation on Gas Diffusion Electrodes for CO_2Electrolysis. *ACS Appl. Mater. Interfaces* **2021**, *13* (13), 15132−15142.
(262) Cofell, E. R.; Park, Z.; Nwabara, U. O.; Harris, L. C.; Bhargava, S. S.; Gewirth, A. A.; Kenis, P. J. A. Potential Cycling of Silver Cathodes in an Alkaline CO_2Flow Electrolyzer for Accelerated Stress Testing and Carbonate Inhibition. *ACS Appl. Energy Mater.* **2022**, *5* (10), 12013−12021.
(263) Dominguez-Ramos, A.; Singh, B.; Zhang, X.; Hertwich, E. G.; Irabien, A. Global Warming Footprint of the Electrochemical Reduction of Carbon Dioxide to Formate. *J. Clean. Prod.* **2015**, *104*, 148−155.
(264) Aldaco, R.; Butnar, I.; Margallo, M.; Laso, J.; Rumayor, M.; Dominguez-Ramos, A.; Irabien, A.; Dodds, P. E. Bringing Value to the Chemical Industry from Capture, Storage and Use of CO_2: A Dynamic LCA of Formic Acid Production. *Sci. Total Environ.* **2019**, *663*, 738−753.
(265) Kaczur, J. J.; Mcglaughlin, L. J.; Lakkaraju, P. S. Investigating Pervaporation as a Process Method for Concentrating Formic Acid Produced from Carbon Dioxide. *J. Carbon Res.* **2020**, *6* (2), 42.
(266) Pérez-Fortes, M.; Tzimas, E. Techno-Economic and Environmental Evaluation of CO_2 Utilsation for Fuel Production. *Synthesis of Methanol and Formic Acid*; Publications Office of the European Union: Luxemburg, 2016.
(267) Georgopoulou, C.; Jain, S.; Agarwal, A.; Rode, E.; Dimopoulos, G.; Sridhar, N.; Kakalis, N. On the Modelling of Multidisciplinary Electrochemical Systems with Application on the Electrochemical Conversion of CO_2 to Formate/Formic Acid. *Comput. Chem. Eng.* **2016**, *93*, 160−170.
(268) Zhai, Y.; Guan, S.; Sridhar, N.; Arun, S.; Agarwal, F. G. US Patent Application 2013/0186771 A1, 2013.
(269) Zhai, Y.; Guan, S.; Sridhar, N.; Agarwal, A. S. US Patent 10253420B2, 2019.
(270) Nwabara, U. O.; Cofell, E. R.; Verma, S.; Negro, E.; Kenis, P. J. A. Durable Cathodes and Electrolyzers for the Efficient Aqueous Electrochemical Reduction of CO_2. *ChemSusChem* **2020**, *13* (5), 855−875.
(271) Verma, S.; Lu, S.; Kenis, P. J. A. Co-Electrolysis of CO_2 and Glycerol as a Pathway to Carbon Chemicals with Improved Technoeconomics Due to Low Electricity Consumption. *Nat. Energy* **2019**, *4* (6), 466−474.
(272) Vass; Endrődi, B.; Janáky, C. Coupling Electrochemical Carbon Dioxide Conversion with Value-Added Anode Processes: An Emerging Paradigm. *Curr. Opin. Electrochem.* **2021**, *25*, 100621.
(273) De Souza, M. B. C.; Vicente, R. A.; Yukuhiro, V. Y.; Pires, C. T. G.; Cheuquepán, W.; Bott-Neto, J. L.; Solla-Gullón, J.; Fernández, P. S. Bi-Modified Pt Electrodes toward Glycerol Electrooxidation in Alkaline Solution: Effects on Activity and Selectivity. *ACS Catal.* **2019**, *9* (6), 5104−5110.
(274) Fan, L.; Liu, B.; Liu, X.; Senthilkumar, N.; Wang, G.; Wen, Z. Recent Progress in Electrocatalytic Glycerol Oxidation. *Energy Technol.* **2021**, *9* (2), 2000804.
(275) Lee, S.; Kim, H. J.; Lim, E. J.; Kim, Y.; Noh, Y.; Huber, G. W.; Kim, W. B. Highly Selective Transformation of Glycerol to Dihydroxyacetone without Using Oxidants by a PtSb/C-Catalyzed Electrooxidation Process. *Green Chem.* **2016**, *18* (9), 2877−2887.

https://doi.org/10.1021/acsenergylett.3c00489
ACS Energy Lett. 2023, 8, 1992−2024

(276) Rumayor, M.; Dominguez-Ramos, A.; Irabien, A. Feasibility Analysis of a CO_2 Recycling Plant for the Decarbonization of Formate and Dihydroxyacetone Production. *Green Chem.* **2021**, *23*, 4840−4851.

https://doi.org/10.1021/acsenergylett.3c00489
ACS Energy Lett. 2023, 8, 1992−2024